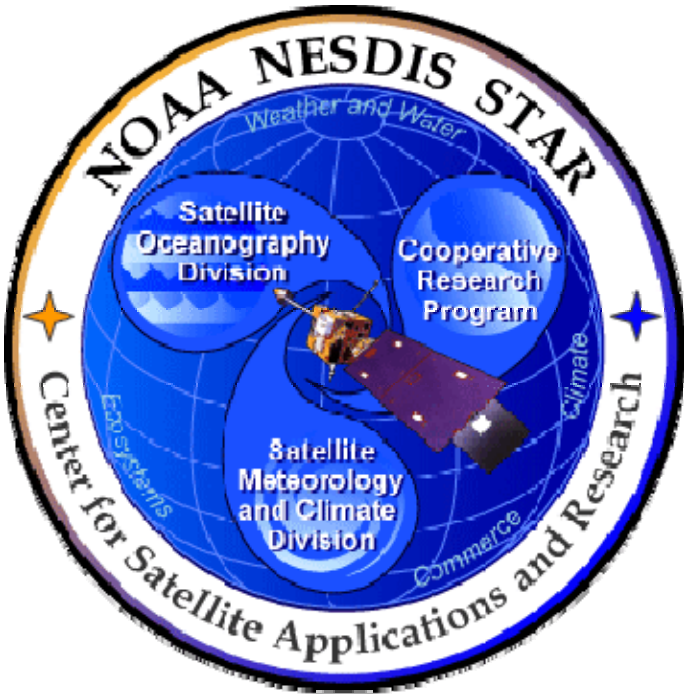

NOAA NESDIS
CENTER for SATELLITE APPLICATIONS and RESEARCH

GOES-R Advanced Baseline Imager (ABI) Algorithm Theoretical Basis Document For Land Surface Temperature

Yunyue Yu, NOAA/NESDIS/STAR
Dan Tarpley, Short & Associates, Inc.
Hui Xu, and Ming Chen, I and M System Group, Inc.

Version 3.0
June 28, 2010

Algorithm Theoretical Basis Document for Land Surface Temperature
Version History SUMMARY

Version	Description	Revised Sections	Date
0.1	New ATBD Document according to NOAA /NESDIS/STAR Document Guideline		6/15/2008
1.0	ATBD Document according to NOAA /NESDIS/STAR Document Guideline		9/30/2008
2.0	ATBD Document 80% readiness		6/26/2009
2.0	Modification made reflecting the responses to AIT and IV&V reviewer's comments, and for including testing results from using MODIS data		9/25/2009
3.0	Revision for reflecting further developments since version 2.0, and modifications and improvement based on the responses to reviewers comments/suggestions on version 2.0 from the IV&V, ADEB, SE members. Detail quality control flags and metadata information are provided. More test and validation results are added as well.	Sections 1 to 5.	6/28/2010

TABLE OF CONTENTS

LIST OF FIGURES

Page

LIST OF TABLES

Page

LIST OF ACRONYMS

ABI	Advanced Baseline Imager
ACM	ABI Cloud Mask
ADEB	Algorithm Development Executive Board
AIT	Algorithm Integration Team
ATBD	Algorithm Theoretical Base Document
AWG	Algorithm Working Group
CONUS	Continental United States
ECMWF	European Centre for Medium-range Weather Forecasts
EOS	Earth Observation Systems
FD	Full Disk
GFS	Global Forecast System
FSC	Fraction of Snow Cover
GOES	Geostationary Operational Environmental Satellite
GS-F&PS	Ground Segment Functional and Performance Specification
IMS	Interactive Multi-sensor snow and ice mapping System
IR	Infrared
IV&V	Independent Verification and Validation
LST	Land Surface Temperature
MODIS	Moderate Resolution Imaging Spectroradiometer
MRD	Mission Requirement Document
MSG	Meteosat Second Generation
NCEP	National center for Environmental Prediction
NESDIS	National Environmental Satellite, Data, and Information Service
NOAA	National Oceanic and Atmospheric Administration
NPOESS	National Polar-orbiting Operational Environmental Satellite System
PIR	Precise Infrared Radiometer
QA	Quality Assurance
RTM	Radiative Transfer Model
SE	System Engineering
SEVIRI	Spanning Enhanced Visible and Infrared Imager
SRF	Spectral Response Function
SST	Sea Surface Temperature
STAR	Center for Satellite Applications and Research
STD	Standard Deviation
SURFRAD	SURFace RADiation network
SW	Split Window
SWA	Software Architecture Document
TIR	Thermal Infrared
TOA	Top Of Atmosphere
UMD	University of Maryland

VIIRS	Visible/Infrared Imager /Radiometer Suite
VVP	Verification and Validation Plan
WV	Water Vapor

ABSTRACT

This Algorithm Theoretical Basis Document (ATBD) describes in detail the procedures for developing and using a land surface temperature (LST) algorithm designed for the GOES-R Advanced Baseline Imager (ABI). It includes a description of the requirements and specifications of the LST products and some specific information about the ABI that is relevant to the derivation of the LST products. The heart of the ATBD is a description of the science of the proposed ABI LST algorithm. The process of algorithm selection is documented. This includes a review of satellite LST research, a selection of candidate algorithms and a description of a large simulated GOES-R ABI data set that was used to derive algorithm coefficients and test the candidate algorithms. The simulated radiances were calculated using sensor spectral response functions (SRF) that are expected from the actual ABI instrument. A description of the expected implementation of the LST algorithm is provided. Ancillary data sets needed for the LST calculation are listed.

Nine split window algorithms were built, which were adapted from the literature, for evaluation as the Day 1 GOES-R LST algorithm. All nine algorithms used explicit spectral emissivity and satellite view angle. Algorithm regression coefficients were derived from the simulated data set and the sensitivity of the algorithms to emissivity error and atmospheric moisture was evaluated. The algorithm least sensitive to error in surface emissivity and atmospheric water vapor was selected for the Day 1 algorithm.

The selected algorithm was applied to GOES Imager and SEVIRI data. The retrieved LSTs were compared against independent ground truth data and the results were analyzed. The properties of the algorithm were examined for selected surface emissivities, time of day and illumination/observation geometry effects and a variety of surface types. The algorithm was found to meet specs with the test data sets. Perfectly cloud free data is assumed in all testing of the ATBD research. A process for routine evaluation of the operational GOES-R LST is described. This includes an automated cloud detection algorithm, routine match-ups against ground truth and methodology for product evaluation. Finally practical matters such as computer resources, instrument performance and its effects on the product are considered.

1. INTRODUCTION

The purpose, users, scope, related documents and revision history of this document are briefly described in this section. Section 2 gives an overview of the land surface temperature (LST) retrieval objectives and operations concept. Section 3 describes the baseline algorithm, its input data requirements, the theoretical background, sensitivity analyses and error budgeting. Test data sets and outputs are presented in Section 4. Some practical considerations are described in Section 5, followed by the assumptions and limitations associated with the algorithm in Section 6. Finally, Section 7 lists the references cited.

1.1. Purpose of This Document

This Algorithm Theoretical Basis Document (ATBD) explains the physical and mathematical background for an algorithm to derive LST product as part of the requirements for the Advanced Baseline Imager (ABI). ABI is the primary visible and infrared instrument to be flown onboard the platform of the Geostationary Environmental Operational Satellite (GOES) R series (GOES-R) of NOAA meteorological satellites. This document provides an overview of the required input data, the physical and mathematical backgrounds of the described algorithm and its predicted performance, sensitivity study of the algorithm, practical considerations, and assumptions and limitations.

1.2. Who Should Use This Document

The intended users of this document are those interested in understanding the physical bases of the LST algorithm and how to use the output of this algorithm for a particular application. This document also provides information useful to anyone maintaining or modifying the original algorithm.

1.3. Inside Each Section

This document covers the theoretical basis for the derivation of the LST product from ABI data. It is broken down into the following main sections:

- **System Overview**: provides objectives of the LST algorithm, relevant details of the ABI instrument, and a brief description of the product requirements.
- **Algorithm Description**: provides all the detailed description of the algorithm including its physical basis, its input and its output.
- **Assumptions and Limitations**: provides an overview of the current limitations of the algorithm and gives the plan for overcoming these limitations with further algorithm development.

1.4. Related Documents

This document may contain information from other GOES-R documents listed in the website provided by GOES-R algorithm working group (AWG):
http://www.orbit2.nesdis.noaa.gov/star/goesr/index.php.

In particular, readers are directed to read the following documents for a good understanding of this ATBD:

GOES-R Series Ground Segment Functional and Performance Specification
GOES-R Series Mission Requirements Document
GOES-R Land Surface Team Critical Design Review
GOES-R Algorithm Theoretical Base Document for ABI Cloud Mask

Other related references are listed in the Reference Section.

1.5. Revision History

Version 0.1 of this document was created by Dr. Yunyue Yu of NOAA/NESDIS, and its intent was to accompany the delivery of the version 0.5 algorithm to the GOES-R AWG Algorithm Integration Team (AIT)**.** The document was then revised following the document guideline provided by the GOES-R Algorithm Application Group (AWG) before the version 1.0 delivery. In 2009 spring and summer, version 2.0 of the document was prepared, which includes some new results conducted from the algorithm Critical Design Review (CDR) and the Test Readiness Review (TRR), as the algorithm 80% readiness document. In 2009 September for version 2.0, modification has been made reflecting the responses to AIT and IV&V reviewer's comments. It also includes testing results from using MODIS data. In this 3.0 version, responses to all the review comments from the AIT, the ADEB, and the Harris are addressed. And, some further development on the algorithm evaluation and testing, quality control flags and metadata definition are included in section 4.

2 OBSERVING SYSTEM OVERVIEW

This section describes objectives of the LST algorithm, details of the ABI instrument, and the product requirements.

2.1 Products Generated

Land surface temperature, a key indicator of the Earth surface energy budget, is widely required in applications of hydrology, meteorology and climatology. It is of fundamental importance to the net radiation budget at the Earth's surface and to monitoring the state of crops and vegetation, as well as an important indicator of both the greenhouse effect and the energy flux between the atmosphere and ground (Norman & Becker, 1995; Li & Becker, 1993; Sellers *et al*., 1998). Satellite LST can be assimilated into climate and atmospheric and land surface models to estimate sensible heat flux and latent heat flux. It can also be applied for analyzing climate change due to its long-term archive from imagery data of geostationary and polar-orbiting satellites. In the United States of America, demands of satellite LST data are from a variety of government agencies including the National Oceanic and Atmospheric Administration (NOAA, Department of Agriculture (DOA), Environmental Protection Agency (EPA), Department of the Interior (DOI), Department of Defense (DOD), as well as from universities and research institutes.

Accuracy of the satellite LST measurement is limited by the atmospheric correction, the complexity of surface emission characteristics, and sensor performance. Among those, variation of surface emissivity is the biggest difficulty in the satellite LST measurement. In the GOES-R program, the LST accuracy requirement is 2.5 K for all the ABI scanning modes (i.e., full disk, CONUS, and mesoscale). A primary objective of the GOES-R LST development team is to provide a state-of-the-art LST algorithm that meets the GOES-R mission requirement. The LST product will be generated in three scanning coverage modes: Continental United States (CONUS), Full Disk (FD) and Mesoscale (M). Note that the LST products are available only for cloud clear and probably clear pixels; and are qualified for four conditions: daytime and nighttime, and dry and moist atmospheres. Specifications of the LST product such as resolution, accuracy and refresh rate are defined in the GOES-R mission requirement document (MRD), which will be described briefly in the next section.

By the time GOES-R is operational retrievals of LST will have been conducted for over forty years from a variety of polar-orbiting and geostationary satellites. For producing an LST climate data record from those programs, consistency of the LST products from different satellite mission is of importance. The GOES-R LST algorithm should have a good historical heritage for consistency among other satellite products.

Currently, surface emissivity variation is still the biggest impediment in satellite LST retrieval. The remote sensing community has been working for years to obtain a time series of accurate

global land surface emissivity maps (e.g., Borbas *et al.*, 2008; Seemann *et al.*, 2008). The GOES-R LST algorithm should potentially benefit from such improvement of emissivity measurement.

Finally, algorithm simplicity and robustness is also a concern in order to produce the LST product as often as every fifteen minutes which is the goal of ABI LST product refresh rate.

2.2 Instrument Characteristics

The ABI will be a mission critical payload on GOES-R, providing over 65% of all the mission data products currently defined. Similar to the current GOES imager, ABI will be used for a wide range of qualitative and quantitative weather, oceanographic, climate, and environmental applications. ABI will offer more spectral bands, higher spatial resolution, and faster imaging rate than the current GOES imager. Its spatial resolution will be nominally 2 km for the infrared bands and 0.5 km for the 0.64 μm visible band. While the instrument will allow a flexible scanning scenario, two basic modes are envisioned. One mode is that every 15 minutes ABI will scan the full disk (FD), and 3 scans of the continental United States (CONUS), plus a selectable 1000 km ×1000 km area every 30 seconds. The second mode is that the ABI can be programmed to scan the FD iteratively. The FD image can be acquired in approximately 5 minutes. The current GOES imager takes approximately 25 minutes for a FD; GOES-R will provide a fivefold increase in the coverage frequency (Schmit *et al.*, 2004, 2007).

ABI has 16 spectral bands; five are similar to the 0.6-, 4-, 11-, and 12-μm windows and the 6.5-μm water vapor band on the current GOES-8/-9/-10/-11 imagers (Menzel and Purdom, 1994; Ellrod *et al.*, 1998), and another is similar to the 13.3 μm on the GOES-12/-N/-O/-P imagers and the GOES-8/-P sounders (Hillger *et al.*, 2003; Schmit *et al.*, 2002). Additional bands on ABI are 0.47 μm for aerosol detection and visibility estimation; 0.865 μm for aerosol detection and estimation of vegetation index and health; 1.378 μm to detect very thin cirrus clouds; 1.6 μm for snow/cloud discrimination; 2.25 μm for aerosol and cloud particle size estimation, vegetation, cloud properties/screening, hot-spot detection, moisture determination, and snow detection; 7.0 and 7.34 μm for midtropospheric water vapor detection and tracking and upper-level sulfur dioxide (SO_2) detection; 8.5 μm for detection of volcanic dust clouds containing sulfuric acid aerosols and estimation of cloud phase; 9.6 μm for monitoring atmospheric total column ozone and upper-level dynamics (Steinbrecht *et al.*1998); and 10.35 μm for deriving low-level moisture and cloud particle size. Each of these bands is often used in conjunction with other bands in a multiple spectral approach for product generation. Figure 2.1 shows the spectral distribution of the ABI channels, compared to the current GOES (GOES-12) imager channels, while channel specification of the ABI is given in Table 2.1. The advanced design of ABI will provide users with twice the spatial resolution, five times the scan rate, and more than three times the number of spectral channels compared to the current GOES imager (Schmit *et al.*, 2007). These improvements will allow tomorrow's meteorologists and climatologists to significantly improve the accuracy of their products, both in forecasting and nowcasting.

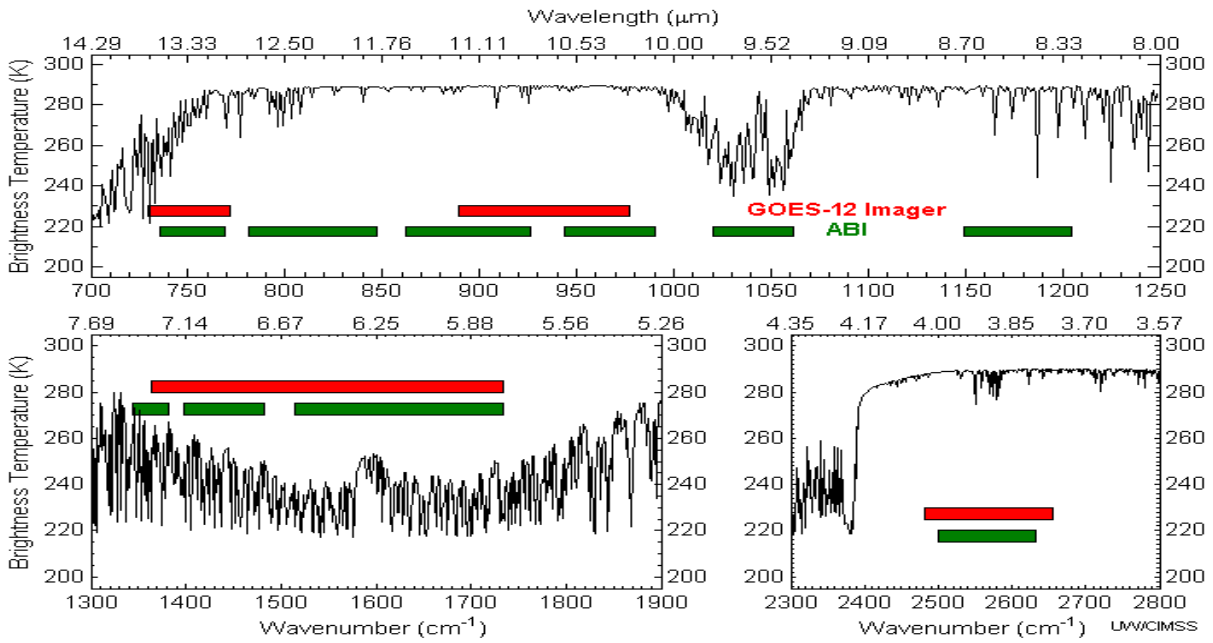

Figure 2.1. Spectral distribution of the ABI channels, compared to the current GOES (GOES-12) Imager channels.

Table 2.1. Spectral characters of Advanced Baseline Imager.

Channel Number	Wavelength (μm)	Bandwidth (μm)	NEDT/SNR	Upper Limit Of Dynamic Range	Spatial Resolution
1	0.47	0.45 – 0.49	300:1[1]	652 W/m^2/sr/μm	1 km
2	0.64	0.59 – 0.69	300:1[1]	515 W/m^2/sr/μm	0.5 km
3	0.86	0.8455 – 0.8845	300:1[1]	305 W/m^2/sr/μm	1 km
4	1.38	1.3705 – 1.3855	300:1[1]	114 W/m^2/sr/μm	2 km
5	1.61	1.58 – 1.64	300:1[1]	77 W/m^2/sr/μm	1 km
6	2.26	2.225 – 2.275	300:1[1]	24 W/m^2/sr/μm	2 km
7	3.9	3.8 – 4.0	0.1K[2]	400K	2 km
8	6.15	5.77 – 6.60	0.1K[2]	300K	2 km
9	7.0	6.75 – 7.15	0.1K[2]	300K	2 km
10	7.4	7.24 – 7.44	0.1K[2]	320K	2 km
11	8.5	8.30 – 8.70	0.1K[2]	330K	2 km
12	9.7	9.42 – 9.80	0.1K[2]	300K	2 km
13	10.35	10.10 – 10.60	0.1K[2]	330K	2 km
14	11.2	10.80 – 11.60	0.1K[2]	330K	2 km
15	12.3	11.80 – 12.80	0.1K[2]	330K	2 km
16	13.3	13.0 – 13.6	0.3K[2]	305K	2 km

[1]100% albedo, [2]300K scene. Shaded channels are used for LST retrieval.

The land surface temperature will be produced for each cloud free land pixel observed by the ABI sensor. The LST retrieval will rely on channels 14 and 15 of the ABI data using split window technique.

2.3 Mission Requirement

The LST requirements were originally defined in the mission requirement document (MRD), and further specified and updated in the Ground Segment Functional and Performance Specification (GS-F&PS). The requirements as of May, 2009 are listed in Table 2.2. In this document we further specify that the LST is the instantaneous temperature of the earth "skin" as viewed from the satellite position, given the particular sun-view geometry.

Table 2.2. GOES-R mission requirements for land surface temperature.

Observational Requirement	LEVEL[1]	Geographic Coverage[2]	Horiz. Res.	Mapping Accuracy	Msmnt. Range (K)	Msmnt. Accuracy[3] (K)	Msmmnt. Precision (K)	Refresh Rate	VAGL[4]	Long-term Stability	Extent Qualifier[5]
LST (Skin): CONUS	T	C	2 km	1 km	213 – 330	2.5	2.3	60 min	3236 sec	TBD	LZA <70
LST (Skin): Hemispheric	T	FD	10 km	5 km	213 – 330	2.5	2.3	60 min	806 sec	TBD	LZA <70
LST (Skin): Mesoscale	T	M	2 km	1 km	213 – 330	2.5	2.3	60 min	159 sec	TBD	LZA <70

[1] T=target, G=goal
[2] C=CONUS, FD=full disk, H=hemisphere, M=mesoscale
[3]The measurement accuracy 2.5K is conditional with 1) known emissivity, 2) known atmospheric correction and 3) 80% channel correction; 5 K otherwise.
[4] VAGL=Vender Allocated Ground Latency.
[5] LZA=local zenith angle.

2.4 Retrieval Strategies

First of all, the ABI cloud mask will be used for all cloud detection. LST retrieval in each scanning mode will be performed on each cloudless (i.e. "clear" and "probably clear" indicated by the cloud mask) land surface pixel, for day and night. A split window technique will be applied for correcting atmospheric absorption in the radiative transfer process of the satellite signal. A specific path correction technique will be applied for better atmospheric correction. Coefficients of the retrieval algorithm will be stratified for different atmospheric conditions. The land surface emissivity information will be applied explicitly in the algorithm and a dynamic climatological emissivity data source will be used for such purpose. Finally, the LST retrieval

quality will be indicated with a set of quality control flags which are either generated in the LST retrieval process or passed from the input data. The quality flags are assigned to each pixel.

3 ALGORITHM DESCRIPTION

A complete description of the algorithm at the current level of maturity (which will improve with each revision) is given in this section.

3.1 Algorithm Overview

The LST is one of the baseline products in the GOES-R ABI processing system. It is on the priority development list of the GOES-R algorithm working group (AWG). The LST algorithm is developed by the GOES-R AWG land team within the land module processing subsystem (Figure 3.1).

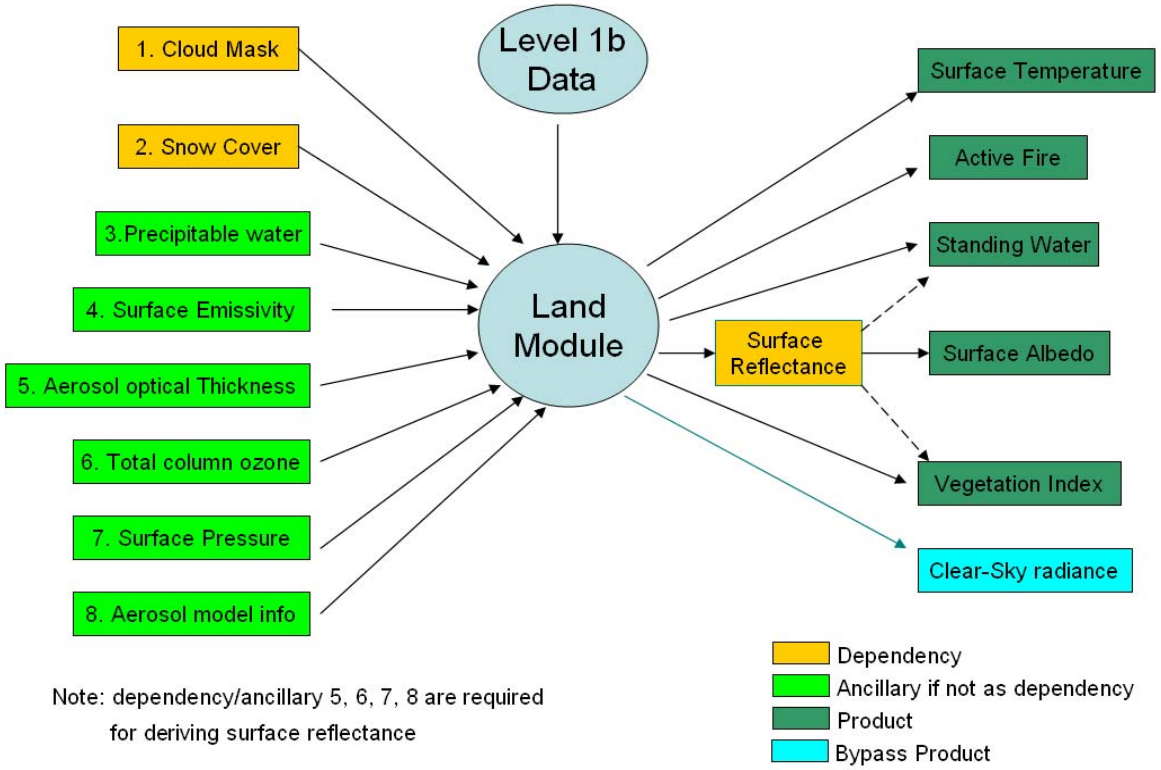

Figure 3.1. Products and dependencies of the land algorithm module. Note that 1) Surface reflectance may be derived as intermediate product in surface albedo derivation (if the MODIS-like algorithm is applied); 2) Aerosol optical thickness and surface albedo may be dependent on the aerosol algorithm and the albedo algorithm; 3) Surface reflectance may be required for deriving standing water and top-of-canopy vegetation index. In addition, the AWG cryospheric team requires the surface reflectance as dependency of its products.

The ABI LST product is based on a split-window technique that corrects for atmospheric absorption, and applies prescribed surface emissivity information. In addition, an atmospheric path length term is applied to further correct for satellite view zenith angle effect (Yu *et al.*,

2009a). Coefficients of the LST algorithm, which were derived using an atmospheric radiative transfer model (RTM), are stratified for daytime and nighttime conditions, as well as for dry and moist atmospheres. The algorithm is then verified using a RTM simulation dataset, and evaluated using proxy dataset and ground measurements.

3.2 Processing Outline

The processing outline of the LST is summarized in Figure 3.2. The LST retrieval for each pixel is started by extracting ABI sensor datasets including brightness temperatures, solar-target-sensor geometry, pixel geolocation and the sensor data quality control flags. Following that, the process extracts ancillary datasets which can be categorized as ABI and non-ABI related datasets. The ABI related ancillary datasets include the ABI cloud mask and snow/ice mask, which are level 2 ABI products and are listed as dependency in Figure 3.1. While a snow/ice mask is required, it may be supplied either as ABI derived ancillary data, if available, or as non-ABI derived ancillary data with more details in the following section. Currently the ABI snow/ice product is the fractional snow coverage; from which the snow/ice mask can be derived, though a threshold is to be determined for such a derivation. The ABI land team is working with other algorithm teams on it since the snow/ice mask is widely required. The non-ABI related datasets include the land/sea mask, the emissivity, and the NCEP water vapor (WV). Note that ABI Emissivity product has been developing since 2009; the LST required emissivity input maybe switched as ABI related ancillary data. Note also that ABI may provide WV product with higher spatial resolution than the NCEP WV does. Once quality of the ABI WV product is validated, it should replace the NCEP WV as the input. In addition, algorithm coefficients and some processing control values are read in this step. Detail information on input datasets will be provided shortly in Algorithm Input sub-section. Next, the ancillary datasets (land/sea mask, snow/ice, emissivity and NCEP WV) are mapped to the ABI pixel location, and land checking process is performed to label each pixel with land/sea, inland water, snow/ice properties. Such ancillary data check information will be recorded in quality control flags of the LST data. Then, the ABI sensor data is filtered using the cloud mask for ensuring that only the cloud clear and probably clear pixels are processed for the LST retrieval. Before calculating LST for each cloudless and land masked pixel, day/night time flag is determined from the solar zenith angle of the sensor geometric data; and dry/moist atmospheric condition flag is determined using the NCEP water vapor information. LST of the pixel is calculated accordingly with the daytime/nighttime and dry/moist flags since the algorithm coefficients are stratified for the conditions. LST will be calculated for snow/ice pixels but indicated in the quality control flags. Meanwhile, flags of large view angle and very cold surface will be indicated for such pixels. Finally, the calculated LST values and their associated quality control flags, which were generated in each of the above steps, are combined with the LST product package and are written to files for user access.

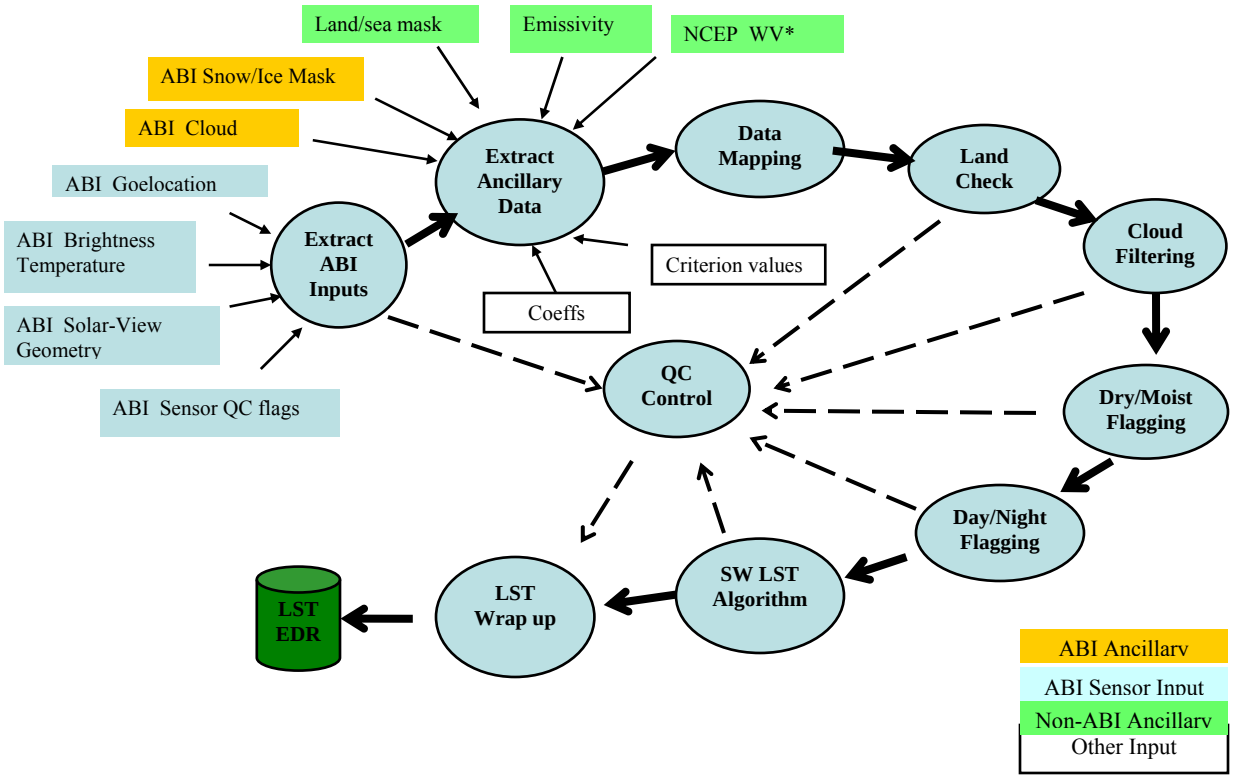

*The ABI WV data may replace the NCEP WV if its quality is verified.

Figure 3.2. High Level Flowchart of the LST production for illustrating the main processing steps.

3.3 Algorithm Input

This section describes the input needed to process the LST product. While the LST is derived for each pixel, ancillary datasets are required as well as the upstream ABI data.

3.3.1 Primary Sensor Data

The list below contains the primary sensor data used by the LST retrieval. By primary sensor data, we mean information that is derived solely from the ABI observations and geolocation information, or the level 1b data. Table 3.1 lists those input sensor data and their descriptions. All input data will be used at the high resolution level and the aggregation method for generating the hemispheric scale LST product at 10 km resolution will only be applied to the output product.

In the table, the channel brightness temperatures are used for LST calculation directly. Latitude and longitude information is needed for mapping the sensor data to ancillary data applied. Solar zenith angle is to determine day and night condition. The view zenith angle is used for atmospheric path correction. Details of the sensor data usage for LST derivation will be described shortly.

Table 3.1. Input list of primary sensor data.

Name	Type	Description	Dimension
Ch14 brightness temperature	input	Calibrated ABI level 1b brightness temperatures at channel 14	grid (xsize, ysize)
Ch15 brightness temperature	input	Calibrated ABI level 1b brightness temperatures at channel 15	grid (xsize, ysize)
Latitude	input	Pixel latitude	grid (xsize, ysize)
Longitude	input	Pixel longitude	grid (xsize, ysize)
Solar zenith	input	ABI solar zenith angles	grid (xsize, ysize)
View zenith	input	ABI view zenith angle	grid (xsize, ysize)
QC flags	input	ABI quality control flags with level 1b data	grid (xsize, ysize)

3.3.2 Derived Sensor Data

There are two ABI derived sensor data sets (or the ABI related ancillary dataset quoted earlier) used by the LST retrieval: 1) the ABI cloud mask (ACM) product, which indicates four cloudiness conditions for each pixel: clear, probably clear, probably cloudy, and cloudy, and 2) snow/ice mask which indicates if the pixel is snow or ice covered. Currently, snow cover is an ABI level-2 product measured as a fraction of snow cover (FSC) with a refresh rate of 60 minutes and ice cover is another ABI level-2 product with a refresh rate of every 180 minutes; and it is expected that an intermediate snow/ice mask will be derived from these ABI level-2 products. Meanwhile we suggest applying a threshold of FSC >50 for generating a snow mask intermediate product. Table 3.2 briefly describes input of the derived sensor data.

Table 3.2. Input list of derived sensor data.

Name	Type	Description	Dimension
Cloud mask	input	ABI level 1cloud mask data	grid (xsize, ysize)
Snow/Ice mask	input	ABI level 2 Snow/Ice mask data	grid (xsize, ysize)
Total Precipitable Water	input	ABI baseline TPW	grid (xsize, ysize)
Land Surface Emissivity	input	ABI level 2 land surface emissivity	grid (xsize, ysize)

The GOES-R AWG sounding team has developed the algorithm to generate the TPW as one of the baseline products, covering CONUS, full disk and mesoscale, with a horizontal resolution of 10 km and accuracy at 1 mm and precision at 3 mm. This product offers better quality, higher spatial and temporal resolutions than the current NCEP forecast data. It is our intention to use the ABI TPW as the LST algorithm input upon availability and further test for meeting the LST requirement. Land surface emissivity is an option-2 ABI product retrieved using time continuity. Currently, it is developed for CONUS only, with a spatial resolution of 10 km and a precision of

0.06 refreshed every 6 hours. Again this product would be the preferred input to LST algorithm because of the higher spatial, temporal resolutions and better quality in comparison to the monthly mean emissivity retrieval. Prior to further test and assessment of the ABI TPW and surface emissivity, the NCEP TPW and the emissivity retrieved from MODIS data have been used for algorithm development and validation. More detailed information is given in the following section of ancillary data.

In case the ABI snow/ice mask is not available at the GOES-R operational, the Interactive multi-sensor snow and ice Mapping System (IMS) will be used for the snow/ice mask.

3.3.3 Ancillary Data

The following table lists and briefly describes the ancillary data required to run the LST. By ancillary data, we mean data that requires information not included in the ABI observations or geolocation data.

Table 3.3 Input of ancillary data.

Name	Type	Description	Dimension
Land/sea mask	input	A land-ocean mask	grid (xsize, ysize)
Water vapor*	input	NCEP water vapor 6-hour forecast data	0.25 deg resolution
Emissivity*	input	MODIS monthly emissivity	0.05 deg resolution
IMS snow/ice mask*	input	Interactive multi-sensor snow and ice Mapping System	0.05 deg resolution

* Alternative input data in case the corresponding ABI product is not available at the GOES-R operation.

- **Land/Sea mask**

  The 1 km resolution land/sea mask will be used for GOES-R ABI products. It is created by SSEC/CIMSS based on NASA MODIS collection 5. Several categories are available in the land/sea mask, including shallow, moderate and deep oceans, land, shoreline, shallow, ephemeral, and deep inland water. LST will be calculated for all land and inland water pixels.

- **Water vapor**

  The water vapor information is extracted from the NCEP analysis and model forecast data. The Aviation model (AVN) provides global forecast every six hours and files in grib format can be downloaded through FTP. Currently we are using the 1° global coverage file, which may be replaced by higher resolution coverage at 0.25° in the future. An index file is available to point each ABI pixel to the corresponding TPW grid in the grib file.

- **Emissivity**

The Global Infrared Land Surface Emissivity is downloaded from the UW-Madison Baseline Fit Emissivity Database (http://cimss.ssec.wisc.edu/iremis/). This global database of infrared land surface emissivity is derived using input from the Moderate Resolution Imaging Spectroradiometer (MODIS) operational land surface emissivity product (MOD11). The baseline fit method (Seemann et al., 2007), based on a conceptual model developed from laboratory measurements of surface emissivity, is applied to fill in the spectral gaps between the six emissivity wavelengths available in MOD11. Emissivity in the baseline fit database is available globally at ten wavelengths (3.6, 4.3, 5.0, 5.8, 7.6, 8.3, 9.3, 10.8, 12.1, and 14.3 microns) with 0.05 degree spatial resolution. Corresponding emissivity values will be extracted and mapped into the ABI full disk area. They can then be applied to the LST algorithm to generate LST products.

- **Snow/Ice mask**

  The IMS snow and ice product is available daily for northern hemisphere. It incorporates a wide variety of satellite imagery (AVHRR, GOES, SSMI, etc.) as well as derived mapped products (USAF Snow/Ice Analysis, AMSU, AMSR-E, NCEP models, etc.) and surface observations. The product is presently used as an operational input into several NWS computer weather prediction models as well as several other governmental agencies. Currently it is available at about 4 km (6144x6144) grid from NSIDC with a slight delay. Near real-time gridded data is available in ASCII format by request (http://www.natice.noaa.gov/ims/).

Details on the derivation of ancillary data can be referred to in the relevant AIT document "Algorithm Interface and Ancillary Data Description Document (AIADDD)". It is worth noting that LST is generated for snow/ice pixels but indicated with QC flags. Therefore the requirement for snow/ice mask is limited for the QC flag control. It is also worth noting that current ABI snow/ice product is quantitative out to 55 degree of LZA and qualitative beyond that, while the LST is required to be out to70 degree. A quality flag is defined to indicate the LST is derived within 55° LZA, or alternative snow/ice mask will be used.

3.3.4 Algorithm Coefficients and Control values

In addition to the sensor data and the ancillary data, algorithm coefficients and some criterion values for algorithm selection and for quality control flags will be ingested as the input data. Table 3.4 lists the chosen LST algorithm coefficients for GOES-R ABI data, while Table 3.5 gives the QC flag criteria. Details of the algorithm selection will be given in the following section.

Table 3.4 LST Algorithm (algorithm 6 in Table 3.6) coefficients for GOES-R ABI. Unit of the input and output is deg K.

Sensor	Conditions	C	A_1	A_2	A_3	D
ABI	Day/Dry	45.257935	0.985361	1.332220	-41.750015	0.035390
	Day/Moist	52.651920	0.930713	2.408630	-35.962742	-0.219514
	Night/Dry	44.597870	0.989985	1.065721	-41.896751	0.083246
	Night/Moist	61.992481	0.892190	2.721928	-33.987152	-0.284960

Table 3.5 Criteria of the LST QC flags.

QC Flag Description	Criteria
Cloud mask	from ABI level-2 product, clear; probably clear; probably cloudy; cloudy
Day/Night flag	daytime (SolZen <= 85°); nighttime (SolZen >85°)
Water vapor flag	dry atmosphere (wv <= 2.0g/cm^2); moist atmosphere(wv>2.0g/cm^2); very moist(wv > 5.0g/cm^2)
Surface type flag	From ancillary data or ABI level-2 products: snow, ice, land, sea
Large viewing angle flag	large view angle (SatZen > 65°)
Other bad quality flag	cold surface(<250K & >=213K); out of range LST (213-330 K)
Emissivity flag	real time emissivity (ABI level-2 product); historical emissivity (MODIS monthly mean)

3.4 Theoretical Description

The ABI LST algorithm development is based on a scientific research conducted by Yu *et al.* (2008, 2009a). Theoretical details of the research are provided in this section.

3.4.1 Physics of the Problem

In clear sky condition, the top of atmosphere (TOA) radiance ($I(\nu)$), which will reach to the satellite sensor, can be described by

$$I(\nu) = I_s(\nu) + I_{atm}(\nu)^{\uparrow} + I_{atm}(\nu)^{\downarrow} \qquad (3.1)$$

where $I_s(\nu)$, $I_{atm}(\nu)^{\uparrow}$ and $I_{atm}(\nu)^{\downarrow}$ represent the radiance contributions from surface emission, atmospheric upwelling and reflected downwelling radiance, respectively; ν is spectrum of the sensing channel. The radiance components and their relationship are illustrated in Figure 3.3.

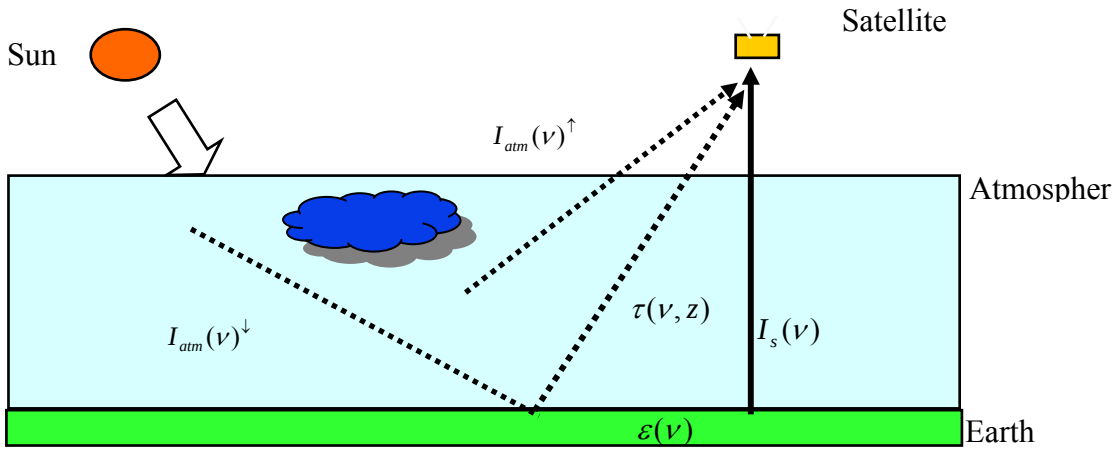

Figure 3.3. Radiation components reached to satellite sensor.

Satellite LST retrievals are usually performed in infrared (IR) bands where the surface emission reaches its maximum, yet atmospheric absorption is significantly small. In IR bands, each of the components in Eq(3.1) can be expressed mathematically by,

$$
\begin{aligned}
I_s(\nu) &= \varepsilon(\nu)\tau_0(\nu)B(\nu,T_s) \\
I_{atm}(\nu)^{\uparrow} &= \int_z^0 B(\nu,T_p(z))\frac{\partial\tau(\nu,z)}{\partial z}dz \\
I_{atm}(\nu)^{\downarrow} &= (1-\varepsilon(\nu))\tau_0(\nu)\int_0^z B(\nu,T_p(z))\frac{\partial\tau(\nu,z)}{\partial z}dz
\end{aligned}
\qquad (3.2)
$$

where ε is the surface emissivity, τ is the atmospheric transmittance (τ_0 is the atmospheric transmittance from surface to top of atmosphere), z is the height from surface, T_s is the surface temperature, $T_p(z)$ is the atmospheric temperature at height z and $B(\nu, T_s)$ is the Planck function. Eqs (3.1) and (3.2) are so-called the radiative transfer equations.

The purpose of the LST algorithm is to retrieve the land surface temperature T_s from the satellite sensor measured radiance I(ν). Physically, in this problem, the surface temperature is basically coupled with two other factors: the surface emissivity and the atmospheric absorptions. Developing an LST algorithm means to find a solution of decoupling the emissivity and the atmospheric absorption effects from the satellite received radiance.

3.4.2 Mathematical Description of the LST Algorithm

An analytic solution to equation (3.1) is not easy, because the integration of the terms requires good knowledge of the atmospheric profiles which is not available in real time. In addition, land surface emissivity is coupled with the surface emission and reflection terms in the equation, so the number of unknowns is always larger than the number of equations, even multiple channels of information are available. In the past thirty-five years, many approaches to the solution have been suggested (e.g., McMillin, 1975, Walton *et al.*, 1998), and widely used for producing the LST product (e.g., Prata, 1993 and 1994; Wan, 1999; Caselles *et al.*, 1997).

3.4.2.1 Candidate Algorithms

McMillin (1975) reported that the atmospheric absorption in thermal IR bands could be corrected using the signal differences between two adjacent channels. This "split window" (SW) technique has been successfully applied for sea surface temperature (SST) for more than 20 years. Its use for LST retrieval, however, is more challenging. First, compared to water, thermal IR (TIR) emissivity for most land surface types varies considerably from unity. This leads to significant errors in the linearization of the radiative transfer equation which forms the basis for the SW technique (McMillin and Crosby, 1984; Yu and Barton, 1994). Second, topographical and vegetation structural variability is complicated and satellite sensed brightness temperatures over a given target can differ significantly from pixel to pixel. Moreover, spatial heterogeneity over land is very large compared to oceans, and a retrieved LST represents a complex integration of the observed ensemble within a pixel. Finally, spatial and temporal variation of atmosphere over land is almost always greater than that over oceans.

For determining a GOES-R operational LST algorithm, we tried to simplify the above complexities by assuming that our prescribed surface emissivity values were sufficiently accurate and the angular and spatial variations described above were negligible. Note the GOES-R mission requirement document (MRD) and the GS-F&PS require use of emissivity values determined *a priori* (GOES-R Mission Requirement Document, 2007). Therefore, for the purposes of this document, we focused primarily on the atmospheric absorption correction issue. The SW technique is therefore a good choice since it is simple and robust for operational use, yet is sufficiently accurate to meet the mission's requirement.

We studied various SW LST algorithms from the literature (Price, 1984; Ulivieri and Cannizaro, 1985; Beck and Li, 1990; Prata and Platt, 1991; Vodal, 1991; Ulivieri *et al*., 1992; Sobrono *et al*., 1993; Sobrino *et al*., 1994;; Wan and Dozier, 1996; Caselles *et al*., 1997; Coll *et al*., 1997; Yu *et al.*, 2008), and adapted nine (Table 3.6) as candidate algorithms for the ABI. Each algorithm consists of a "base" SW algorithm plus a path length correction. The base algorithms were adapted from the literature and represent a variety of formulations in terms of using the thermal infrared brightness temperatures and surface emissivity values. The path length correction, which is the last term in each algorithm, was added for additional atmospheric correction (Sikorski *et al.*, 2002; Walton *et al*., 1998). Geometric analysis shows that the atmospheric path length at 60^o of the satellite zenith angle is about 2 times larger than that at the nadir. Yu *et al*. (2008) showed that, if an algorithm's coefficients are determined for typical column water vapor amounts, algorithm accuracy can degrade significantly at large view angles unless a corrective term is applied. Therefore, we used the term, $(T_{11}-T_{12})(\sec\theta-1)$, for path length correction. A detail description of this term is in Yu *et al.* (2008).

Table 3.6. Candidate split window LST algorithms. Each algorithm is composed of two parts: the base split window algorithm and path length correction (the last term in each algorithm). The base split window algorithms are adapted from those published split window algorithms as referred in the references, while the path length term is particularly added for additional atmospheric correction.

No	Formula[#]	Reference
1	$T_s = C + (A_1 + A_2 \frac{1-\varepsilon}{\varepsilon} + A_3 \frac{\Delta\varepsilon}{\varepsilon^2})(T_{11} + T_{12}) + (A_4 + A_5 \frac{1-\varepsilon}{\varepsilon} + A_6 \frac{\Delta\varepsilon}{\varepsilon^2})(T_{11} - T_{12}) + D(T_{11} - T_{12})(\sec\theta - 1)$	Wan & Dozier (1996); Becker & Li (1990).
2	$T_s = C + A_1 \frac{T_{11}}{\varepsilon} + A_2 \frac{T_{12}}{\varepsilon} + A_3 \frac{1-\varepsilon}{\varepsilon} + D(T_{11} - T_{12})(\sec\theta - 1)$	Prata & Platt (1991); modified by Caselles *et al.* (1997).
3	$T_s = C + A_1 T_{11} + A_2 (T_{11} - T_{12}) + A_3 (1 - \varepsilon_{11}) + A_4 \Delta\varepsilon + D(T_{11} - T_{12})(\sec\theta - 1)$	Coll & Valor (1997).
4	$T_s = C + A_1 T_{11} + A_2 (T_{11} - T_{12}) + A_3 \frac{1-\varepsilon}{\varepsilon} + A_4 \frac{\Delta\varepsilon}{\varepsilon^2} + D(T_{11} - T_{12})(\sec\theta - 1)$	Vidal (1991).
5	$T_s = C + A_1 T_{11} + A_2 (T_{11} - T_{12}) + A_3 (T_{11} - T_{12})\varepsilon_{11} + A_4 T_{12} \Delta\varepsilon + D(T_{11} - T_{12})(\sec\theta - 1)$	Price (1984).
6	$T_s = C + A_1 T_{11} + A_2 (T_{11} - T_{12}) + A_3 \varepsilon + D(T_{11} - T_{12})(\sec\theta - 1)$	Uliveri & Cannizzaro (1985).
7	$T_s = C + A_1 T_{11} + A_2 (T_{11} - T_{12}) + A_3 \varepsilon + A_4 \frac{\Delta\varepsilon}{\varepsilon} + D(T_{11} - T_{12})(\sec\theta - 1)$	Sobrino *et al.* (1994).
8	$T_s = C + A_1 T_{11} + A_2 (T_{11} - T_{12}) + A_3 (1 - \varepsilon) + A_4 \Delta\varepsilon + D(T_{11} - T_{12})(\sec\theta - 1)$	Ulivieri *et al.* (1992).
9	$T_s = C + A_1 T_{11} + A_2 (T_{11} - T_{12}) + A_3 (T_{11} - T_{12})(T_{11} - T_{12}) + A_4 (1 - \varepsilon_{11}) + A_5 \Delta\varepsilon + D(T_{11} - T_{12})(\sec\theta - 1)$	Sobrino *et al.* (1993).

[#]Note:
T_{11} and T_{12} represent the top-of-atmosphere brightness temperatures of ABI channels 14 and 15, respectively;
$\varepsilon=(\varepsilon_{11}+\varepsilon_{12})/2$ and $\Delta\varepsilon=(\varepsilon_{11}-\varepsilon_{12})$, where ε_{11} and ε_{12} are the spectral emissivity values of the land surface at ABI channels 14 and 15, respectively;
θ is the satellite view zenith angle.

As with most SW algorithms, our candidate algorithms explicitly use land surface emissivity values. This contrasts with algorithms such as Sun and Pinker (1993; 1994) and Sikorsky *et al.* (2002) where emissivity information is indirectly incorporated through the use of different coefficient sets determined for different land surface types. The latter approach must be tolerant to within-class emissivity variability which can be as significant as between-class variability. We prefer the algorithms of emissivity explicit since such algorithms allow easy incorporation of periodically updated land cover maps (e.g., annual maps from EOS/MODIS or seasonal from NPOESS/VIIRS), emissivity maps that accommodate within class variability (Yu *et al.*, 2005), maps that include directional variability (Yu *et al.*, 2006), or other related map improvements.

We expect that these and other emissivity map developments will be significantly improved by the launch of GOES-R in 2014.

3.4.2.2 Algorithm Selection

To select a suitable algorithm for the GOES-R ABI, we analyzed the accuracy and sensitivity of the candidate SW algorithms using a comprehensive simulation dataset. The accuracy of the best performing algorithm was further studied using ground LST data from the SURFace RADiation (SURFRAD) network data and corresponding GOES-8 satellite data. We discuss these two analysis approaches in sequence below.

3.4.2.2.1 Simulation Model and Processes

The MODTRAN atmospheric radiative transfer model (Berk *et al*., 2000) has been widely used in satellite remote sensing studies for over three decades. It is a moderate spectral resolution model, up to cm^{-1} in frequency. We used MODTRAN version 4, revision 2, released in 2000. The radiative transfer simulation procedure is illustrated in Figure 3.4.

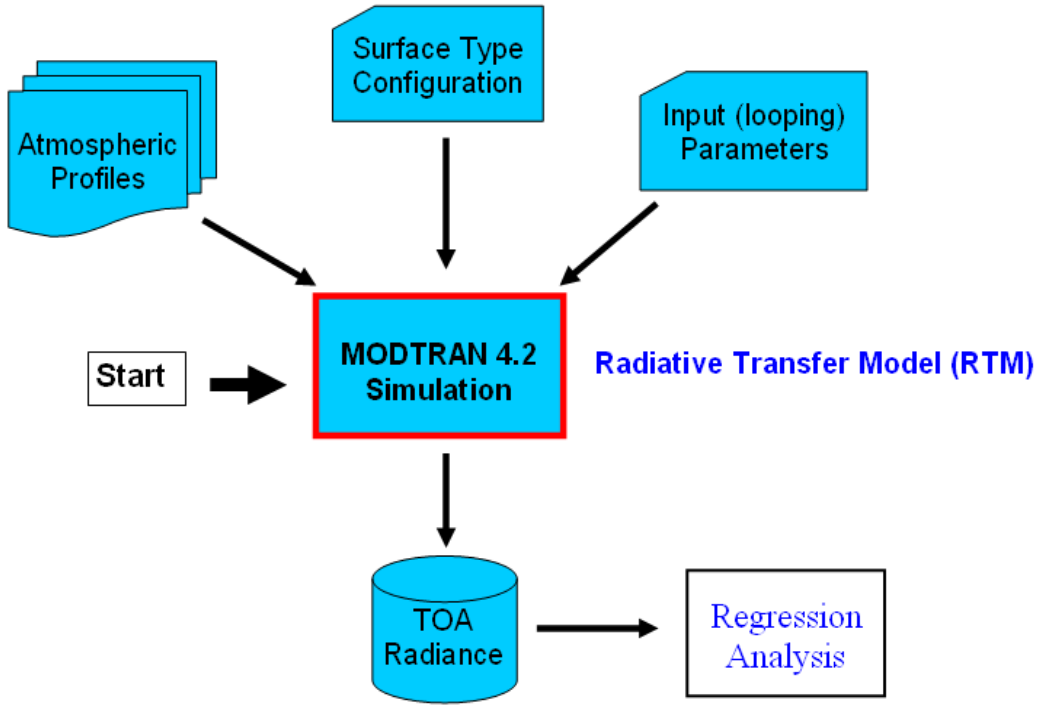

Figure 3.4. Radiative transfer simulation procedure.

We configured MODTRAN's atmosphere using 126 atmospheric profiles: 60 for daytime and 66 for nighttime; the nighttime is determined when solar zenith angle is larger than 85^0. The profiles were generated from cloud-free radiosonde data available from the CrIS F98-Weather Products Test Bed Data Package (NOAA88, Rev. 1.0). The profiles represented a variety of atmospheric conditions, spanning a column water vapor range from 0.2 to 7.5 g/cm^2 and a surface air

temperature range from 240 to 306 K. The profiles are fairly evenly distributed over the ranges as shown in Figure 3.5; they spanned a latitude range from 60º South to 70º North.

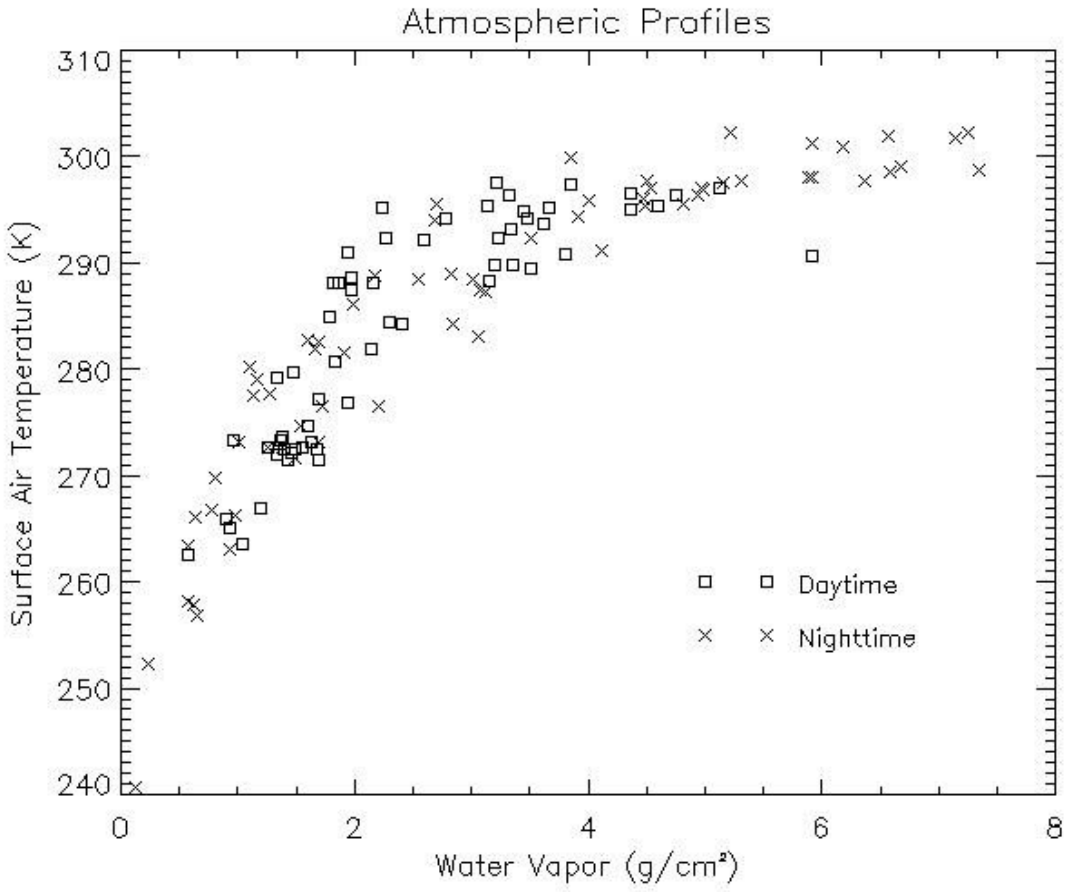

Figure 3.5. Distributions of total column water and surface air temperatures of the atmospheric profiles used in the simulation analyses.

To simulate a wide range of environmental conditions using a limited profiles set, we followed Yu *et al.* (2005) and varied the prescribed LST for each profile in a range as T_{air} *- 15 < LST <* T_{air} *+ 15 K*, where T_{air} is the surface air temperature of the profile, with a *1 K* increment. For each prescribed LST, we iterated the prescribed sensor view zenith angle from *0* to *70º*.

Twenty six emissivity values were assigned for each simulation configuration defined by the atmospheric profile, the prescribed LST, and the view zenith angle. The emissivity values were adapted from Snyder *et al.* (1998). We describe development of 78 virtual surface types from these data further below.

3.4.2.2.2 Regression Analyses

Upon simulating the top-of-atmosphere radiances, we then conducted regression analyses for the algorithm development. The regression procedure is illustrated in Figure 3.6.

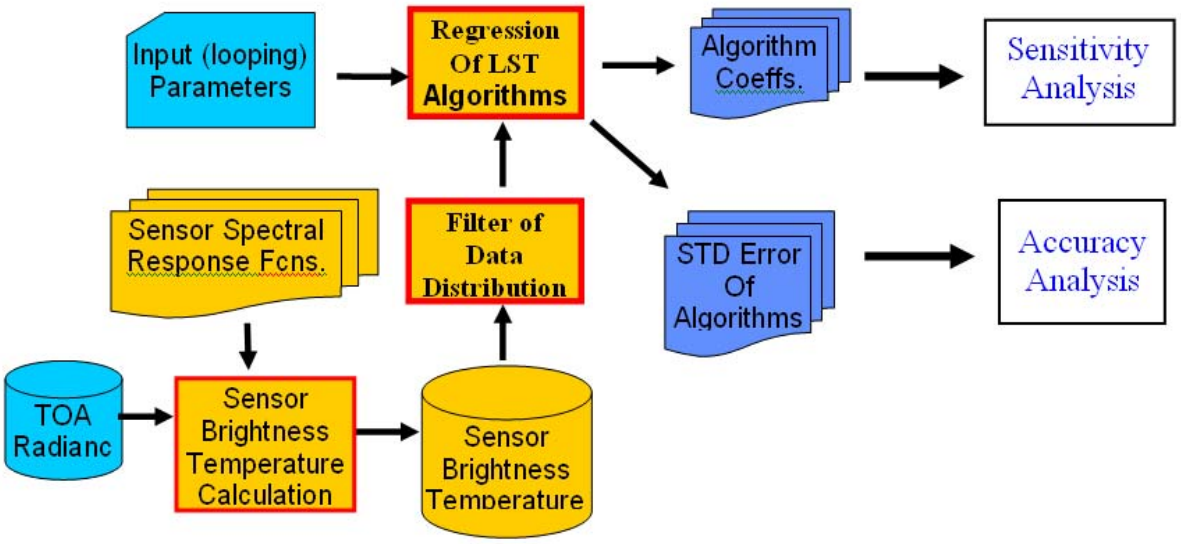

Figure 3.6. Procedure of the algorithm regression analyses.

We first determined the mean channel radiance by integrating over the sensor spectral response function (SRF). The channel radiances were converted into corresponding brightness temperatures using the Planck function. Because ABI is still in development, measured SRFs are not currently available. Instead, the GOES-R AWG has recommended a "Gaussian Boxcar Hybrid" function as SRFs of the ABI, for corresponding algorithm development uses. We expect that using modeled, rather than measured, SRFs will not significantly affect our results since Yu *et al.* (2008) demonstrated that the SW LST algorithms are not very sensitive to SRF variations in the thermal infrared channels.

After running the MODTRAN simulations with iterations of atmospheric profiles, the surface temperatures and the view zenith angles, we obtained 9840 daytime data pairs (where a "pair" represents the prescribed LST and the associated modeled brightness temperatures in ABI channels 14 and 15) and 10660 nighttime data pairs for each emissivity value.

Because water vapor is the most significant atmospheric absorber in the thermal bands, we stratified the simulation data according to the water vapor content: 1) "dry" atmosphere, where the total column water vapor is less than 2.0 g/cm^2, and 2) "moist" atmosphere, where the water vapor content is larger than 2.0 g/cm^2. Similar data stratification was used in the official MODIS LST algorithm (Wan and Dozier, 1996). The stratification acknowledges the capacity of warm atmospheres to hold more water vapor, as is shown in Figure 3.5, and the degradation of LST algorithm performance with increasing water vapor.

Due to significant differences in the discontinuity between LST and air temperature, during daytime and nighttime, many LST retrieval algorithms (or accompanying coefficient sets) were specified uniquely for daytime or nighttime use. We also performed regressions separately for the daytime and nighttime datasets. In addition, to better simulate real satellite data, we added Gaussian-distributed random noise to both the simulated brightness temperatures and the surface

emissivity values. The standard deviations of the sensor Noise Equivalent Delta Temperature (NEΔT) and the surface emissivity noise are 0.1 K and 0.005 (unitless), respectively. The NEΔT value is the design requirement for ABI in channels 14 and 15; the assumed emissivity noise standard deviation is 2.5 times the digitization error of the MODIS emissivity product, which is a candidate for the ABI LST derivation.

To prescribe a wider range of surface conditions, 78 "virtual" land surface types were developed. First, 26 spectral emissivity values at wavelengths around 11 μm and 12 μm were calculated from Snyder *et al*.'s emissivity classification data (1998). Of those, 14 represent the means of Snyder's 14 surface classes and the other 12 are those values combined with the estimated uncertainties. We then recombined the 11 μm and 12 μm emissivity values and constructed additional 52 "virtual surface types". Each virtual surface type was carefully assessed manually against the variability in Snyder's original samples to ensure that the virtual types were realistic and yet had adequate variation. Figure 3.7 shows emissivity distribution of the 78 virtual surface types at the ABI channels 14 (~11μm) and 15 (~12μm).

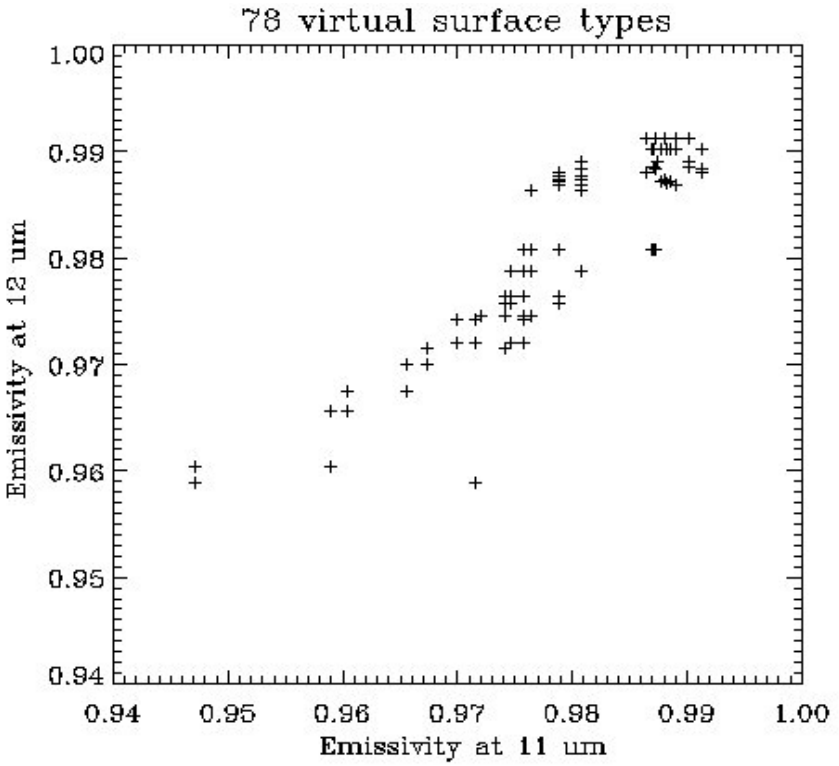

Figure 3.7. 78 virtual surface type emissivity values used in the algorithm regression analyses.

Before conducting regression analysis with the simulated data and candidate algorithms, we also considered the natural Gaussian-like distribution of land surface and surface air temperatures as noted in Justin *et al.* (NGST technical report, personal communication, 2006). That report used NCEP and ECMWF datasets for VIIRS LST algorithm analysis. We therefore applied a Gaussian function to filter the simulation data before running the algorithm regression process. Figure 3.8 shows the filtering results for the daytime dataset. A similar process was applied on the nighttime dataset.

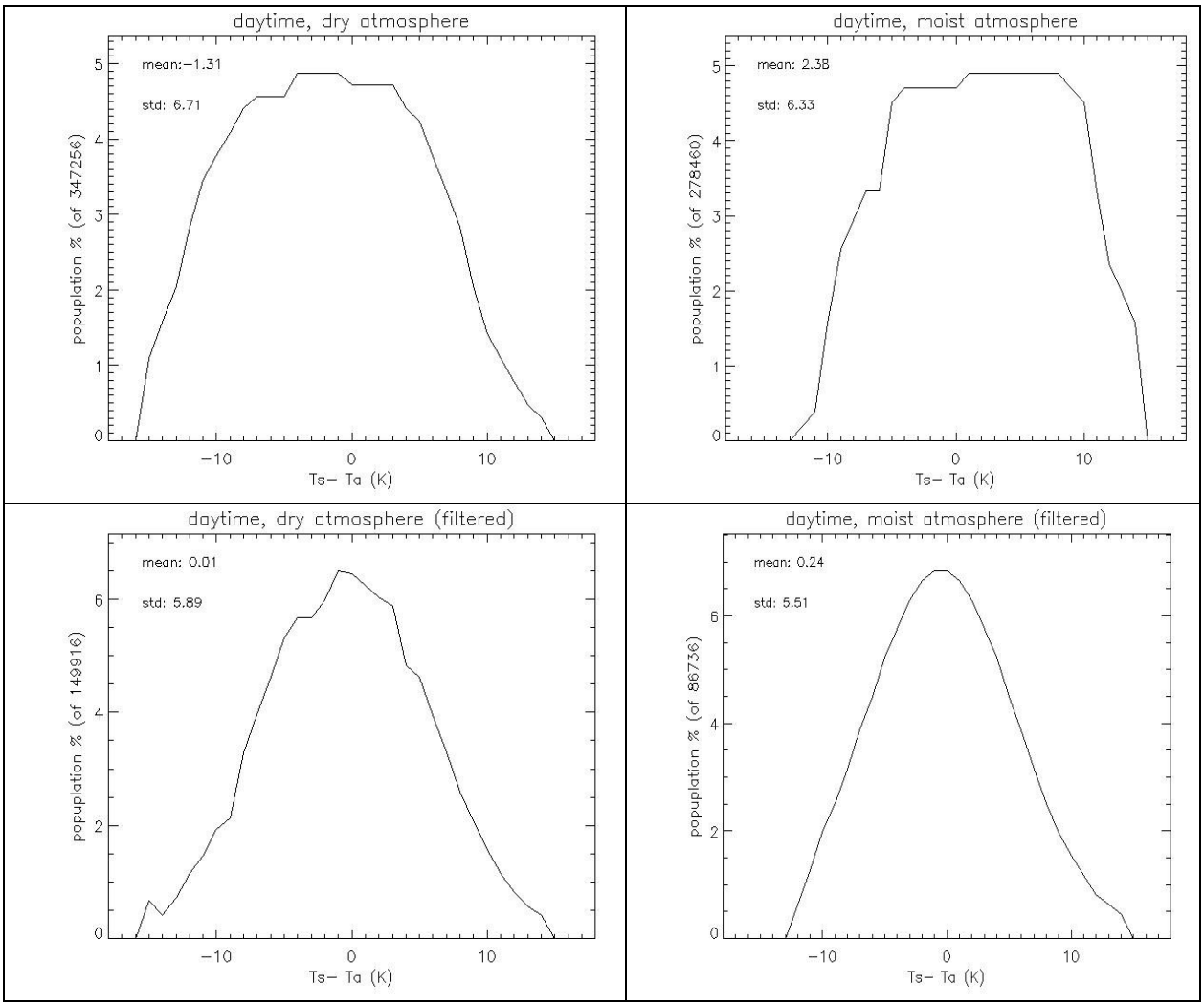

Figure 3.8. Daytime simulation data distribution in terms of the land surface and surface air temperature differences. The original simulation data (top panels) are pretty much evenly distributed in range of the temperature differences. The filtered data for both the dry (left) and moist (right) atmospheres are shown in the bottom panel.

3.4.2.2.3 Regression Results

For each of the 9 algorithms, we calculated the bias and standard deviation of the regressions. Figure 3.9 shows scatter plots of the regression results for the daytime dry atmosphere cases. It indicates that all algorithms perform well for an LST range from about 255 K to 305 K. The standard deviation (STD) of the differences between the prescribed LSTs and the retrieved LSTs ranged from 0.35 K (algorithms 1, 3, 4, 7, 8, 9) to 0.47 K (algorithms 2 and 5). Similar accuracy is observed for the moist atmosphere cases, where the STD ranged from 0.65 K (algorithm 9) to 0.75 K (algorithms 2, 6). For the nighttime cases, similar regression accuracies are observed. STDs of the algorithms under different atmospheric conditions are listed in Table 3.7.

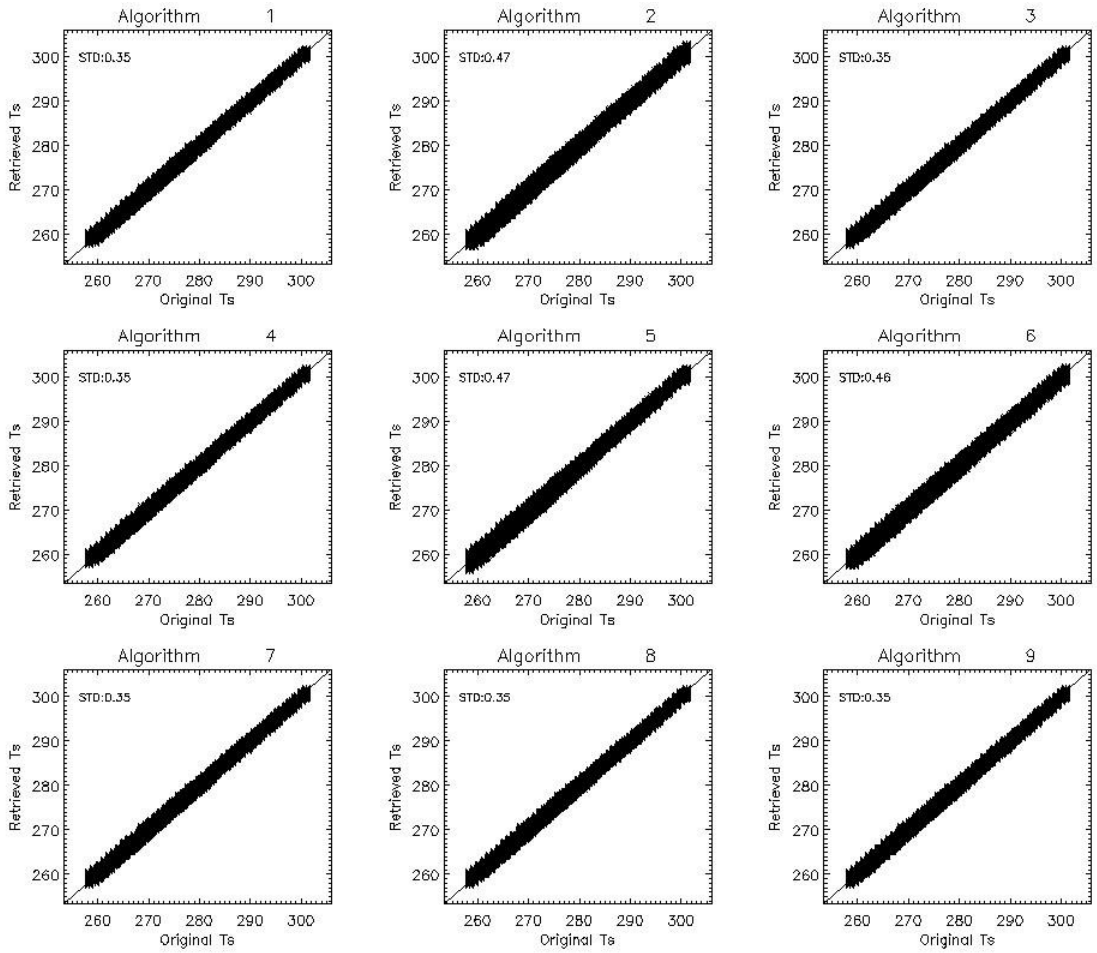

Figure 3.9. Scattergram plots of the regression results for the dry atmosphere. Standard deviation (STD) errors of the regression are given in each plot (Daytime).

Table 3.7. Standard deviation errors (K) of the Regression analysis.

No	Daytime		Nighttime	
	Dry	Moist	Dry	Moist
1	0.35	0.70	0.32	0.92
2	0.47	0.75	0.47	0.96
3	0.35	0.70	0.33	0.92
4	0.35	0.70	0.32	0.92
5	0.47	0.72	0.47	0.94
6	0.46	0.75	0.45	0.95
7	0.35	0.70	0.33	0.92
8	0.35	0.70	0.33	0.92
9	0.35	0.65	0.31	0.89

To have a closer look at error distributions, we produced histogram plots of the regression fits in Figures 3.10-3.11 and Figures 3.12-3.13 for daytime and nighttime results, respectively. Figures 3.10-3.13 reveal that there is no significant bias in any of the algorithms, and the error distributions are fairly symmetric (Gaussian-distribution-like) around zero. That means, all

algorithms performed well and the retrieval noise level (less than 1.0 K) is smaller than the GS-F&PS requirement. Note that since the regression bias is zero for all the algorithms, the STD equals the accuracy of the regression statistics. We therefore used the STD as the accuracy metric in the simulation analyses.

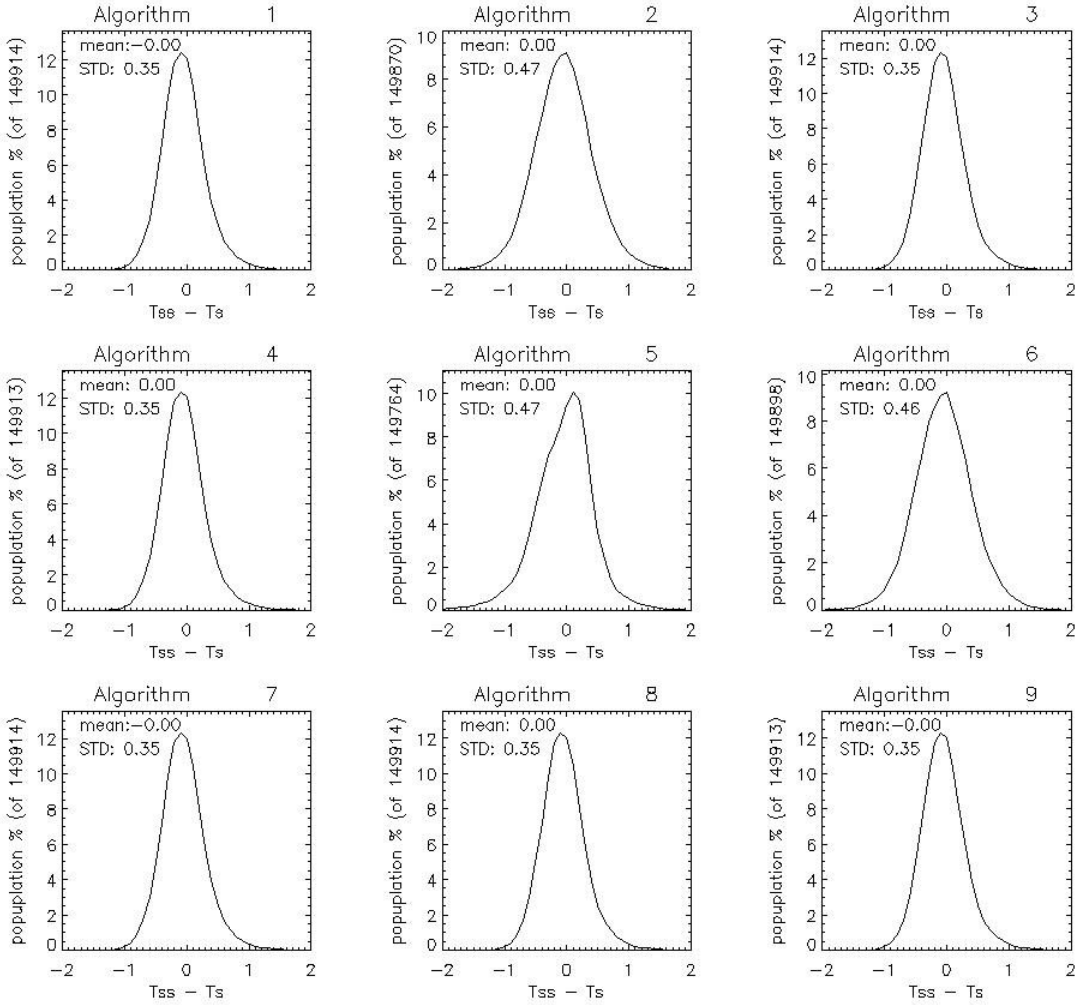

Figure 3.10. Histogram plots of the regression results for the dry atmosphere (Daytime). Standard deviation (STD) and mean errors of the regression are given in each plot.

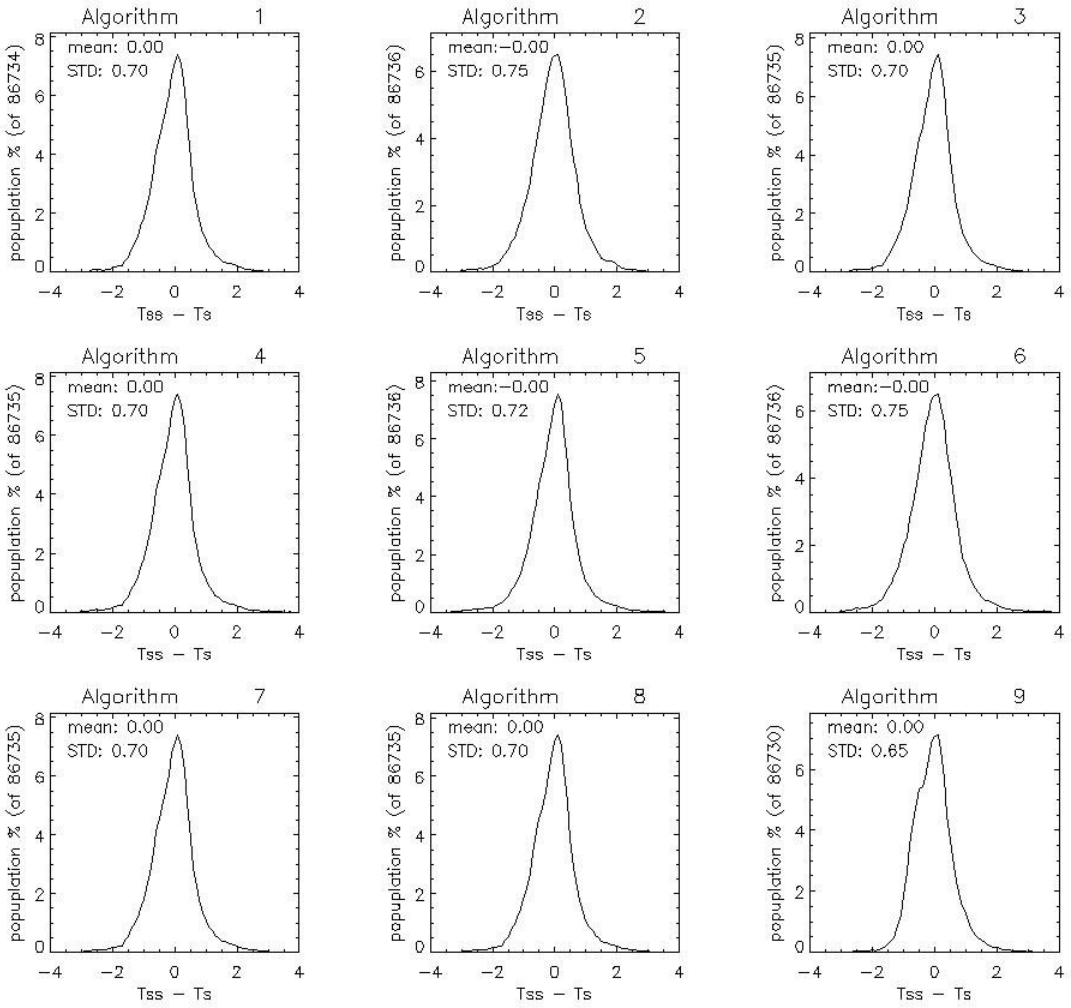

Figure 3.11. Histogram plots of the regression results for the moist atmosphere (Daytime). Standard deviation (STD) and mean errors of the regression are given in each plot.

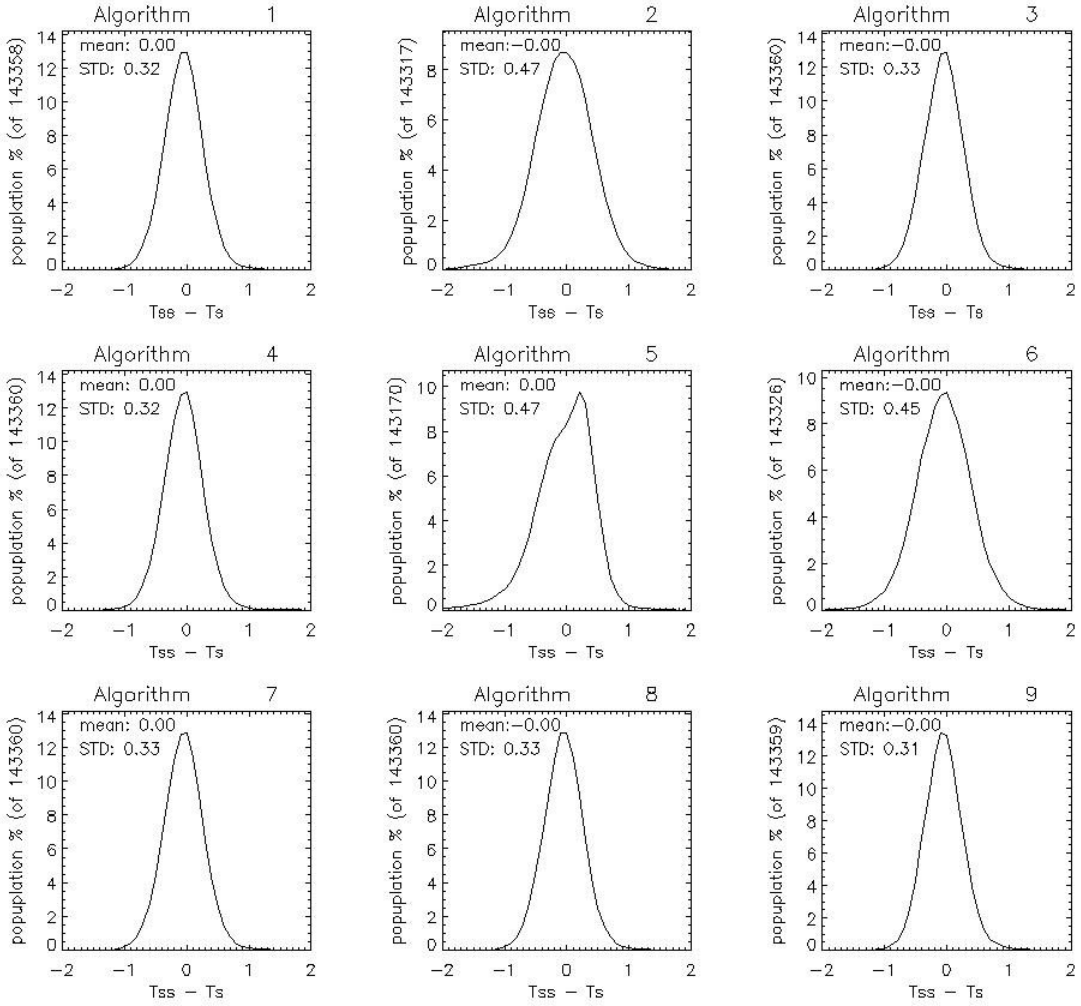

Figure 3.12. Histogram plots of the regression results for the dry atmosphere (Nighttime). Standard deviation (STD) and mean errors of the regression are given in each plot.

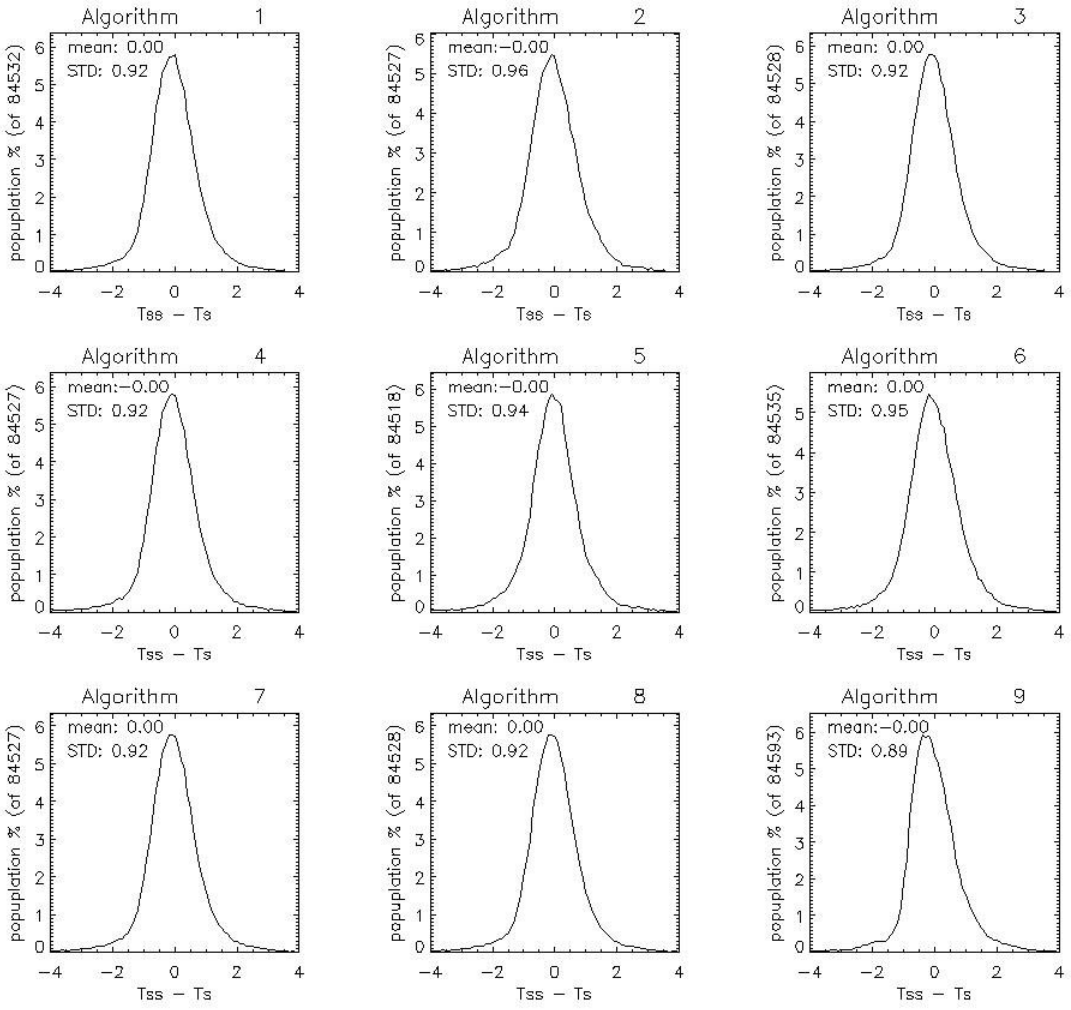

Figure 3.13. Histogram plots of the regression results for the moist atmosphere (Nighttime). Standard deviation (STD) and mean errors of the regression are given in each plot.

Compared to the daytime algorithm performance, the standard deviation of the nighttime for the moist atmosphere cases is slightly worse for each algorithm. This is because the nighttime atmospheric profiles used in the simulation process are moister than the daytime atmospheric profiles, as shown in Figure 3.5. For the dry atmosphere cases, the regression standard deviation of each algorithm is similar between the daytime and the nighttime.

3.4.2.3 Variation and Uncertainty Estimation

Two important error sources in LST retrieval are the surface emissivity uncertainty and the atmospheric water vapor absorption. We therefore analyzed the sensitivities of the candidate LST algorithms (Table 3.6) in terms of those two factors. The simulation dataset described above is used in the following estimations. The ABI LST retrieval algorithm will be determined from the results of the variation and uncertainty estimation.

3.4.2.3.1 Emissivity Uncertainty

Analytically, the maximum LST uncertainty δT_s due to the emissivity uncertainty can be described as,

$$\delta T_s = \sqrt{\delta T_1^{\,2} + \delta T_2^{\,2}} \tag{3.3}$$

where δT_1 and δT_2 represent the 11 and 12 micron band uncertainties resulting from the uncertainties of the mean emissivity (ε) and emissivity difference ($\Delta\varepsilon$), respectively. Using algorithm 7 (Table 3.6) as an example, these two components are

$$\delta T_1 = (A_3 - \frac{A_4}{\varepsilon^2})\delta\varepsilon \quad \text{and} \quad \delta T_2 = \frac{A_4}{\varepsilon}\delta(\Delta\varepsilon) \tag{3.4}$$

Therefore, the maximum LST uncertainty for algorithm 7 is

$$\delta T_s = \sqrt{((A_3 - \frac{A_4}{\varepsilon^2})\delta\varepsilon)^2 + (\frac{A_4}{\varepsilon}\delta(\Delta\varepsilon))^2} \tag{3.5}$$

Considering that $\varepsilon=(\varepsilon_{11}+\varepsilon_{12})/2$ and $\Delta\varepsilon=(\varepsilon_{11}-\varepsilon_{12})$, and assuming the emissivity uncertainties in each band are the same, i.e., $\delta\varepsilon=\delta\varepsilon_{11}=\delta\varepsilon_{12}$, the maximum uncertainty of the emissivity difference is $\delta(\Delta\varepsilon)=|\delta\varepsilon_{11}|+|\delta\varepsilon_{12}|=2\delta\varepsilon$. Thus, the LST uncertainty, δT_s, due to the emissivity uncertainty can be calculated using the above equation.

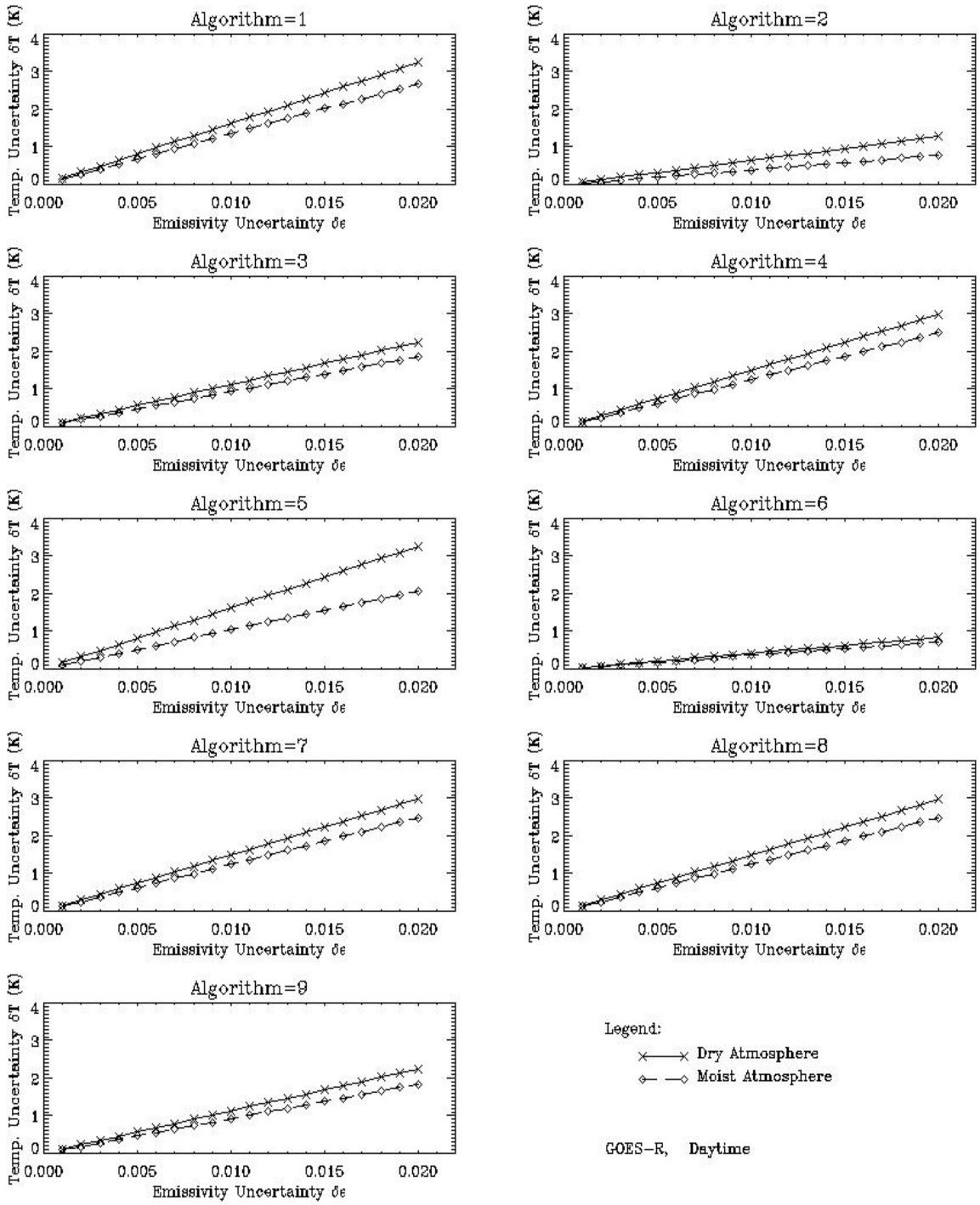

Figure 3.14. Uncertainty of the retrieved LSTs along with the surface emissivity uncertainty for daytime algorithm. In the plots, it is assumed that mean emissivity ε=0.97, the emissivity difference $\Delta\varepsilon$= 0.005 and the surface temperature is at about 298 K.

Emissivity sensitivities of the algorithms were estimated using equation (3.3), and are presented in Figure 3.14, for the daytime case. For illustration purpose, we assumed that 1) the mean emissivity (ε) and emissivity difference ($\Delta\varepsilon$) are 0.97 and 0.005, respectively, and 2) the brightness temperatures are 295 K and 294 K for channels 14 and 15 of the ABI sensor,

respectively. Results show that the LST uncertainty (δT) increases approximately linearly, and that uncertainty can be significant (up to 3 K) for fairly small uncertainty in emissivity. Thus, the algorithms are very sensitive to the emissivity error. Similar sensitivity results were observed for the nighttime cases, and therefore are not shown here. Note, however, that the predicted LST uncertainty calculated using equation (3.3) represents an extreme situation where all of the emissivity errors worsen the LST retrieval (i.e., the errors always compound rather than cancel each other). In practice, the final LST error may be significantly smaller, since emissivity errors at each channel may cancel each other and the temperature errors δT_1 and δT_2 may cancel each other.

In a relative sense, the sensitivity is lowest for algorithm 6, followed by algorithm 2. This is because, in algorithms 2 and 6, the emissivity difference ($\Delta\varepsilon$) is not used, and uncertainty of $\Delta\varepsilon$ can be double that of the mean emissivity. This implies that, to reduce the LST algorithm sensitivity to the emissivity error, the emissivity difference should not be included in the algorithm formulation. Note that emissivity sensitivity for the dry atmosphere is higher than that for the moist atmosphere since the LST algorithms for dry atmospheres are less affected by the atmospheric absorption and therefore are more accurate (Table 3.7).

3.4.2.3.2 Water Vapor Uncertainty

Stratifying our regressions by water vapor regime, we assume that water vapor content can be well estimated *a priori*. In practice, water vapor information is usually available from satellite soundings, ground radiosondes and/or operational numerical weather prediction model forecasts. Nevertheless, two errors may occur. First, the water vapor value may be mis-measured due to a variety of error sources. Second, due to spatial resolution differences between the ABI data and water vapor data, both “dry” and “moist” atmospheric conditions may occur within the unit spatial area over which the water vapor was estimated (which may contain from several to more than ten GOES-R pixels). Therefore, the coefficient set of the LST algorithm for dry atmospheres may be incorrectly applied in a moist atmospheric condition, and vice-verse. To test the sensitivity of the algorithms to this error, we applied the algorithm coefficient sets derived for moist atmospheres to dry atmospheric conditions; and vice-versa.

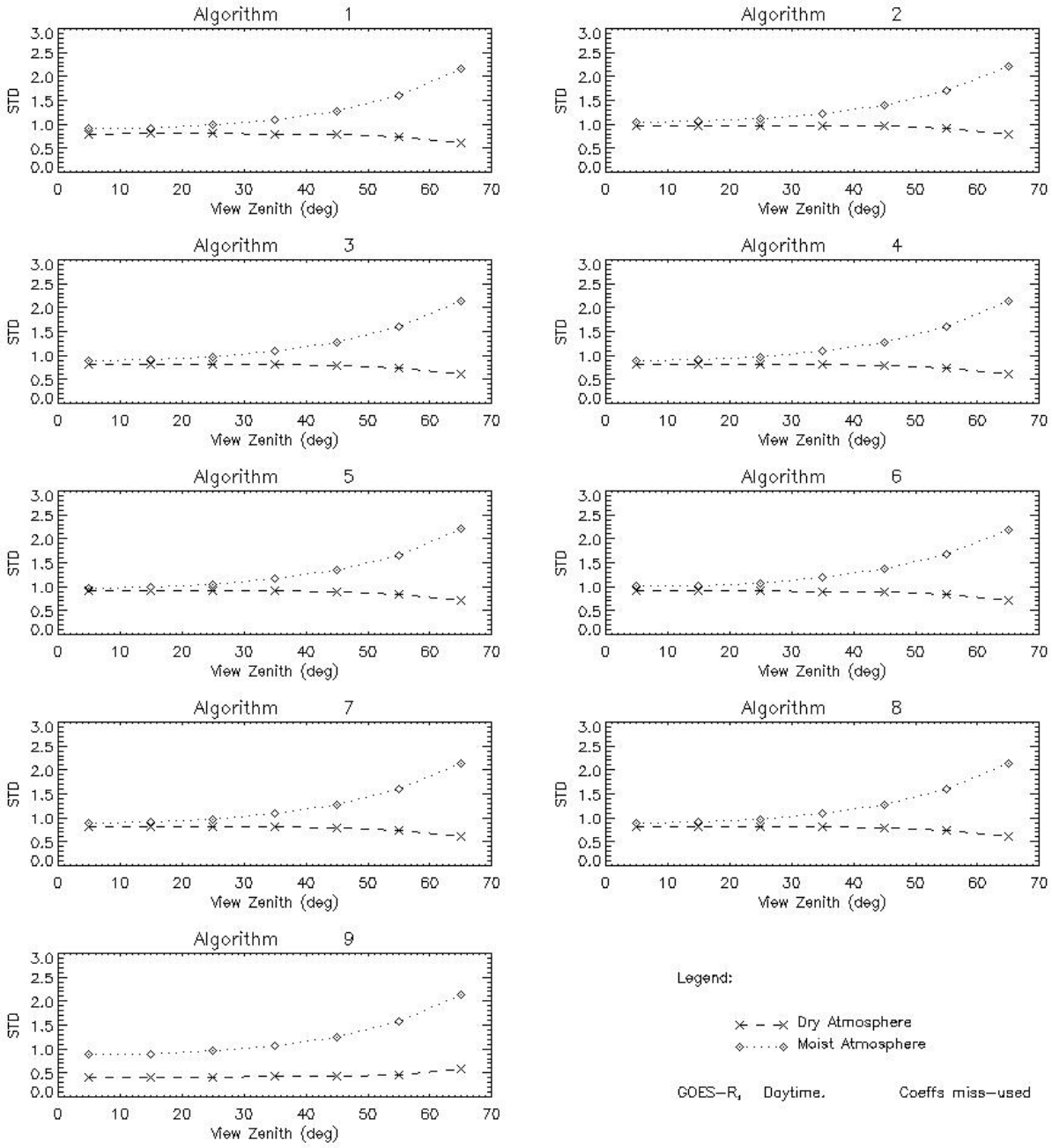

Figure 3.15. Standard deviation errors when algorithm coefficients are wrongly applied (daytime cases). The dash lines (marked as Dry Atmosphere) represent the errors when the coefficients derived for moist atmosphere are applied for the dry atmospheric LST retrieval, while the dot lines (marked as Moist Atmosphere) represent the errors when the coefficients derived for dry atmosphere are applied for the moist atmospheric LST retrieval.

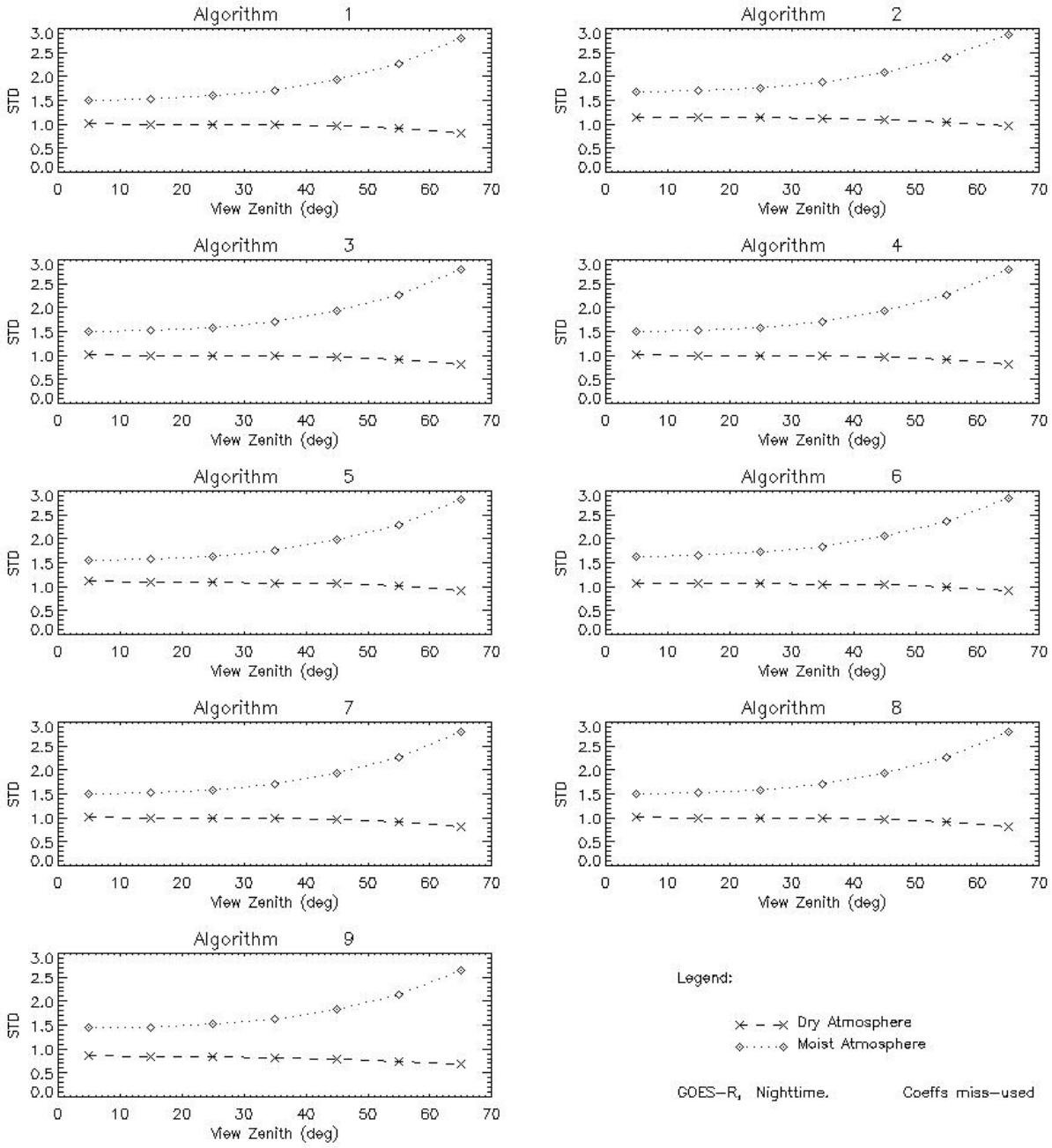

Figure 3.16. Same as Figure 3.15, except for the nighttime cases.

The water vapor sensitivity of the algorithms is illustrated for daytime and nighttime cases in Figures 3.15 and 3.16, respectively. In these cases, the STD is calculated separately in each 10-degree range of view zenith angles from 0 to 70 degrees. Note that, for all algorithms, the algorithm coefficients derived for dry atmospheric conditions are more sensitive if they are wrongly applied for the moist atmospheric conditions. This is particularly true for the nighttime cases since they are moister than the daytime cases. Further, for the moist atmospheric condition cases (the dot lines), such water vapor sensitivity increases when the satellite zenith angle increases. This is because the atmosphere is getting moister when the total column water vapor

along the view path increases with the increase of satellite zenith angle. For the dry atmospheric condition cases (the dash lines), the STD is significantly increased (comparing to the values in Table 3.7), but it does not increase with the view zenith angle. In fact, the STD of the LST errors decreased (and is approaching the values of the moist atmospheric cases in Table 3.7) when the zenith angle increases. This implies that even for the dry atmospheric conditions, the coefficient set for the moist atmospheric condition may be applicable when the satellite zenith angle is large.

3.4.2.3.3 Large Satellite View Angle

In addition, the GOES-R sensor view geometry may have significant impact on the variation of atmospheric absorption due to the radiative transfer path length increase from nadir to the edge of the scan. Considering that altitude of GOES-R satellite is about 36,000 km and the Earth radius is about 6700 km, the relationship between the satellite zenith angle (θ) and the satellite viewing angle (θ_v) is (Sun and Pinker, 2004)

$$\begin{aligned} \sin\theta &= \frac{Satellite\ \ Altitude\ +\ Earth\ \ Radius}{Earth\ \ Radius}\sin\theta_v \\ &\approx 6.37\sin\theta_v \end{aligned} \qquad (3.6)$$

Therefore, the maximum satellite viewing angle (about 8.7 degrees) corresponds to 74.48 degrees of view zenith angle. Such a large view zenith angle may have great impact on LST retrieval since, for instance, when the zenith angle is increased from 0 to 60 degrees, the atmospheric path length is doubled. We therefore assessed candidate algorithm sensitivity to the varying zenith angles using the simulation datasets.

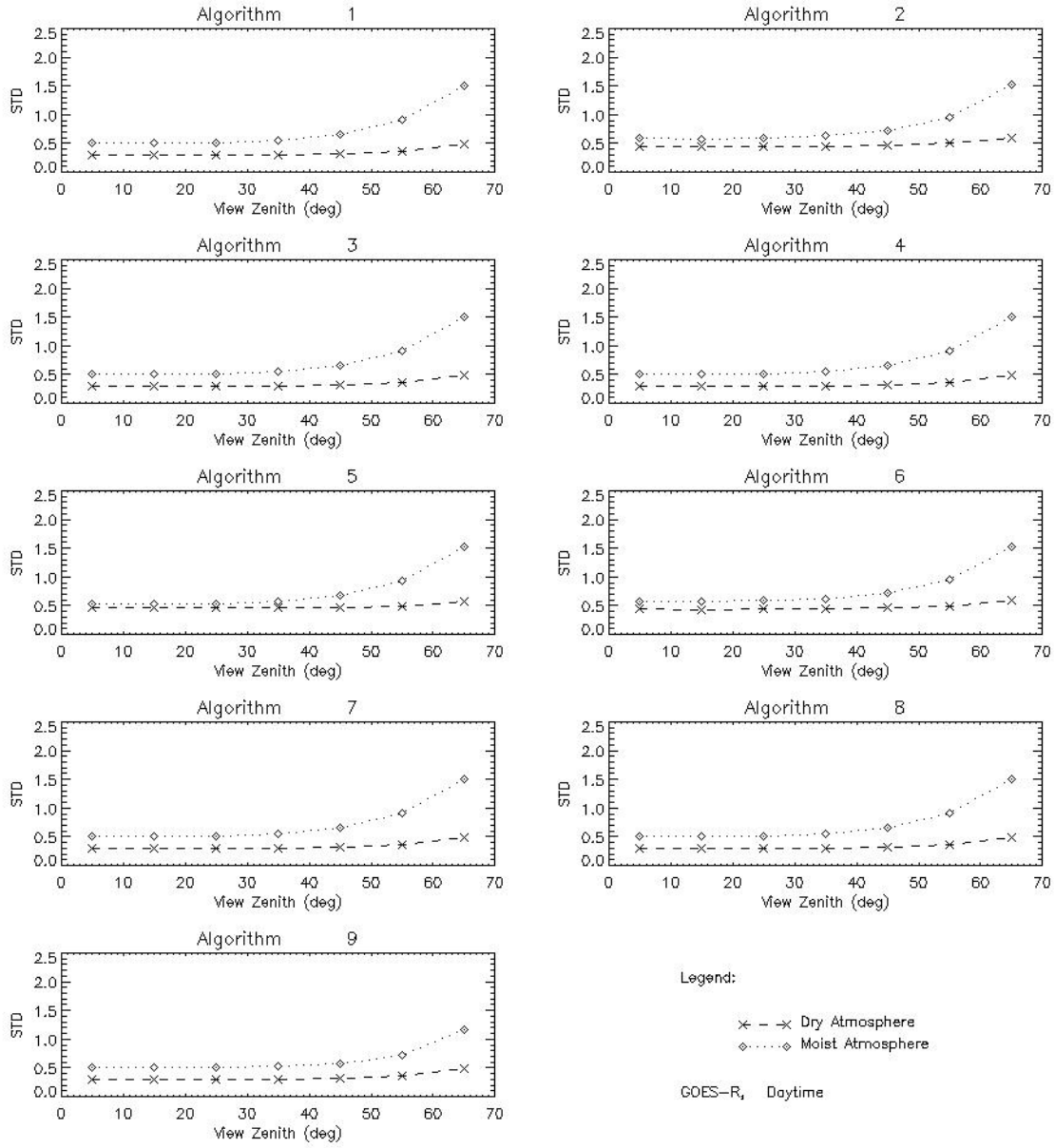

Figure 3.17. Daytime algorithm standard deviation errors in different satellite view zenith angles.

The algorithm STD error distributions with satellite zenith angle are shown for the daytime cases in Figure 3.17. It indicates that, for the moist atmospheric conditions, the STD error gets significantly worse when the zenith angle is larger than 45 degrees. For dry atmospheric conditions, the increase in STD is insignificant. Similar trends were observed for the nighttime cases (not shown).

Overall, similar water vapor sensitivity was found in all the algorithms, while algorithms 2 and 6 had significant smaller emissivity sensitivity than the other algorithms. Because simplicity is an advantage in operational procedures, algorithm 6 was chosen as the best candidate for further evaluation.

3.4.2.3.4 Summary of Algorithm Selection

We note that all algorithms listed in Table 3.6 give similar retrieval accuracy. This primarily indicates the accuracy limitation of the current SW technique. The accuracy difference between the moist and dry atmospheric conditions implies that water vapor contamination is a major concern for the GOES-R LST retrieval. The largest errors are expected with SW algorithms when the atmosphere is moist and the satellite zenith angle is larger than 45 degrees. Accuracy of the retrieval under dry atmospheric conditions is significantly better than that under moist atmospheric conditions. Similar results were observed in Yu *et al.* (2008).

Emissivity sensitivity is a more serious problem. This is because the emissivity effect is coupled with the atmospheric absorption effect in the radiative transfer process; while the atmospheric absorption effect is linearized in the SW technique, the emissivity effect cannot be similarly linearized. A trade-off in current SW applications occurs since emissivity information improves retrieval accuracy, but inaccurate emissivity information may induce significant error. It is worth pointing out that the same conflict also occurs in all the SW LST algorithms, e.g., the LST algorithm developed for the NPP VIIRS sensors (Sikorski *et al*., 2002), that stratify the algorithm coefficients for different land surface types instead of using the emissivity information explicitly in the algorithm. For such algorithms, the emissivity uncertainty of a certain surface type may also induce significant LST retrieval error.

Our results demonstrate that, although using both the mean emissivity and the emissivity difference of the two thermal channels provide the best retrieval accuracy, such algorithms are too sensitive to the emissivity uncertainty and should not be used in operational practice. As a compromise, we recommend algorithm 6, which only requires the mean emissivity information, as the selected algorithm for generating the GOES-R LST product.

Finally, we emphasize that all the results discussed to this point assume perfect cloud detection. That is, all these results are for truly cloud clear pixels. Residual cloud effects in pixels detected as clear will add significant noise to the LST retrievals.

3.4.3 Algorithm Output

There are three LST products generated corresponding three ABI scan modes. As for the CONUS and Mesoscale modes, full resolution (i.e. 2 km) LSTs are produced. Output of the full resolution LST products mainly contains two data arrays: the LST values and associated quality control flags, as are described in Table 3.8. To minimize storage request of the LST product, the LST value is stored in a short integer using the following scaling equation:

$$T_{int} = T_s \times scaling_{factor} - offset \qquad (3.7)$$

where T_{int} is the unsigned integer from the retrieved LST, T_s. The scaling_factor and offset values are 100 and 10000, respective. User is directed to the product metadata for the scaling information.

Table 3.8. Algorithm output data.

Name	Type	Description	Dimension

LST values	Short Integer	Retrieved land surface temperature value for each pixel of the scanning mode. Scaling factor is 100, offset is 10000, corresponding to Eq (3.7).	grid (xsize, ysize)
QC flags	Short Integer	Bit-based quality control flags for each pixel of the scanning mode: Land, cloudiness, sensor data quality, day/night, dry/moist, very moist, large view zenith, very cold surface, etc.	grid (xsize, ysize)

Another 2-byte short integer is used for the product quality control flags for each pixel, which may be comprised of a total of 16 bits holding the test results (yes/no) for each of the various tests and flags shown in Figure 3.2. The quality control flags are defined in Table 3.9.

Table 3.9. Quality control flags of the full resolution LST product.

Byte	Bit	Flag	Source	Effect
1	0	Empty		Reserved for future use
	1	QF*	LST	0=good, 1=bad
	2	Availability	SDR	00=normal, 01=out of space, 10=bad data, 11=missing data
	3			
	4	Surface Type	Land/sea Mask	00=land, 01=snow/ice, 10=in-land water, 11=sea
	5			
	6-7	Cloud Index	Cloud Mask	00=clear, 01=probably clear, 10=probably cloudy, 11=cloudy
2	0	Atmospheric Condition	LST	00=dry atmosphere (wv<=2.0g/cm^2); 01=moist atmosphere(wv>2.0g/cm^2); 10= very moist(wv>5.0/cm^2)
	1			
	2	Day/Night	SDR	0=day (solar zenith <= 85 deg), 1=night
	3	View Angle	LST	0=normal, 1=large view angle (LZA>55 deg)
	4	LST Quality	LST	00=normal, 01=cold surface (<250 K & >=213K), 10= out of range (213-330K)
	5			
	6	Emissivity Quality	LST	0=normal, 1=historical emissivity
	7	Empty		Reserved for future use

*The GOES-R AWG Algorithm integration Team (AIT) recommended that an overall quality flag (QF) is defined for simply indicating the data can be used (good) or not (bad). The "good" is defined when Availability is 00, and the Cloud Index is 00 or 01; otherwise, the QF value is "bad".

Note that the overall quality flag, QF, can be separated as a 1-byte flag for user convenience, which is recommended by the GOES-R AWG Algorithm Integration Team.

In producing the Full Disk LST product, LST value and the QC flags described above are produced first for each original pixel (which is in 2 km resolution); an aggregation process is then applied over 5 by 5 pixels for generating the 10 km resolution Full Disk LST product if all of the 5 by 5 pixels are cloud free. The aggregated LST is the mean of the 25 pixels. Quality control flags for the Full Disk LST product are similar to those for the CONUS and Mesoscale LST products, with a few redefinitions as shown in Table 3.10.

Table 3.10. Quality control flags of the Aggregated LST product.

Byte	Bit	Flag	Source	Effect
1	0	Empty		Reserved for future use
	1	QF*	LST	0=good, 1=bad
	2	Availability	SDR	00=normal, 01=out of space, 10=bad data, 11=missing data
	3			
	4	Surface Type*	Land/sea Mask	00=land, 01=snow/ice, 10=in-land water, 11=sea
	5			
	6-7	Cloud Index	Cloud Mask	00=clear, 01=probably clear, 10=probably cloudy, 11=cloudy
2	0	Atmospheric Condition*	LST	00=dry atmosphere (wv<=2.0g/cm^2); 01=moist atmosphere(wv>2.0g/cm^2); 10= very moist(wv>5.0/cm^2)
	1			
	2	Day/Night	SDR	0=day (solar zenith <= 85 deg), 1=night
	3	View Angle	LST	0=normal, 1=large view angle (LZA>55 deg)
	4	LST Quality*	LST	00=normal, 01=cold surface (<250 K & >=213K), 10= out of range (213-330K)
	5			
	6	Emissivity Quality	LST	0=normal, 1=historical emissivity
	7	Empty		Reserved for future use

*Redefined for the Full Disk LST product only.

In the table, the largest flag value of the 5 by 5 pixels is assigned as the flag of the aggregated pixel for these flags: QF, Availability, Cloud index, View angle, and Emissivity quality. The mixed pixel with Day and Night is flagged as Day.

As for the redefined flags, the mixed surface type (11) is for the pixel aggregated from land (00), snow/ice (01), and/or in-land water (10); the original sea flag is replaced. The mixed atmospheric condition (11) is defined as the mix of dry (00) and moist (01); one or more very moist pixels in the aggregation remain the very moist. For the LST quality, the aggregated pixel contains the normal and cold surface (or out of range) is flagged as cold (or out of range); or it is flagged as mixed if the cold surface and out of range occur in the containing pixels.

In addition to the pixel level LST values and quality control flags, metadata are needed in the LST product describing the common and LST specific information about the product. The GOES-R AWG and the Land Team recommend following metadata that (Table 3.11) should be included in generating the ABI LST products.

Table 3.11. Metadata defined for the LST product file.

METEDATA	TYPE	DEFINITOIN
DateTime	common	*Date and time of swath beginning and swath end*
Bounding Box	common	*Product resolution (nominal at nadir), number of rows and number of columns, byte per pixel, data type, byte order information, location of box relative to nadir (pixel space)*
Product Name	common	The ABI LST
Ancillary Data	common	*Ancillary data name used to produce the product: version*

		number, origin (where it was produced), name
Satellite	common	GOES-R
Instrument	common	Advanced Baseline Imager
Altitude	common	*Altitude of the satellit*e
Nadir	common	*Pixel in the fixed grid*
Position	common	*Latitude and longitude of the satellite positio*n
Projection	common	*Grid Projectio*n
Mode	common	*Type of Scan mode*
Version	common	*Product version number*
Compression	common	*Data compression type (method) used*
Location	common	*Location where the product is produced*
Contact	common	*Contact information of the producer/scientific supporter*
document	Common	*Citations to documents (i.e., ATBD*)
Product Unit	LST	Degree Kelvin
Scaling Factor	LST	100
Offset	LST	10000
Statistics	LST	*Mean, minimum, maximum, and standard deviation of all the available LSTs*
Good pixels	LST	*Percentage of good LST retrieval (in range 230-330K*)
Total Pixels	LST	*Total pixels LSTs are retrieved (cloudless land surface pixels*)

Note: the definitions in *italic* words are determined at running.

It is noted that LST values will not be calculated for the pixels indicated as cloudy or probably cloudy, bad/out of space/missing data, ocean. Inland water pixel is considered as land pixel and the LST will be calculated over it.

4 TEST DATASETS AND OUTPUTS

4.1 Simulated and Proxy Input Data Sets

The selected algorithm (6) must be verified using real satellite data, and be validated using ground measurement. Since ABI data was not available during the development phase, we used data from other satellite sensors as proxies: the Spinning Enhanced Visible and Infra-red Imager (SEVIRI) onboard the European Meteosat Second Generation (MSG) satellite, the Moderate Resolution Imaging Spectroradiometer (MODIS) on both the Terra and Aqua satellites, and the Imagers of U.S. Geostationary Operational Environmental Satellites (GOES) series 8. The data from these satellite sensors are considered as good proxies of ABI since they have TIR split window channels as the ABI does. Table 4.1 lists the sensor spectral specifications of the MSG/SEVIRI, GOES-8 Imager, as well as ABI.

Table 4.1. Similarity of SEVIRI, MODIS, and GOES-8 Imagers to ABI in channel spectrum.

Sensor	Channel No.	Wavelength Center (μm)	Bandwidth (μm)	Sensor Noise (NEΔT K)
ABI	14	11.2	10.8 ~ 11.6	0.10@300K
	15	12.3	11.8 ~ 12.8	0.10@300K
SEVIRI	10	10.8	9.8 ~ 11.8	0.13@300K
	11	12.0	11.0 ~13.0	0.21@300K
GOES-8	4	10.7	10.2 ~ 11.2	0.14@300K
	5	12.0	11.5 ~ 12.5	0.26@300K
MODIS-Terra	31	11.03	10.78 ~ 11.28	0.05@300K
	32	12.02	11.77 ~ 12.27	0.05@300K
MODIS-Aqua	31	11.03	10.78 ~ 11.28	0.05@300K
	32	12.02	11.77 ~ 12.27	0.05@300K

It is worth noting that algorithm coefficients applied for different proxy sensor inputs are different although the algorithm bears the same formulation throughout all the tests described in this section. This is because the central wavelengths and spectral response functions of the proxy split window channels are slightly different from those of GOES-R ABI window channels and from each other. Table 4.2 lists the algorithm coefficients for SEVERI, MODIS, GOES-8, respectively. To calculate the algorithm coefficients applicable to different proxy inputs, we used the same simulation dataset and regression procedure as we did with ABI window channels (Section 3.4.2.2), but used the corresponding central wavelengths and spectral response functions of the proxy split window channels in the simulation model. All following references in this section to "the algorithm" will refer to algorithm 6, since this is the selected and going to be tested.

Table 4.2. Algorithm coefficients for SEVERI, MODIS and GOES-8.

Sensor	Conditions	C	A_1	A_2	A_3	D
SEVIRI	Day/Dry	37.99915	1.010679	1.235773	-40.3856	0.408706
	Day/Moist	34.21294	1.006243	1.920798	-36.5879	0.215784
	Night/Dry	37.74266	1.010398	1.017359	-39.8323	0.467824
	Night/Moist	48.3898	0.951504	2.267945	-34.9662	0.259702
GOES-8	Day/Dry	35.02255	1.018212	1.263787	-39.3879	0.609744
	Day/Moist	27.91336	1.02632	1.990878	-35.7585	0.421895
	Night/Dry	36.160667	1.012895	1.02223	-38.9095	0.669541
	Night/Moist	45.10002	0.962238	2.444521	-34.5557	0.453345
MODIS-Terra	Day/Dry	30.83924	1.037948	1.668957	-40.6564	0.965683
	Day/Moist	22.85736	1.049361	2.986492	-37.0393	0.585346
	Night/Dry	35.27473	1.020291	1.220296	-39.9625	1.020330
	Night/Moist	45.96710	0.967989	3.749331	-36.6638	0.580914
MODIS-Aqua	Day/Dry	34.63325	1.024765	1.902572	-40.8006	0.739355
	Day/Moist	32.26877	1.023235	3.257209	-39.0953	0.562345
	Night/Dry	37.43817	1.013047	1.808079	-40.2709	0.546225
	Night/Moist	59.38677	0.918527	4.415647	-36.2407	0.491050

4.1.1 SEVIRI Data and Ground Observation Data

MSG SEVIRI provides 11 spectral channels with a spatial resolution of 3 km and a temporal resolution of 15 minutes. The MSG/SEVIRI full disk data have been collected every 30 minutes through a Man-computer Interactive Data Access System (McIDAS) at the University of Wisconsin Space Science and Engineering Center (SSEC) Data Center. They have been tested using the selected LST algorithm and compared with LST observed at available ground stations.

4.1.1.1 SEVIRI Data

A large amount of the MSG/SEVIRI full disk data were collected for the LST algorithm tests in the early development stage. The SEVIRI full-disk dataset provides all the necessary sensor inputs (Table 3.1) of the algorithm except for the ancillary data. The algorithm coefficients applied for SEVERI sensor inputs are listed in Table 4.2. The sensor spectral response functions used to calculate the algorithm coefficients were obtained from the EUMETSAT homepage (http://www.eumetsat.int/Home/Main/what_we_do/satellites/Meteosat_second_generation); emissivity values were obtained from the MODIS global emissivity database (Borbas *et al*., 2008; Seemann *et al*., 2008); and the water vapor data were obtained from 6-hour model forecasts for the National Centers for Environmental Prediction (NCEP). The SEVIRI LST values were then calculated using the algorithm.

Since the GOES-R cloud mask is not readily available or easily adaptable because of the input requirements, a preliminary snow and cloud classification procedure has been developed to filter out bad pixels in the SEVIRI images. The procedure for cloud detection for the MSG SEVIRI full disk data is shown below:

Night Time (SolarElevation ≤ 10)

T9<230 » general cloud

For water area:

T9 <290 or T4-T9 < -6

» cloud over night water

For land area:

T9 <275 or T4-T9 < -6

» cloud over night land

Day Time (SolarElevation >10)

T9<230 » general cloud

For water area:

T9 ≤ 272 or T4-T9 >15 » cloud over water

(T9 ≤ 295 & T9 >272 &

R1N>20 or R2>15 or T4-T9>15) » cloud over water

For land area:

T9 ≤ 265 or T4-T9 >20 » cloud over land

(265 <T9 ≤ 290 & NDVI ≤ 0.3 &

R1 > 50 or R2 >45 or T4-T9 >20) » cloud over land

Where T4 and T9 are the brightness temperatures of the SEVIRI sensor data at channels 4 (3.9μm) and 9 (10.8μm), respectively. R1 and R2 are the reflectance at visible and near infrared channels 1 (0.635μm) and 2 (0.81μm), R1N is the normalized visible reflectance to count for the bidirectional effect (with a solar zenith angle and satellite zenith angle as 50° and a relative azimuthal angle of 0°). NDVI is calculated by (R2-R1)/(R2+R1).

4.1.1.2 Cardington Data

The UK Met Office maintains a ground station at the Cardington Site in Bedfordshire, UK (52°06' N, 00°25' W). Two *Kipp & Zonen CG4* Pyrogeometers are used for measuring the incoming and outgoing longwave irradiance with a spectral range of 4.5 to about 40 μm and have a field of view of 180°, with a cosine response. The data held at the British Atmospheric Data Centre (BADC) are stored in ASCII format. We have downloaded its 1 minute measurement data through the restricted access: http://badc.nerc.ac.uk/browse/badc/ukmo-cardington. The observed upwelling ($F^{\uparrow}$) and downwelling ($F^{\downarrow}$) radiative fluxes are converted to temperature as follows:

$$F^{\uparrow} = \varepsilon\sigma T_s^4 + (1-\varepsilon) F^{\downarrow} \qquad (4.1)$$

where ε is the monthly mean surface emissivity extracted from the CIMSS baseline fit emissivity database for 11 & 12 μm and σ is the Stefan-Boltzman constant ($\sigma = 5.67051 \times 10^{-8}$ $Wm^{-2}k^{-4}$). Station LST is then calculated using the following equation:

$$Ts = \left[\frac{F^{\uparrow} - (1-\varepsilon)F^{\downarrow}}{\varepsilon\sigma} \right]^{\frac{1}{4}} \qquad (4.2)$$

4.1.1.3 Gobabeb Data

Supported by the Land Surface Analysis - Satellite Applications Facility (LSA-SAF), Karlsruhe Institute of Technology (KIT) of Germany operates four permanent validation stations for LST retrieved from TIR satellite measurements (Göttsche and Olesen, 2009; Olesen and Göttsche,

2009). Courtesy by Drs. Göttsche and Olesen, we have acquired the Gobabeb station observation data for 2008 and 2009. The Gobabeb tower is located at 23°33'S, 15°03'E, 408 m elevation. Two down-looking *Heitronics KT-15.85 IIP* radiometers measure the surface-leaving radiance (9.6-11.5μm) from the gravel plain with the fields of view (FOV) about 13 m^2 each. A third radiometer (*Kipp & Zonen CNR1*) at the 2 m level measures sky radiance, in terms of broad-band shortwave (SW) and longwave (LW) radiative fluxes. Validation station Time series of KT-15 brightness temperatures (2 x ground, 1 x sky) from Gobabeb. Brightness temperatures from the surface pointing radiometers are converted to radiances, which are then corrected for reflected downwelling radiance using the monthly mean surface emissivity extracted from the CIMSS baseline fit emissivity database for 11 μm and measured downwelling radiance. LST is then obtained from the corrected surface leaving radiances.

4.1.1.4 Le Bray Data

Atitar and Sobrino (2009) published their comparison results of SEVIRI LST with the *in situ* data through their one-day field campaign at the Le Bray station on July 27, 2007. Courtesy of Sobrino, we obtained the one day data and applied the *in situ* LST to the comparison with GOES-R LST algorithm products.

Le Bray is located at 44°42'00" N, 00°46'00" W, 60 m elevation, about 20 km SW of Bordeaux, France. The SEVIRI Viewing Angle at the station location is 51°. The two radiometers [*Raytek (R) and Everest (Ev)*] have been installed in a tower of 33-m altitude, in the forest zone of Le Bray. They are oriented at nadir with fields of view of 6° and 4°, respectively, with a single band of 8-14 micrometers. Surface temperature measurements are available every 5 minutes for the day of field campaign.

4.1.1.5 Match-up SEVIRI and Station Observation Data

The match-up of SEVIRI and station data for LST comparison was carried out on all cloud free pixels that are spatially and temporally close to both data sets. Since MSG SEVIRI data have a fixed lat/lon coordinates for the full disk image, it is easy to locate the nearest pixel according the ground station's lat/lon location. Then the one minute data for the 15^{th} and 45^{th} minute of the hour were used to compare with the corresponding satellite data. For the Gobabeb station data comparison, the pixel to the northeast of the tower location was actually used because it is more representative of the tower measurement surface and the surrounding homogenous gravel plain .

4.1.2 GOES-8 and SURFRAD Match-up Data

To evaluate the selected GOES-R LST algorithm in depth, we collected ground reference LST data estimated from the observations of six SURFRAD stations, and compared the satellite retrieved LST values. The proxy sensor inputs of the algorithm are from the GOES-8 Imager observations.

4.1.2.1 GOES-8 Data

The GOES-8 Imager dataset were prepared by the GOES-R AWG proxy team. It is 4-km in spatial resolution and 1-hour in temporal resolution. In this validation effort, we selected the Imager pixels that were spatially nearest to the SURFRAD locations. Available in this dataset are the hourly brightness temperature measurements from the five channels of GOES-8 and the associated illumination and viewing geometry. The thermal infrared channels of GOES-8 Imager

are listed in Table 4.1. In the time domain, we used only the SURFRAD values that were closest to the GOES-8 measurements. The maximum temporal difference between the SURFRAD and the satellite measurements was less than 2 minutes since the SURFRAD daily files provide measurements every 3 minutes. A whole year of 2001 was used in this comparative analysis.

4.1.2.2 SURFRAD Data

The SURFRAD network has been operational in the United States since 1995. It provides high quality *in situ* measurements of upwelling and downwelling radiation, along with other meteorological parameters such the atmospheric water vapor. A detailed description of the SURFRAD network and associated instrumentation can be found in Augustine *et al*. (2000; 2005). Table 4.3 gives brief information about the six SURFRAD stations related to this work. We used one year (2001) of SURFRAD data over the six stations. The year 2001 was chosen because GOES-8 data were still available for that year and GOES-8 had a split window instrument, unlike later satellites in the series. Surface type information for the sites, which were used to estimate the surface emissivity, was obtained from the University of Maryland (UMD) land classification dataset (Hansen and Reed, 2000). The algorithm coefficients applied to GOES-8 proxy inputs are listed in Table 4.2.

Table 4.3. Ground data collected from six SURFRAD Stations were used for the algorithm validation.

Site No.	Site Location	Lat(N)/Lon(W)	Surface Type*
1	Pennsylvania State University, PA	40.72/77.93	Mixed Forest
2	Bondville, IL	40.05/88.37	Crop Land
3	Goodwin Creek, MS	34.25/89.87	Deciduous Forest
4	Fort Peck, MT	48.31/105.10	Grass Land
5	Boulder, CO	40.13/105.24	Crop Land
6	Desert Rock, NV	36.63/116.02	Open Shrub Land

*IGBP surface types.

.

The SURFRAD ground LST values were calculated from upwelling and downwelling radiation measurements, in the spectral range from 3 μm to 50 μm, obtained by a precise infrared radiometer (PIR). The SURFRAD PIR is calibrated annually using a laboratory blackbody such that its measurement estimates the total energy emitted from a blackbody rather than the instrument limited spectrum (Augustine *et al*., 2000; 2005). Equation 4.1 and 4.2 are used for the ground LST calculation.

The emissivity in equation (4.2) was estimated by mapping the UMD surface type classification to the Snyder *et al*. land surface emissivity classification. The mapping method is described in (Yu *et al.*, 2005). Note that the mapped emissivities are spectral emissivity values at around 11 and 12 μm (the SW channels). We assumed that the mean emissivity of the channel emissivities is applicable to equation (4.2).

4.1.2.3 Cloud Filtering

As addressed in Section 2, the LST retrieval algorithm will be performed only on each cloudless land surface pixel. An accurate cloud screening procedure for satellite Imager data is crucial for reliable algorithm performance. In the operational cal/val system, however, the best available cloud filtering is required in order to distinguish which problems of the LST retrieval are caused by the algorithm or instrument and which are caused by cloud contamination. The ABI cloud mask, developed as an independent GOES-R product, will be used for all cloud detection in the final operational integrated GOES-R product system. But for pre-launch and early stage algorithm tests, particularly for tests by using proxy data, the GOES-R ABI cloud mask (ACM) is not readily applicable.

First, the ACM algorithm makes extensive use of information from NWP fields, coupled with a Radiative Transfer Model (RTM) to generate the expected clear-state for the spectral and temporal tests. For many off-line LST validation tests, this is impractical. Second, although the ACM is designed to work when only a sub-set of the expected channels is provided (e.g., running with fewer SEVERI proxy channels), the performance of the cloud mask is sensitive to imagery artifacts or instrument noise. Specific ACM calibrations are therefore required because the ACM algorithm compares the observed values to those from a forward radiative transfer model. Third, the LST validation tests will use extensive ground-based observations. Some of these ground-based observations may provide extra information for the detection of cloudy scenarios (e.g., downward long wave radiations). Basically, the GOES-R ACM algorithm relies only on the primary sensor information derived from the ABI observations and geolocation data. Therefore, to serve the special purpose of various pre-launch and offline LST validation tests, a practical and feasible cloud screening algorithm is essential and indispensable. The cloud-screening schemes described in this section will mainly serve this purpose.

Our cloud-screening scheme is designed with reference to the first version of GOES-R cloud mask ATBD, and optimized with respect to the available GOES-8 channels and SURFRAD observations. It is basically a threshold-testing scheme with the threshold value of each cloud parameter specified with an analytic optimization function. Eight parameters are chosen to characterize the essential differences of a cloudy pixel from a clear one:

- BT_{ch4} - $Max(BT_{ch4})$, difference between channel 4 brightness temperature and its maximum record over the previous 10 days,
- BT_{ch3} - BT_{ch4} , brightness temperatures difference of channel 3 and channel 4,
- BT_{ch4} - BT_{ch5}, brightness temperatures difference of channel 4 and channel 5,
- BT_{ch2} - BT_{ch4}, brightness temperatures difference of channel 2 and channel 4,
- $Reflectance_{ch1}$, channel 1 reflectance
- *StdDev (PIR)*, standard deviation of downwelling sky irradiance measured at the SURFRAD site during the past 15 minutes,
- $StdDev(BT_{ch4})$, deviation of 3 by 3 pixel array of channel 4 brightness temperature,
- Difference between SURFRAD LST and the match-up GOES-8 pixel channel 4 brightness temperatures.

These parameters enable us to identify the possible spectral, spatial and temporal singularities of a target pixel due to cloud. The underlining physics with these parameters may be referred to the relevant GOES-R ATBD and in the published literature. In general, selection of cloud detection parameters always involves assumptions of the different radiometric characteristics of a cloudy

state from its clear-sky counterpart. For instance, most clouds would cause enhanced reflectance and lower IR brightness temperatures. Snow cover, which also has increased reflectance, can be identified from image sequences, since snow pixels generally tend to be static from one hour to the next while clouds move.

In comparison with the GOES-R ACM algorithm, the above cloud-detection scheme has some distinct features. First, instead of using complicated RTM to evaluate clear-state reference values, the current scheme specifies clear-state values from historical time-series records. Second, apart from the satellite data, the SURFRAD ground measurements are also used in the cloud filtering. For most cloud-free (or cloudy) conditions during daytime, the solar irradiance time series is a smoothly (or highly irregular) varying curve, except when thin cloud occurs which has very little effect on the variation of solar irradiance. In most of such exceptional circumstances, the sky downwelling irradiance profile shows enhancements which enable the detection of clouds. Besides, an optimization function is introduced to specify the threshold values for each of the above parameters.

Just like other threshold-testing schemes, the most essential step leading to successful cloud detection is to specify pertinent threshold values for the involved parameters. Proper setting of threshold values would maximize the sensitivity to the presence of cloud and minimize the false detection of cloud. The threshold optimization is formulized with the assumption that within an optimized parameter domain, the scheme would produce maximum counts of valid cloudy/clear decision. Listed in Table 4.4 are the optimized threshold value settings with respect to one year (2001) dataset of the SURFRAD and GOES-8 Imager observations.

Table 4.4 Threshold Value Settings of the Cloud-Screening Algorithm.

Cloud-Screening Parameters	Threshold Values
BT_{ch4}_ - Max(BT_{ch4})	≥ -10K
BT_{ch2} - BT_{ch4}	-1.0K ~ 10.0K(day), -3.0K ~ 1.0K(night)
BT_{ch3} - BT_{ch4}	-70.0K ~ 25.0K(dry)
BT_{ch4} - BT_{ch5}	-3K ~ 3.0K
$Reflectance_{ch1}$	≤ 0.2
StdDev(BT_{ch4})	≤1.5K (dry), ≤ 0.8K(moist)
StdDev (PIR)	$1.2wm^{-2}$

The cloud screening is implemented as an automated process where threshold testing is performed one after another through all the above cloud parameters, Note that during nighttime, only the infrared channels of the satellite data and the downwelling sky irradiance of the SURFRAD data were used for the cloud filtering.

4.1.2.4 Match-up GOES and SURFRAD LST Data

To get pairs of valid match-up LSTs from the GOES-8 and SURFRAD data, we take three general steps: 1) geo-location match-up, 2) time match-up and, 3) cloud screening for clear-sky cases. We first pick up the GOES Imager pixel that is spatially nearest to one of the SURFRAD locations, and then search the SURFRAD time segment that is closest to the Imager data time stamp in the time series of the matched SURFRAD station. The geo-location match-up accuracy is limited by the accuracy of GOES-8 Imager data, which is about 4 km; while the time match-up accuracy is basically determined by Imager scanning time and temporal interval of the SURFRAD measurement, which is approximately about 5 minutes.

Once the valid match-up are confirmed, LSTs of that specific location and time are calculated separately from the GOES-8 data and the SURFRAD data. If a cloudless data pair is further confirmed following the cloud screening scheme, the matched LST pair is archived together with other relevant ancillary data.

4.1.3 MODIS Data

MODIS is an instrument that serves as the keystone instrument for global studies of atmosphere, land, and ocean processes (Salomonson *et al.,* 1989). It scans $\pm 55^{o}$ from nadir, has 36 bands with bands 1-19 and band 26 in the visible and near infrared range, and remainder bands in the thermal range from 3 to 15 μm. It provides daylight reflection and day/night emission spectral imaging of any point on the Earth every 1-2 days. The thermal infrared bands have an IFOV of approximately 1km at nadir.

MODIS is very useful for the development of various land surface product data because of its global coverage, radiometric resolution and dynamic ranges for a variety of land cover types, and high calibration accuracy in multiple thermal infrared bands designed for retrievals of LST and atmospheric properties. Particularly, the thermal infrared bands 31 and 32 of MODIS bear

similar central wavelength and band width to GOES-R channel 14 and 15 (Table 4.1), which makes them very suitable for the pre-launch testing/validation of the GOES-R LST algorithm. 10 weeks' MODIS data were collected by the GOES-R AWG proxy data team, and will be ingested to the GEOS-R mainframe by AIT members to retrieve the LST values with the selected GOES-R LST algorithm. This 10-week data collection is composed of four different data periods that fall into four seasons, respectively. Listed in Table 4.5 are the four different time periods together with the swath data types included in the 10-week collection. In addition, MODIS LST product data (MOD/MYD11-L2) of the same time periods was prepared to evaluate the GOES-R LST algorithm performance through comparison with MODIS product LST. Only the MOD/MYD11 swaths passing over the six SURFRAD sites (Table 4.3) during the selected data periods were collected, which enable us to make cross-comparison among GEOES-R LST, MODIS LST and SURFRAD LST at the available surface observation sites.

Not all of the data listed Table 4.5 are the necessary inputs of the GOES-R LST algorithm. The GOES-R product system provides several options in the emissivity and TPW inputs. The LST output shown in this document used the emissivity values from the MODIS global emissivity database (Borbas *et al.*, 2008; Seemann *et al.*, 2008), and the water vapor data from the 6-hour model forecasts of the National Centers for Environmental Prediction (NCEP).

Table 4.5. 10-week MODIS Swath data collected by GOES-R AWG Proxy Data Team

Satellites	Data Periods	Swath Data Sets/Types
Terra and Aqua	08/01-08/31, 2006 02/01-02/14, 2007 04/01-04/14, 2007 10/01-10/14, 2007	• Calibrated Radiances 5-Min L1B Swath 1km (MOD/MYD021KM, collection 5) • Geolocation Fields 5-Min L1A Swath 1km (MOD/MYD03,collection 5) • Temperature and Water Vapor Profiles 5-Min L2 Swath 5km (MOD/MYD07, collection 5) • Clouds 5-Min L2 Swath 1km and 5km (MOD/MYD06, collection 5) • Cloud Mask and Spectral Test Results 5-Min L2 Swath 250m and 1km (MOD/MYD35_L2, collection 5)

4.2 Output from Simulation/Proxy Datasets

4.2.1 Test Outputs

4.2.1.1 SEVERI Proxy Test Outputs

Figure 4.1 gives an example of the test results using SEVIRI proxy inputs. Overall, the LST values are reasonable and the spatial distribution of the LST is consistent with our understanding in the region. An animation of a time series (about one-month) of the LSTs was generated (not

shown here) for illustrating the LST daily and diurnal variations over the region. The results are also very reasonable.

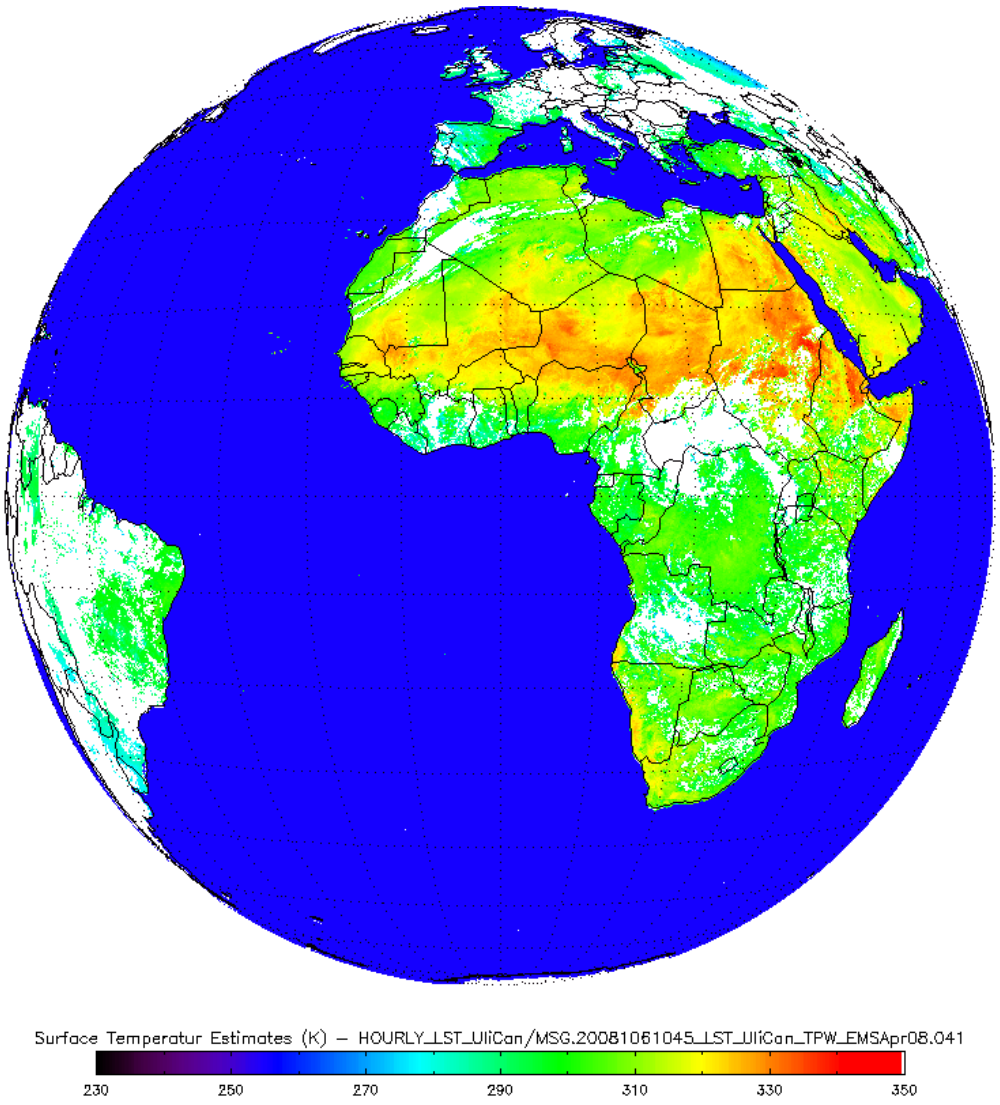

Figure 4.1. Sample LST image derived from one MSG/SEVIRI full disk data, as proxy of the GOES-R ABI data. Emissivity and water vapor information were from the MODIS monthly emissivity product and from the NCEP forecasting model, respectively. The data was sensed at 10:45 UTC time, on April 15th, 2008. Blue and white colors are masks of ocean and cloud areas, respectively. The color scale bar indicates the temperature range from 230 K to 350 K.

More than one year of SEVIRI and the Cardington station data have been processed and compared for the calculated LST results. Figure 4.2 shows the scatterplot between LST calculated from SEVIRI and surface measurements using the available data from February 2007 to March 2009.

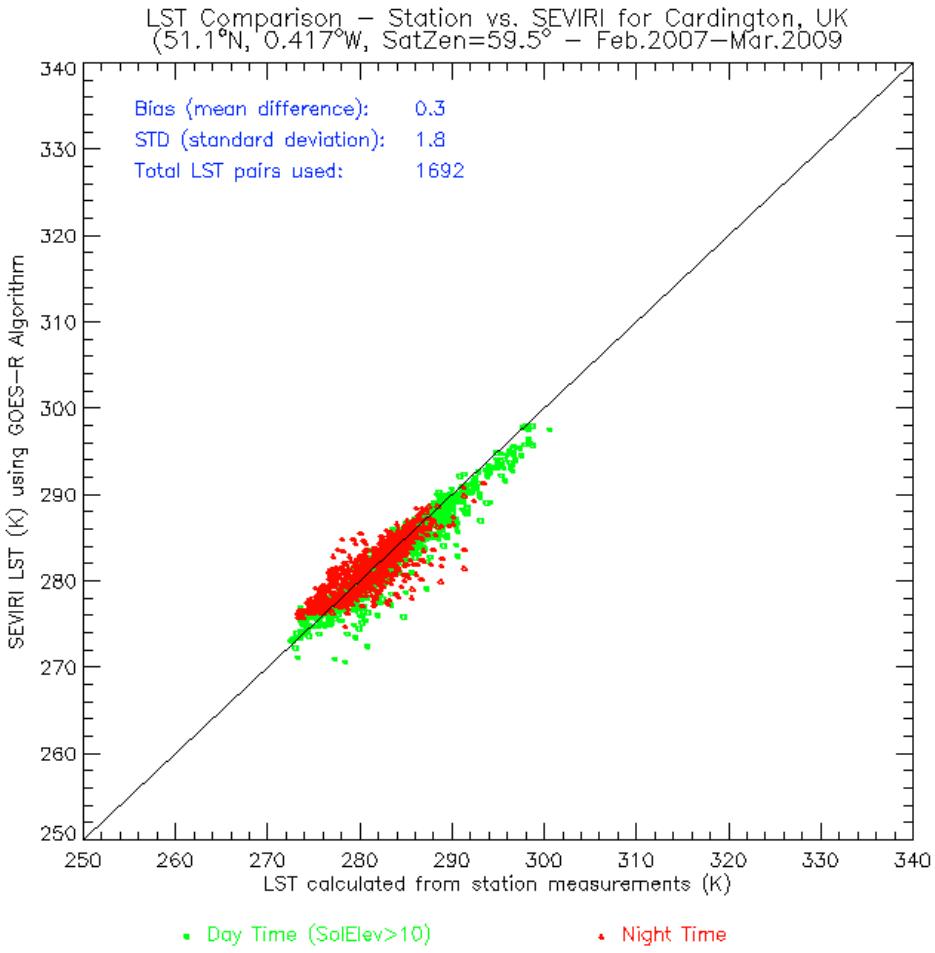

Figure 4.2. Scatter plots of LSTs derived from SEVIRI data vs. LSTs estimated from Cardington station. Datasets are stratified for daytime (Green) and night time (red) atmospheric conditions.

Similarly, available SEVIRI and the Gobabeb station data have been processed and compared for the calculated LST results. Figure 4.3 shows the scatter plots between LST calculated from SEVIRI and surface measurements using the available data from January 2008 to March 2009. The much increased sample size reflects the much better chance of getting cloud free pixels in southern Africa than in the UK. The consistent bias between the validation and the satellite derived data has been noted. The cause of the bias is unknown yet. It is probably because the emissivity value used for the ground LST estimation is lower than the reality, or it is because ground radiometer is biased during the period, etc.. Further investigations will be conducted during the period of algorithm intensive validation.

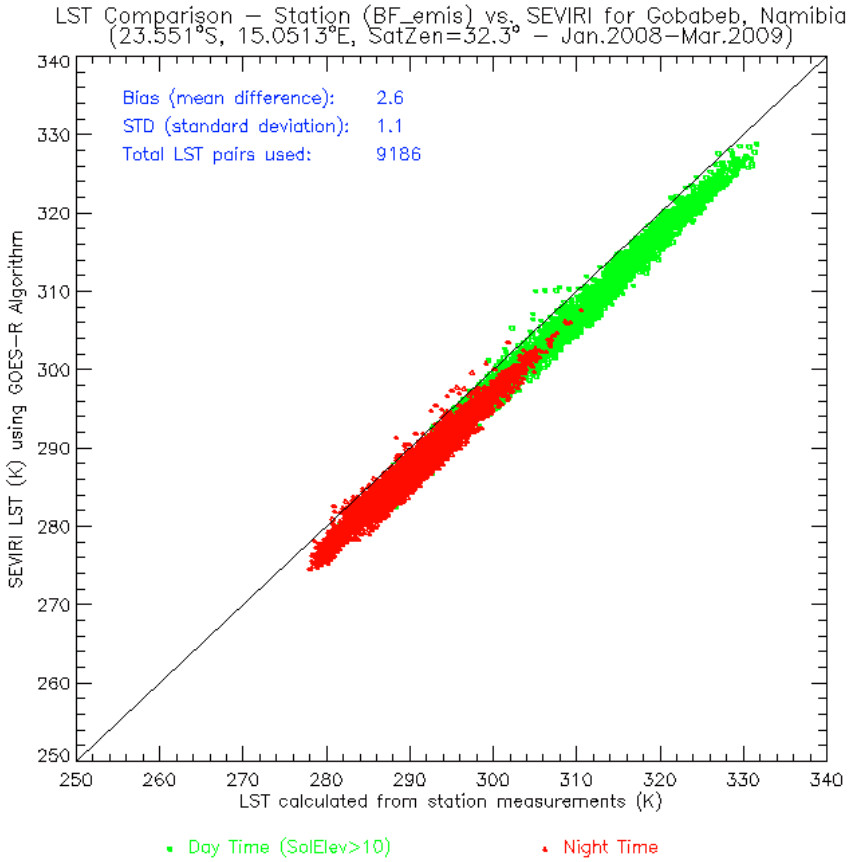

Figure 4.3. Scatter plots of LSTs derived from SEVIRI data vs. LSTs estimated from Gobabeb station. Data sets are stratified for daytime (Green) and night time (red) atmospheric conditions.

Finally, Figure 4.4 shows the comparison of SEVIRI generated LST using the adjusted GOES-R LST algorithm and the *in situ* surface temperature measurements from the radiometers during the one day field campaign as provided by J. Sobrino. This result is fairly close to that published by Atitar and Sobrino (2009). It is reassuring/encouraging that similar trends are demonstrated in the comparison of surface measured LST and the satellite generated LST using different split window algorithms.

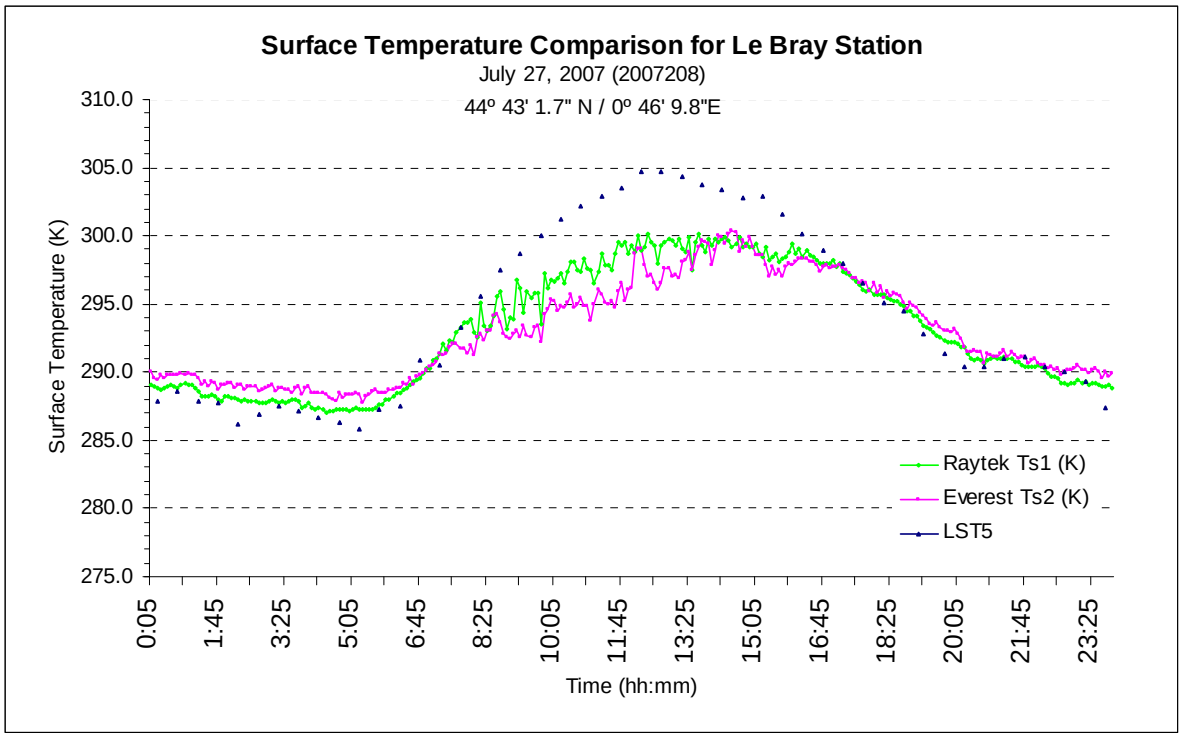

Figure 4.4. Comparison of LST from SEVIRI algorithm (LST5) and LST from radiometers (Ts1 & Ts2) with the one day experimental data provided by José Sobrino.

4.2.1.2 GOES-8 Proxy Test Outputs

Listed in Table 4.6 are the numbers of match-up data pairs from the SURFRAD and GOES-8 comparative test over the six SURFRAD sites in the year 2001. Except in March and July at Site 1 (Pennsylvania State University in State College, PA), each site/month/diurnal phase combination is well represented (at least 8 observations; typically many more). This match-up data size apparently indicates the feasibility of using practical cloud-screening algorithm for the pre-launch algorithm test purpose, and meanwhile allows us to perform meaningful statistical analysis for each site.

Table 4.6. Numbers of Match-up data Pairs of GOES-8 at the SURFRAD Sites in Year 2001.

Month	Site 1		Site 2		Site 3		Site 4		Site 5		Site 6	
	Day	Night	Day	Night	Day	Night	Day	Night	Day	Night	Day	Night
1	48	17	55	64	107	107	58	48	100	67	100	51
2	43	30	38	38	73	57	55	34	41	54	64	48
3	0	0	51	71	94	62	93	79	41	63	123	34
4	94	18	39	80	81	34	62	61	81	57	139	35
5	71	22	27	59	127	65	75	83	82	45	168	75
6	50	26	82	102	82	51	65	50	86	64	187	60
7	6	4	91	77	40	8	27	38	40	43	173	74
8	43	30	129	113	41	38	82	137	56	45	107	52
9	115	57	95	108	124	49	79	110	116	85	189	98
10	103	38	62	95	184	39	90	79	74	58	115	61
11	114	34	43	129	146	70	64	53	116	53	131	88
12	40	38	67	66	124	71	73	70	107	74	113	56
Total	727	314	779	1002	1223	651	823	842	940	708	1609	732

The output of match-up data pair comparisons over the six SURFRAD sites are shown in Figures 4.5 and 4.6, with the data pairs stratified into day/night and for dry/moist atmospheric phases, respectively. Different colors are used for marking the data pairs of different phases, that is, red for daytime phase or dry phase; blue for nighttime phase or moist phase.

As shown in Figures 4.5 and 4.6, the data sizes (data pairs) of different phases are fairly enough to establish their individual statistical analysis (see Section 4.2.2.2).

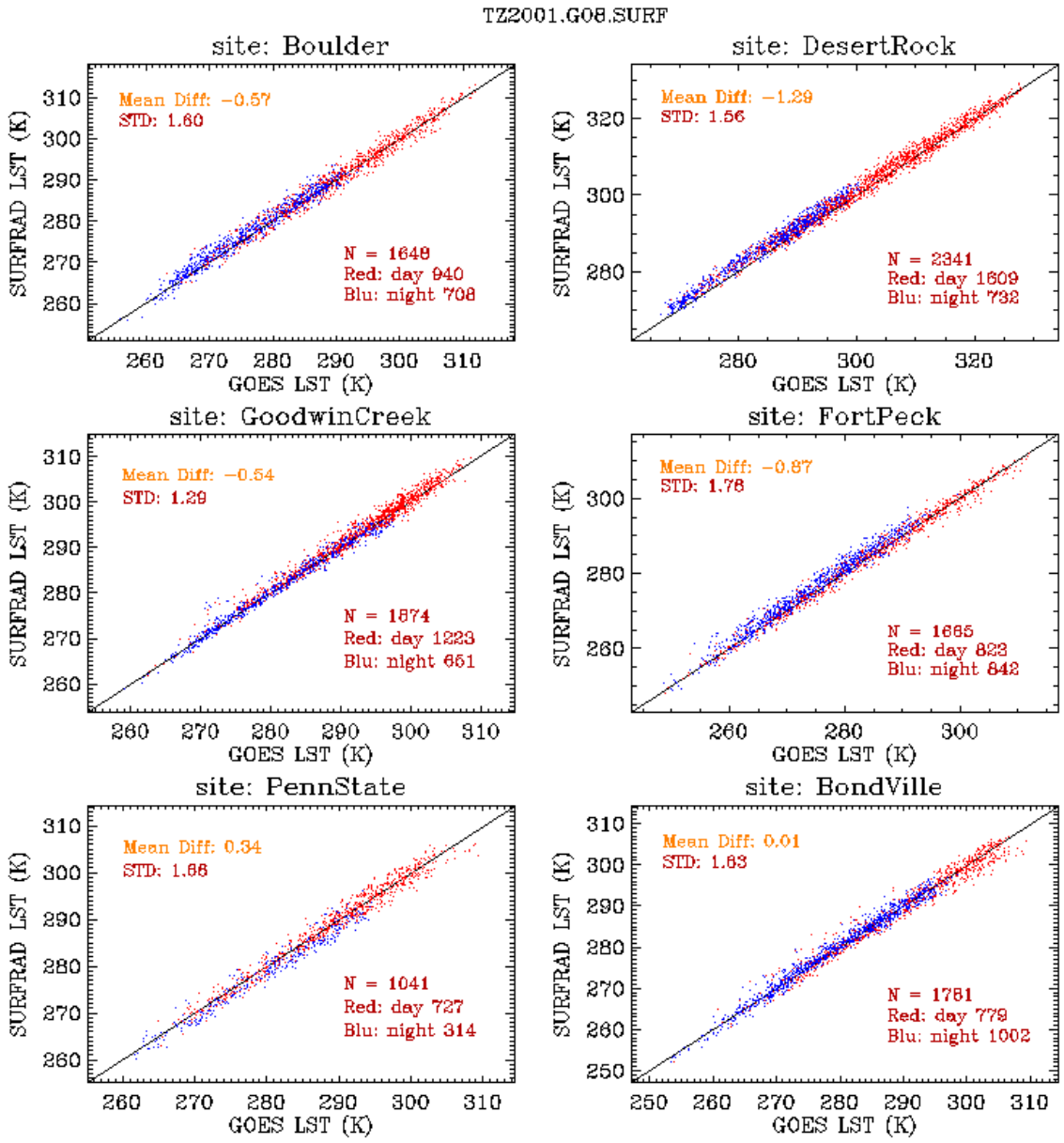

Figure 4.5. Scatter plots of LSTs derived from GOES-8 Imager data vs. LSTs estimated from SURFRAD stations in year 2001. Data sets are stratified for daytime (red) and night time (blue) atmospheric conditions.

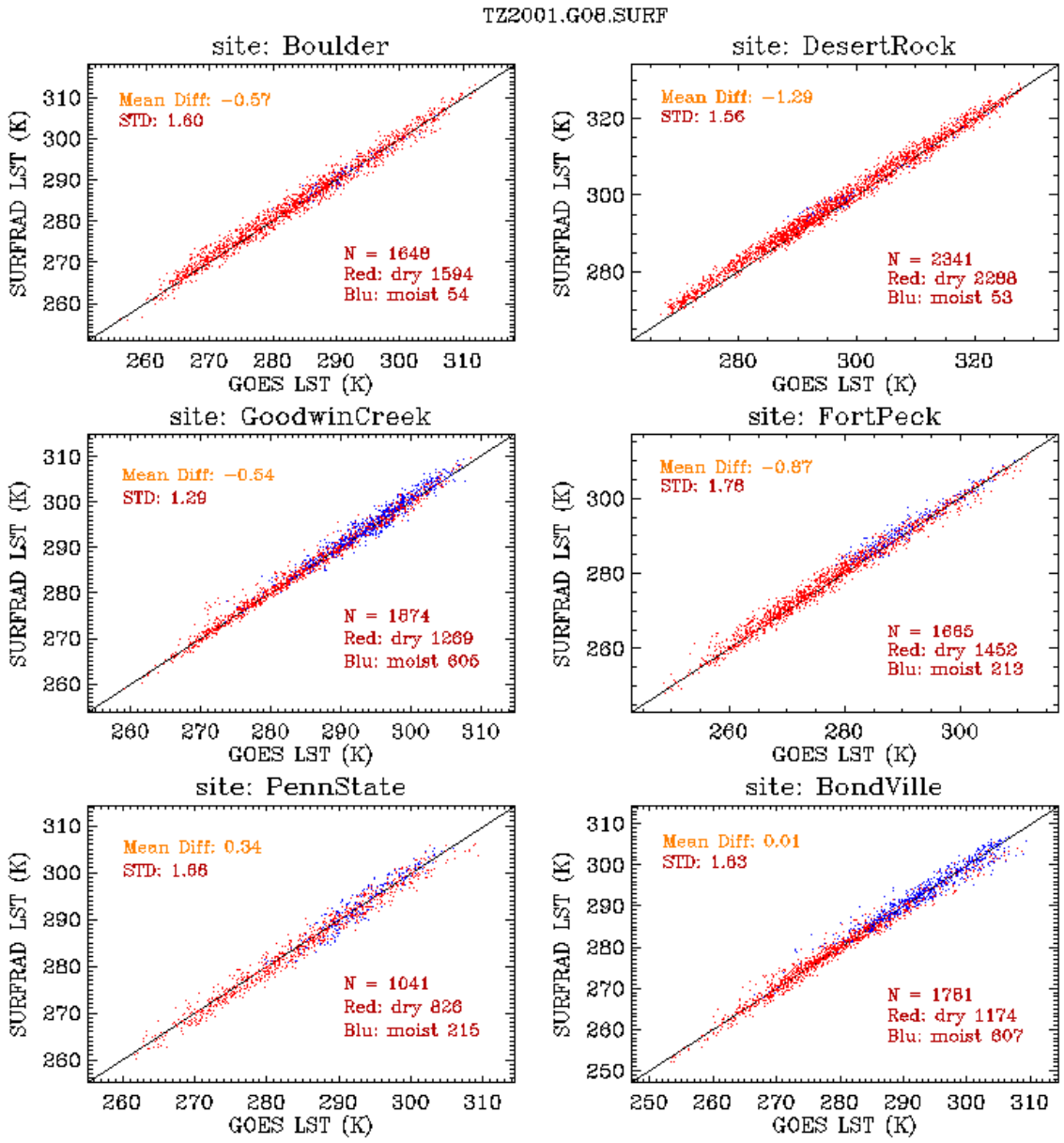

Figure 4.6. Same as Figure 4.4, except the data sets are stratified for dry (red) and moist (blue) conditions.

4.2.1.3 MODIS Proxy Test Outputs

The LST outputs of the GOES-R algorithm with the 10-week MODIS proxy inputs are 2-dimension data arrays which bear the original MODIS swath geo-location structure.

Shown in Figure 4.7 is a sample from the 10-week MODIS proxy test outputs. The areas filled with background color (white) are the areas without the LST retrieval (e.g., cloudy pixels, watery regions.

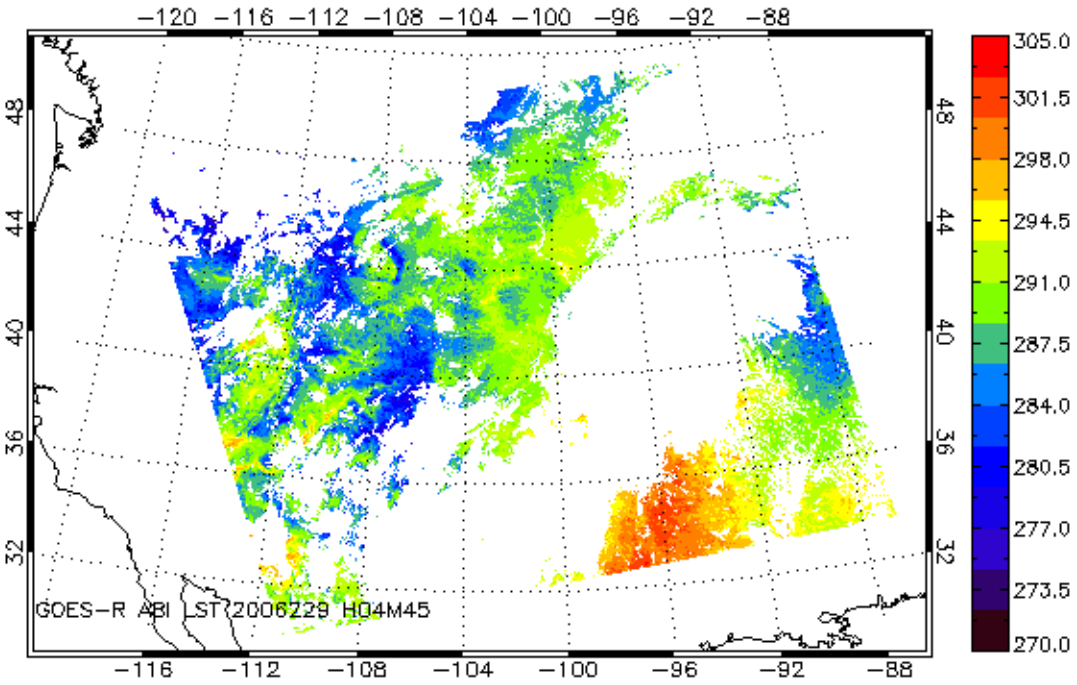

Figure 4.7. A sample LST output of the GOES-R algorithm with the inputs of MODIS TERRA proxy data of 08/17/2006 04:45GMT. The emissivity input in this case run is from the MODIS global emissivity database (Borbas *et al.*, 2008).

Several hundreds of such swaths are available from the 10-week MODIS proxy dataset. Only those swaths with one of the six SURFRAD station enclosed were collected and analyzed, for performing cross-comparison among GOES-R ABI LST, MODIS product LST and SURFRAD LST through the match-up observations. It is worth noting that the cloud screening of the 10-week MODIS proxy data test was based on the MODIS cloud product data (MOD/MYD35_L2). LST retrieval was performed only at Clear or Probably Clear pixels; pixels of Cloudy and Probably Cloudy were excluded. The match-up among GOES-R LST, MODIS LST and ground-based LST was performed only in the case where the matched GOES-R pixel and MODIS pixel both have retrieval values. A T-test screening was applied in the match-up process to further filtering out the "outlier" scenes that fall out 95% confidence level In addition, ground-based cloud information was utilized to confirm the removal of all the T-test outliers.

The resultant match-up GOES-R ABI LST (from the proxy MODIS data) and SURFRAD LST pairs were shown in Figures 4.8 and 4.9. Since the MODIS is onboard the polar-orbiting satellite which has only two over-pass observations a day, it is expected that the number of the match-up data pairs at each the SURFRAD site is significantly smaller comparing to the GOES and SURFRAD match-up dataset; therefore, it does not allow further data stratification over finer time scales as we did in the GOES-8 and SURFRAD Test. However, the number of match-up data pairs is still fairly good (normally larger than 30) for an overall evaluation of the differences among the three LST datasets.

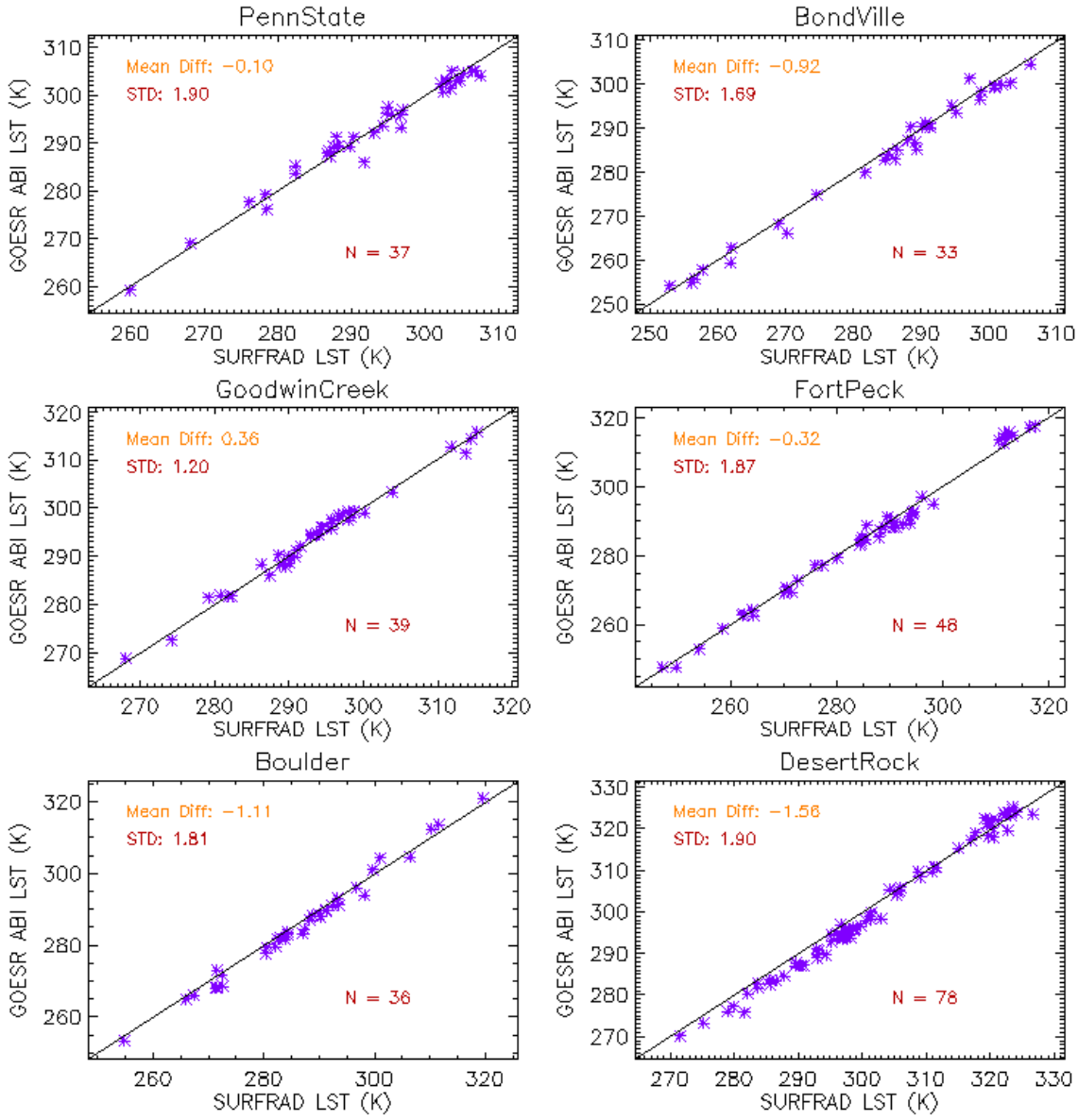

Figure 4.8. Scatter plots of GOES ABI LSTs with MODIS TERRA proxy inputs vs. the Matched SURFRAD LSTs at each SURFRAD station.

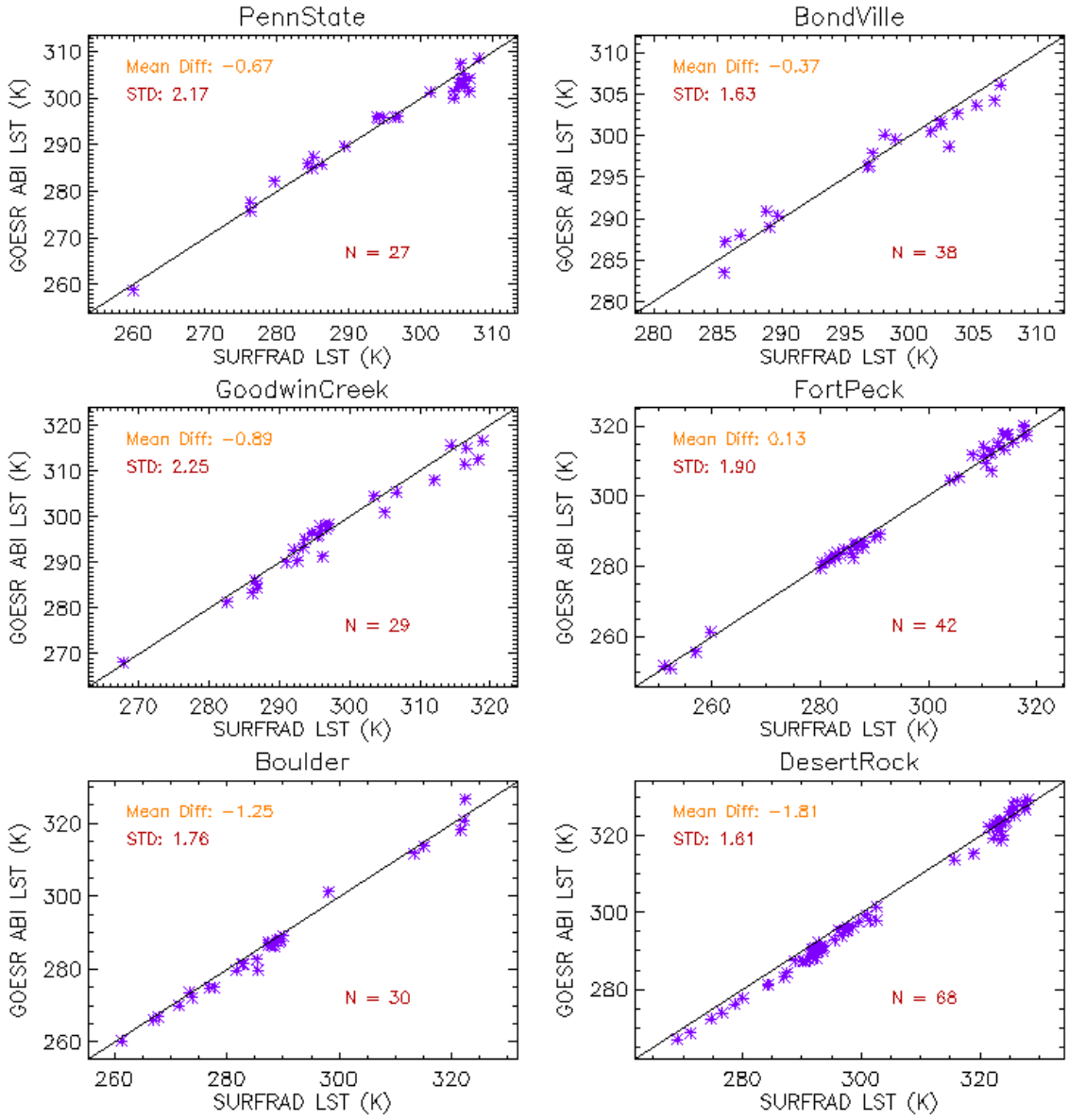

Figure 4.9. Scatter plots of GOES ABI LSTs with MODIS AQUA proxy inputs vs. the matched SURFRAD LSTs at each SURFRAD station.

Moreover, the comparison of GOES-R ABI LST with MODIS product LST can be performed over the entire swath, and be aggregated over a group of swaths, e.g., all the swaths passing over the a specific SURFRAD stations. As an example, the GOES-R ABI LST of Figure 4.7 is compared with the corresponding MODIS TERRA LST swath, and is shown in Figure 4.10. A slight positive bias of GOES-R ABI LST from MODIS LST may be easily identified from this figure. An overall accuracy and precision estimation will be addressed in Section 4.2.2.

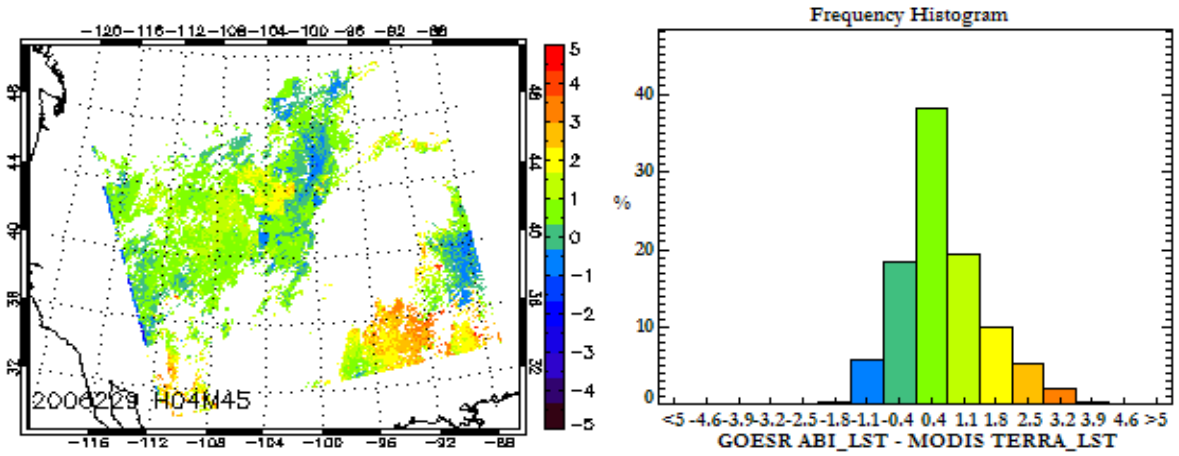

Figure 4.10. Image and histogram plot of LST difference between the proxy GOES-R LST and the MODIS LST. The data is sampled from MODIS Terra, on August 17, 2006.

4.2.2 Precision and Accuracy Estimates

4.2.2.1 Estimation Based on GOES-8 Proxy Data

For each SURFRAD site, overall accuracy and precision are estimated by calculating the mean LST difference and standard deviation between the GOES-8 proxy LST and SURFRAD LST, over all the available data pairs. Accordingly, the accuracy and precision under different atmospheric conditions (e.g., day/night) are evaluated over the corresponding subsets, respectively. The calculation results are summarized in Table 4.7.

It is seen that the exact accuracy and precision values are different from site to site. Nevertheless, the absolute value of overall accuracy is generally less than 1K (except the site number 6), which indicates that the selected GOES-R algorithm is efficient in spite of the distinct land surface properties of the six sites. The overall standard deviation (precision) is around 1.5K at all the sites. The low standard deviation values also imply the high repeatability and reliability of the estimations. By using the estimated standard deviation of each site, the confidence level of the estimated accuracy value is generally over 90% under Z-test (test for large sample data size).

In general, the accuracy of nighttime is lower than that of day time. Of the six sites, there are four sites (sites 1, 4, 5, 6) whose nighttime accuracies are lower than the corresponding daytime accuracies. The difference may be over 1.3K at Fort Peck station although the data sizes are similar for daytime and night time. Different cloud contamination may be one of the reasons. But as shown in Figure 4.5, the portion of moist data pairs is even higher at Goodwin Creek (moist data set may be easily subject to cloud contamination), while day/night difference at Goodwin Creek is smaller than that at Fort Peck. Moreover, no obvious outliers are found from the moist data set in Figure 4.5. In contrast, the daytime/night time precision values of the six sites are all around 1.5K, which are also similar to their individual overall precisions.

Table 4.7. Accuracy and Precision (deg K) Estimations of Daytime, Nighttime and overall.

Site	Overall			Day			Night		
	N	Acc.	Prec.	N	Acc.	Prec.	N	Acc.	Prec.
1	1041	0.34	1.66	727	0.01	1.56	314	1.09	1.66
2	1781	0.01	1.63	779	0.35	1.89	1002	-0.26	1.34
3	1874	-0.54	1.29	1223	-0.75	1.27	651	-0.14	1.24
4	1665	-0.87	1.76	823	-0.20	1.59	842	-1.52	1.68
5	1648	-0.57	1.60	940	-0.31	1.64	708	-0.90	1.49
6	2341	-1.29	1.56	1609	-1.00	1.56	732	-1.93	1.35

Shown in Table 4.8 are the accuracy/precision values for the four seasons, respectively. It is worth noting that the seasonal precision values are still around 1.5K. But the seasonal accuracy patterns vary from site to site. It is unsure whether such distinct seasonal patterns might be related to the different surface covers and regional climates. All these statistical features will be further studied in the future.

Table 4.8. Accuracy and Precision (deg K) Estimations of Four Seasons

Site	Winter			Summer			Fall			Spring		
	N	Acc.	Prec.	N	Acc.	Prec.	N	Acc.	Prec.	N	Acc.	Prec.
1	216	0.39	1.46	159	-0.06	1.96	461	0.41	1.52	205	0.41	1.86
2	328	0.26	1.62	594	-0.09	1.44	532	0.27	1.76	327	-0.50	1.63
3	539	-0.45	1.27	260	-0.63	1.45	612	-0.43	1.26	463	-0.73	1.23
4	338	-0.31	1.62	399	-1.29	1.67	475	-0.69	1.62	453	-1.09	1.95
5	443	-0.41	1.68	334	-0.85	1.42	502	-0.65	1.44	369	-0.38	1.83
6	432	-1.57	1.39	653	-1.23	1.64	682	-0.96	1.50	574	-1.55	1.57

4.2.2.2 Estimation Based on 10-week MODIS Proxy Data

As shown in Figures 4.8 and 4.9, the match-up data size (data pairs) from the 10-week MODIS Proxy Test is fairly enough for an overall accuracy and precision estimation. The overall accuracy and precision can be calculated in the same way as in the GOES-8 and SURFRAD Match-up Test. The results were summarized in Table 4.9 and Table 4.10.

It is seen in Tables 4.9 and 4.10 that ABI LSTs are mostly lower than the ground LST (SURFRAD LST), while the MODIS LSTs are the lowest. In average, the biases between the ABI LST and MODIS LST and the biases between ABI LST and the SURFRAD LST are mostly less than 1 K, while the bias between the MODIS LST and the SURFRAD LST are mostly larger than 1 K. That means, referring to the SURFRAD ground measurements the ABI LST is more accurate than the MODIS LST. The larges bias between the ABI LST and the ground LST

occurs at the Desert Rock (site 6), which is -1.56 K from the proxy of MODIS Terra data and -1.81 K from the proxy MODIS Aqua data, respectively. Precisions of the ABI LSTs to the ground LSTs are in a range from 1.20 K to 2.25 K. Note that the two extreme cases occur in the same site (Goodwin Creek, site 3) but from different MODIS proxies. It implies that the proxy data from the two sensors can be significantly different. Such difference may be introduced from the surface directional emissivity feature, or cloud contamination effect.

Table 4.9. Accuracy and Precision (deg K) Estimations of the ABI LSTs with MODIS TERRA proxy data.

Site	ABI LST – TERRA LST		ABI LST – SURFRAD LST	
	Acc.	Prec.	Acc.	Prec.
1	0.90	0.67	-0.10	1.90
2	0.53	0.90	-0.92	1.69
3	1.43	1.15	0.36	1.20
4	0.61	0.51	-0.32	1.87
5	0.53	0.67	-1.11	1.81
6	-0.19	0.35	-1.56	1.90

Table 4.10. Accuracy and Precision (deg K) Estimations of the ABI LSTs with MODIS AQUA proxy data.

Site	ABI LST – AQUA LST		ABI LST – SURFRAD LST	
	Accuracy	Precision	Accuracy	Precision
1	0.50	0.81	-0.67	2.17
2	0.80	1.15	-0.37	1.63
3	1.72	1.64	-0.89	2.25
4	0.65	0.72	0.13	1.90
5	0.39	0.58	-1.25	1.76
6	-0.61	0.45	-1.81	1.61

Considering that atmospheric absorption generally makes the satellite LST lower than the "true" value, the positive bias of the GOES-R LST from the MODIS LST may suggest better performance of the atmospheric absorption correction in the ABI LST algorithm. To further investigate this feature, we compared ABI LSTs and the MODIS LSTs using the 10-week MODIS swath data that over passed the SURFRAD ground sites. Accuracy and precision of calculated from each the swath data were aggregated, and is given in Table 4.11. It is seen again that the accuracy of the ABI LST to the MODIS LST is positive for all the swath data over the 6 SURFRAD sites, both for the MODIS Terra and Aqua.

Table 4.11. Aggregated Accuracy and Precision Estimations of the ABI LSTs with MODIS proxy data.

Site	ABI LST – TERRA LST		ABI LST – AQUA LST	
	Accuracy	Precision	Accuracy	Precision
1	0.90	0.71	0.86	0.78
2	0.92	0.75	0.89	0.82

3	1.00	0.79	0.92	0.88
4	0.74	0.61	0.62	0.66
5	0.65	0.68	0.64	0.80
6	0.54	0.66	0.46	0.79

In summary, we provided quantitative performance assessment of the GOES-R ABI LST algorithm with a variety of test datasets, including the SEVIRI proxy, the GOES-8 Imager proxy and MODIS AQUA and TERRA proxies. The assessment results indicate that the selected ABI LST algorithm can meet both the accuracy and precision requirements (Table 2.2).

4.2.3 Error Budget

There are a variety of sources that may introduce error in the satellite LST retrieval, yet it is very hard to quantitatively identify each source. Most of the error sources are coupled to each other. In our algorithm development, we tried to reduce the LST retrieval error by 1) stratified the algorithm coefficients for different atmospheric moisture conditions, 2) applied a path correction term for large view zenith angle, and 3) applied emissivity explicitly for counting the emissivity variance. Our test and evaluation results indicate that the algorithm can meet the accuracy and precision requirements of the GOES-R mission. However, it must be pointed out that several issues remain unsolved in the algorithm and in the test and evaluation process.

First, the algorithm is still sensitive to the surface emissivity though it is the least sensitive algorithm among those we tested (Table 3.6). A 3% emissivity uncertainty may introduce up to 1 K (Figure 3.14) LST retrieval error. Second, the residual of the atmospheric correction can be up to 0.9 K (Table 3.7), and additional errors may be introduced if the water vapor information is not right (Figures 3.15 and 3.16). Errors will also be introduced in the algorithm coefficient generation using the MODTRAN radiative transfer model. This is mainly because limited samples of the atmospheric profiles, solar-view geometries, surface emissivity values and the prescribed surface temperatures were used in the simulation process. Also, the simulated sensor response function used in generating the sensor brightness temperature maybe an error source.

In the algorithm evaluation process, as mentioned earlier, there are several issues that should be further studied in the match-up dataset comparisons. Difference between the satellite pixel-size measurement and the ground spot-size measurement must be characterized for a high quality validation procedure. More accurate broadband emissivity values are needed to better estimate the ground LSTs.

Cloud contamination is still a problem even if we have used a stringent cloud filtering procedure in generating the match-up dataset. It is found that a little threshold value or procedure change will have significant impact to the output match-up data pairs, though the overall validation results are not obviously affected.

All the above factors may potentially degrade the algorithm performance when it is applied for the real GOES-R satellite data.

5 PRACTICAL CONSIDERATIONS

5.1 Numerical Computation Considerations

The LST algorithm selected is mathematically simple, and requires no complicated mathematical routines. In operations it will be robust and fast enough in terms of the algorithm latency requirement (< 15 minutes, goal) using current computer power. There is no specific numerical computation requirement needed. For storage consideration, LST values should be saved in two-byte integers, with scale factors (intercept and slope) defined for the entire dataset. Quality flags for each pixel value should be bit-flag definitions, to minimize data storage.

5.2 Programming and Procedural Considerations

The LST algorithm is a pixel-by-pixel algorithm, implemented in sequential mode. Because of the algorithm simplicity, it requires small amount of code, with basic mathematical routines. However, since the LST algorithm requires ancillary datasets such as emissivity data and the total column atmospheric water vapor data, pre-calculated lookup tables may be needed for mapping the ancillary datasets to the ABI pixel geolocation. Besides, the algorithm processing routines should be programmed in block functions for integration ease.

5.2.1 Configuration of Retrieval

The primary adjustable parameters for the LST retrieval are the algorithm coefficients that are stratified for four atmospheric conditions. Criterion values for the dry, moist and very moist atmospheric conditions should also be adjustable in order to optimize the algorithm if needed from results of post-launch validation. Source of ancillary datasets should be configurable for the best dataset. And finally, it should be kept in mind that metadata used for the product may be modified, reduced and added in late phase of the product generation.

5.3 Quality Assessment and Diagnostics

The LST retrieval will be assessed and monitored. First, a set of quality control flags will be generated with the LST product for retrieval diagnostics, as is presented in Section 3.4.3. The quality control flags will indicate the retrieval conditions, including the land/non-land surfaces (i.e., ocean, snow, ice, water etc.), atmospheric water vapor status (i.e., dry, moist and very moist conditions), day and night, large view angle, very cold surface, etc. Details are shown in Table 3.9. LST maps and statistical information will be generated and reviewed for quality assessment.

5.4 Exception Handling

The algorithm will handle exceptions through the quality control flags. In calculating the LST for each pixel, quality control flags from input datasets will be examined and skipped for bad sensor data (e.g., missing or no sensor data). Cloudy pixels (i.e., "cloud" and "probably cloud") will also be skipped. Availability of other ancillary datasets such as emissivity and water vapor will also be checked and the retrieval will be skipped if either is not available. New quality control flags will be generated for indicating the exceptions.

In case the ABI derived sensor data are used as input to the LST algorithm, if the ABI snow mask, land surface emissivity, and TPW are not available, alternative ancillary data should be checked first for LST algorithm input before skipping the LST calculation.

5.5 Algorithm Validations

The algorithm testing described in Section 4 is preliminary. More substantial algorithm and product validations are necessary pre and post launch of the GOES-R satellite. A detailed validation plan for the GOES-R ABI product of land surface temperature has been is addressed in the Validation Plan Documentation, which has been submitted to the GOES-R AWG for review in March 2009.

5.5.1 Pre-launch Validations

Further validations using the SURFRAD ground measurements and GOES-8, -10 Imager data will be performed. First, a two-measurement statistical method developed by Flynn (2007) and Yu *et al*. (2009b) will be applied to analyze statistical features (such as noise and correlation) of the LSTs estimated from the SURFRAD data and from the GOES Imager data. Further, a three-measurement method (Yu *et al.* 2009c) will be applied for the accuracy estimation of the LST algorithm. LST diurnal cycle derived using the GOES Imager data will be analyzed for assessing the algorithm (Vinnikov *et al*., 2008). In addition, a ground site characterization study will be performed on the SURFRAD stations for better comparisons between the satellite retrieved LSTs and the ground estimated LSTs.

Similar validations will be performed using MSG/SEVIRI data. The corresponding ground measurement data will be collected through collaborative relationship with the European colleagues.

In addition to using the geostationary satellite data for the algorithm validation, polar orbiting satellite data may also be used for multi-satellite data comparisons. For instance, the Earth Observation Systems (EOS) satellite produces LSTs from its Moderate Resolution Imaging Spectroradiometer (MODIS) data, and the National Polar-orbiting Operational Environmental Satellite System (NPOESS, scheduled launch in 2010) will produce LSTs from its Visible/Infrared Imager/Radiometer Suite (VIIRS). The multi-satellite data comparison may provide better assessment of the algorithm.

5.5.2 Post-launch Validations

There are two stages in performing the Post-launch validation. At the early stage, which is normally within one to three months after the launch, the algorithm will be calibrated using new sensor response functions and noise features, determined from the on-orbit sensor calibration procedure. The algorithm will also be tuned from the results of using the available ancillary datasets. After that, a long-term validation facility and procedure will be performed for assessing and monitoring the LST product. At that time, algorithm improvement may be available from improving the cloud detection method, the quality of ancillary data, the ground estimation, etc.

6 ASSUMPTIONS AND LIMITATIONS

6.1 Assumptions

First of all, because the LST algorithm requires ancillary datasets, it is assumed that following data are available before the LST retrieval is performed:

- the ABI cloud mask,
- a high quality dynamic land surface emissivity dataset,
- water vapor dataset.

Specifications on sensor will perform as described in the GS-F&PS. Algorithm coefficients will be calibrated using real values of the sensor response functions. And, most importantly, a national validation network facility will be established after the first launch of GOES-R satellites.

6.2 Limitation

The algorithm described in this document performs in the infrared spectral bands. It is applicable only on cloudless pixels. LST effects due to roughness and/or structure of land surface, the emissivity directional feature and its variation in a pixel are not handled in the algorithm. The retrieved LST value is an effective land surface skin temperature over isothermal mixed pixel. The retrieval accuracy may be reduced significantly in regions with heavy atmospheric water vapor loading (e.g. > 5.0 g/cm^2). Also, the retrieval may be questionable in regions with very low LST and where the surface air temperature is higher than LST.

6.3 Pre-launch Product Improvements

There are two general areas of preplanned product improvement, better and more accurate validation against ground truth and refinement of the LST algorithm.

6.3.1 Improved Validation Methods

The difficulties with comparison of satellite retrievals with ground observations are well known and common to many of the satellite products. They include incompatibility between surface point measurements and pixel-sized satellite observations, unknown error characteristics of ground truth and satellite retrievals and calibration uncertainties in the satellite and ground data. Efforts to develop and prove new methods of evaluating errors in both ground and satellite data will be pursued in the pre-launch period. A method of comparing two data sets (Flynn 2006, Yu et al. 2009b), where both have unknown errors, will be evaluated. The method applies a linear fitting model to the satellite and ground based data and uses the result to estimate precision of

both data sets. A related method to make use of three independent observations (Ground observations at SURFRAD, GOES-East and GOES-West) is also being studied (Yu et al., 2009c). These methods are expected to allow statistically significant error estimates to be made about each source of data and thereby help specify the error in the satellite LST.

Clearly, the properties of the land surface, specifically land surface cover and emissivity, are very important to its retrieved LST. It is planned to characterize the land surface around the ground truth sites (SURFRAD and CRN) in as much detail as possible. This will help understand differences between the *in situ* point measurements and the pixel-sized satellite LST. High resolution ASTER data, from the Terra satellite, archived at the EROS Data Center will be used in this effort. Maps of land use, vegetation type, vegetation fraction and emissivity will be developed for approximately 10 x 10 km areas around each ground truth site.

An automated calibration/validation system is being developed. It will be implemented first using real time GOES and Meteosat SEVIRI data as proxies for the ABI. LST algorithms of the GOES-R ABI type will be used, but with coefficients specified for the split window bands on the GOES Imagers and the SEVIRI. In addition, studies of the GOES-R algorithm as applied to MODIS data will also be done. Knowledge gained from these studies will be used to improve the algorithm.

6.3.2 Algorithm Improvement

The large diurnal variability of LST is something that is conceptually understood, but which is poorly described quantitatively and not explicitly accounted for in the algorithm. The amplitude of the diurnal cycle is determined by surface cover, specifically the green vegetation fraction and soil moisture. The Bowen ratio over bare dry soil is high and over transpiring vegetation is low, and therefore green vegetation fraction in each pixel is important to LST and its diurnal range, with diurnal variation much larger in low vegetation pixels. A second contributor to LST variation is the fraction of surface shadowing seen from the observing satellite. This effect arises because shaded surfaces are significantly cooler than sunlit surfaces, so the apparent shadow fraction in a pixel is important. It, of course, varies according to the relative geometry of the sun and satellite and is changing throughout daylight hours. All of these factors should be factored into the LST algorithm and work on that problem is planned.

In addition, we are working on an inversion method that can derive the LST and the surface emissivity simultaneously using multi-channel and multi-observation measurements. Originally, such method was applied to the EOS/MODIS mission through its day and night observations over a pixel (Wan, 2008). The method can be applied to GOES-R ABI data better since it provides multiple observations over a pixel in a short time interval, which ensures constant emissivity during the time which is the baseline of the inversion method. We simplified the method significantly and have had the output stable and faster (Yu et al., 2009d).

7 REFERENCES

Aminou, D., and coauthors, "Meteosat Second Generation: A comparison of on-ground and on-flight imaging and radiometric performances of SEVIRI on MSG-1," *Proceedings of 'The 2003 EUMETSAT Meteorological Satellite Conference', Weimar, Germany, 29 September – 3 October 2003*, pp. 236–243, 2003.

Atitar, Mariam and José Antonio Sobrino, (2009) A Split-Window Algorithm for Estimating LST From Meteosat 9 Data: Test and Comparison With In Situ Data and MODIS LSTs, IEEE GEOSCIENCE AND REMOTE SENSING LETTERS, VOL. 6, NO. 1, PP122-126, JANUARY 2009.

Augustine, J. A., J. J. DeLuisi, C. N. Long, "SURFRAD- A National Surface Radiation Budget Network for Atmospheric Research", Bull. Amer. Meteor. Soc., 81, 2341-2357, 2000.

Augustine, J. A., G. B. Hodges, C. R. Cornwall, J. J. Michalsky and C. I. Medina, "An Update on SURFRAD- The GCOS Surface Radiation Budget Network for the Continental United States", J. Atmos. Oceanic Technol., 22, 1460-1472, 2005.

Becker, F., and Z. L. Li., "Towards a local split window method over land surfaces", Int. J. Remote Sensing, vol. 11, pp. 369-393, 1990.

Berk, A., G. P. Anderson, P. K. Acharya, J. H. Chetwynd, M. L. Hoke, L. S. Bernstein, E.P. Shettle, M.W. Matthew and S.M. Alder-Golden , MODTRAN4 Version 2 Users's Manual, Space Vehicles Directorate, Hanscom AFB, MA 01731-3010, April 2000.

Borbas, E. E., L. Moy, S. W. Seemann, R. O. Knuteson, P. Antonelli, J. Li, H-L Huang, I. Trigo, I. de Meteorologia, L. Zhou, A GLOBAL INFRARED LAND SURFACE EMISSIVITY DATABASE AND ITS VALIDATION, P2.7, AMS Annual meeting, New Orleans, January, 2008.

Caselles, V., C. Coll, and E. Valor, "Land surface temperature determination in the whole Hapex Sahell area from AVHRR data," Int. J. Remote Sens., vol. 18, no. 5, pp. 1009–1027, 1997.

Coll, C., E. Valor, T. Schmugge, and V. Caselles, "A procedure for estimating the land surface emissivity difference in the AVHRR channels 4 and 5," Remote Sensing Application to the Valencian Area, Spain, 1997.

Ellrod, G. P., Detection and analysis of fog at night using GOES multispectral infrared imagery, NOAA Tech. Rep. NESDIS 75, 22 pp., 1998.

EUMETSAT homepage, http://www.eumetsat.int/groups/ops/documents/document/pdf_ten_052562_msg1_spctrsp.pdf

Flynn, L., "Comparisons Two Sets of Noisy Measurements", NOAA Technical Report, NESDIS Office of Research and Applications, 2006.

Geostationary Operational Environmental Satellite (GOES), GOES-R Series, Advanced Baseline Imager, Performance and Operational Requirements Document (PORD), Implementation Review, 2004: DOORs Implementation Version 2.0, 417-RABIPORD-0017, (January 23), 36-p.

GOES-R Program Office, GOES-R Series Mission Requirements Document (MRD), P417-R-MRD-0070, 2007.

GOES-R Series Ground Segment (GS) Project Functional and Performance Specification (F&PS) Version 1.10 May 8, 2009. http://www.star.nesdis.noaa.gov/star/goesr/MRD/FPS_1.10.pdf

Göttsche, Frank and Folke Olesen, A SIMPLE PHYSICALLY BASED MODEL OF DIURNAL CYCLES OF LAND SURFACE TEMPERATURE, extended abstract submitted to EUMETSAT Meteorological Satellite Conference, held in Bath, U.K., 21-25 September 2009.

Hansen, M., and B. Reed, "A comparison of the IGBP DISCover and University of Maryland 1 km global land cover products", International Journal of Remote Sensing 21 (2000) (6–7), pp. 1365–1373, 2000.

Hillger, D., W. Ellrod, P. Gary, Detection of Important Atmospheric and Surface Features by Employing Principal Component Image Transformation of GOES Imagery, Journal of Applied Meteorology, Vol. 42, No. 5, pp. 611–629, 2003.

Li, Z-L, and F. Becker, Feasibility of land surface temperature and emissivity determination from AVHRR data, Remote Sensing of Environment, vol. 43, pp. 67-85, 1993.

McMillin, L. M., "Estimation of sea surface temperatures from two infrared window measurements with different absorption", Journal of Geophysical Research 80 (C36), pp. 5113–5117, 1975.

McMillin, L. M., and D. S. Crosby, "Theory and validation of multiple window sea surface temperature technique", J. Geophys. Res., 89, 3655-3661, 1984.

Menzel, W. P., and J. F. W. Purdom, Introducing GOES-I: The First of a New Generation of Geostationary Operational Environmental Satellites, Bull. Amer. Meteor. Soc., 75, 757–781, 1994.

Norman, J. M., and F. Becker, Terminology in thermal infrared remote sensing of natural surfaces, Remote Sensing Rev. 12:159-173, 1995.

Olesen, Folke-S. and Frank-M. Göttsche, VALIDATION OF LAND SURFACE TEMPERATURES OBTAINED FROM METEOSAT-MVIRI AND SEVIRI WITH IN-SITU MEASUREMENTS, extended abstract submitted to EUMETSAT Meteorological Satellite Conference, held in Bath, U.K., 21-25 September 2009.

Prata, A. J., and C. M. R. Platt, "Land surface temperature measurements from the AVHRR," in Proc. 5th AVHRR Data Users Conf., Tromso, Norway, Jun. 25–28, pp. 438–443. EUM P09, 1991.

Prata, A. J., "Land surface temperatures derived from the AVHRR and the ATSR, 1, Theory," J. Geophys. Res., 98(D9), 16,689–16,702. 1993.

Prata, A. J., "Land surface temperatures derived from the AVHRR and the ATSR, 2, Experimental results and validation of AVHRR algorithms," J. Geophys. Res., 99(D6), 13,025–13,058. 1994.

Price, J. C., "Land surface temperature measurements from the split window channels of the NOAA-7/AVHRR", J. Geophys. Res., vol. 89, pp. 7231–7237, 1984.

Salomonson, V.,W. Barnes, P. Maymon, H. Montgomery, and H. Ostrow, ‘‘MODIS: advanced facility instrument for studies of the Earth as a system,’’ *IEEE Trans. Geosci. Remote Sens.*, vol. 27, no. 2, pp. 145-153, 1989.

Schmetz J, Pili P, Tjemkes S, Just D, Kerkmann J, Rota S, Ratier A., "An introduction to Meteosat Second Generation (MSG)", *Bulletin of the American Meteorological Society,* 83, 977-992, 2002.

Schmid J, "The SEVIRI Instrument", Proceedings of the 2000 EUMETSAT Meteorological Satellite Data User's Conference, Bologna, Italy, 29 May – 2 June 2000, 2000.

Schmit T. J., W. F. Feltz, W. P. Menzel, J. Jung, A. P. Noel, J. N. Heil, J. P. Nelson III, G. S. Wade, "Validation and use of GOES sounder moisture information", Wea. Forecasting, 17, 139-154, 2002.

Schmit, T.J., J. Li, M.M. Gunshor, C.C. Schmidt, W.P. Menzel, J. Gurka, and J. Sieglaff, Study of the Advanced Baseline Imager (ABI) on the GOES-R and beyond, 84th AMS Annual Meeting, Seattle WA, 2004.

Schmit, T. J., W. Paul Menzel , J. Gurka , M. Gunshor, "The ABI on GOES-R, 3rd Annual Symposium Future National Operational Environmental Satellite Systems", San Antonio, January 16, 2007.

Schumann W, Stark H, McMullan K, Aminou D, Luhmann H-J., "The MSG System", *ESA bulletin,* 111, 2002.

Seemann, S.W., E. E. Borbas, R. O. Knuteson, G. R. Stephenson, H.-L. Huang, Development of a Global Infrared Land Surface Emissivity Database for Application to Clear Sky Sounding Retrievals from Multi-spectral Satellite Radiance Measurements.J. Appl. Meteor. Climatol., Vol. 47, 108-123, 2008.

Sellers, P. J., F. G. Hall, G. Asrar, D.E Strebel, and R. E. Murphy, The first ISLSEP field experiment (FIFE), Bull. Amer. Meteorol. Soc., Vol. 69, no. 1, 22-27, 1998.

Sikorski, R. J., P.S. Kealy, and W. J. Emery, Land Surface Temperature Visible/Infrared Image radiometer Suite Algorithm Theoretical Basis Document, Version 5, Raytheon Systems Company, 2002. Available: http://npoesslib.ipo.noaa.gov/atbd/viirs/.

Snyder, W. C., Z. Wan, and Y. Z. Feng, "Classification-based emissivity for land surface temperature measurement from space", Int. J. Remote Sensing, vol. 19, no. 14, pp. 2753-2774, 1998.

Sobrino, J. A., Z. L. Li, M. P. Stoll, and F. Becker, "Improvements in the split-window technique for land surface temperature determination," IEEE Trans. Geosci. Remote Sens., vol. 32, no. 2, pp. 243–253, Mar. 1994.

Sobrino, J. A., Z. L. Li, M. P. Stoll, and F. Becker, "Determination of the surface temperature from ATSR data," in Proc. 25th Int. Symp. Remote Sens. Environ., Graz, Austria, Apr. 4–8, pp. II-19–II-109, 1993.

Sun, D. and Pinker, R.T. Estimation of land surface temperature from a Geostationary Operational Environmental Satellite (GOES-8). Journal of Geophysical Research, D, Atmospheres v.108, no. D11, 3 June 2003. S

Sun, D., and R. Pinker, “Case study of soil moisture’s effect on land surface temperature retrieval”, IEEE Trans. Geos. Remote Sens. Lett., 1 (2), 127-130, 2004.

Ulivieri, C., and G. Cannizzaro, “Land surface temperature retrievals from satellite measurements,” Acta Astronaut., vol. 12, no. 12, pp. 985–997,1985.

Ulivieri, C., M. M. Castronouvo, R. Francioni, and A. Cardillo, “A SW algorithm for estimating land surface temperature from satellites,” Adv. Space Res., vol. 14, no. 3, pp. 59–65, 1992.

Vidal, A., “Atmospheric and emissivity correction of land surface temperature measured from satellite using ground measurements or satellite data,” Int. J. Remote Sens., vol. 12, no. 12, pp. 2449–2460, 1991.

Vinnikov, K. Y., Y. Yu, M. K. Rama Varna Raja, D. Tarpley, M. Goldberg, “Diurnal-seasonal and weather-related variations of land surface temperature observed from geostationary satellites”, *Geophys. Res. Lett.*, **vol. 35**, L22708, doi:10.1029/2008GL035759, 2008.

Walton, C. C., Pichel, W. G., Sapper, J. F., and May, D. A., “The development and operational application of non-linear algorithms for the measurement of sea surface temperatures with the NOAA polar-orbiting environmental satellites”, Journal of Geophysical Research, 103, 27 999–28 012, 1998.

Wan, Z., and J. Dozier, “A generalized split-window algorithm for retrieving land-surface temperature measurement from space”, IEEE Trans. Geosci. Remote Sensing, vol. 34, pp. 892–905, 1996.

Wan, Z., "MODIS Land-Surface Temperature Algorithm Basis Document (LST ATBD): version 3.3," (April 1999).

Wan, Z., “New refinements and validation of the MODIS Land-Surface Temperature/Emissivity products”, Remote Sensing of Environment 112 (2008):59–74.

Yu, Y., and I. J. Barton, “A non-regression-coefficients method of sea surface temperature retrieval from space”, Int. J. Rem. Sens., 15, 1189-1206, 1994.

Yu, Y., J. L. Privette, and A. C. Pinheiro, “Analysis of the NPOESS VIIRS land surface temperature algorithm using MODIS data,” IEEE Trans. Geosci. Remote Sens., vol. 43, no. 10, pp. 2340–2350, Oct. 2005.

Yu, Y., Ana C. Pinheiro, J L. Privette, “Correcting land surface temperature measurements for directional emissivity over 3-D structured vegetation”, SPIE San Diego , July, 2006.

Yu, Y., J. P. Privette, and A. C. Pinheiro, “Evaluation of split window land surface temperature algorithms for generating climate data records”, IEEE Trans. Geosci. Remote Sensing, vol. 46, No. 1, pp. 179-192, 2008.

Yu, Y.**,** D. Tarpley, J. L. Privette, M. K. Rama Varna Raja, K. Vinnikov, H. Xu, “Developing algorithm for operational GOES-R land surface temperature product”, *IEEE Trans. Geosci. Remote Sens.*, **vol. 47**, no. 3, pp. 936-951, 2009a.

Yu. Y.,, J. L. Privette, Mitchell Goldberg, and D. Sun, “Evaluation of the GOES land surface temperature algorithm using tower-based measurements from SURFRAD network”, Proc., Second Conference on Earth Observation for Global Change, Chengdu, China, 2009b.

Yu. Y., M. Chen, K. Vinnikov, D. Tarpley, and H. Xu, “A Three-measurement Model Developed for Evaluating Satellite Land Surface Temperature Product”, SPIE 2009, San Diego, 2009c.

Yu. Y., H. Xu, D. Tarpley, and M. Goldberg, “A Simplified method for measuring land surface temperature and emissivity using thermal infrared split-window channels”, IGARSS 2009, Proc., Cape Town, 2009d.